



THESIS

3



This is to certify that the

dissertation entitled

Real-Time Analysis of Light Alkenes at Elevated
Temperatures and Pressures by Fiber Optic
Near Infrared Spectroscopy

presented by

Engin Deniz Yalvac

has been accepted towards fulfillment
of the requirements for

Ph.D. degree in Chemistry



Major professor

Date 12/11/96

LIBRARY
Michigan State
University

**PLACE IN RETURN BOX to remove this checkout from your record.
TO AVOID FINES return on or before date due.**

DATE DUE	DATE DUE	DATE DUE
_____	_____	_____
_____	_____	_____
_____	_____	_____
_____	_____	_____
_____	_____	_____
_____	_____	_____
_____	_____	_____

MSU Is An Affirmative Action/Equal Opportunity Institution

c:\circ\date\date\date\pm3-p.1

**REAL-TIME ANALYSIS OF LIGHT ALKENES AT ELEVATED TEMPERATURES
AND PRESSURES BY FIBER OPTIC NEAR INFRARED SPECTROSCOPY**

By

Engin Deniz Yalvac

A DISSERTATION

Submitted to

Michigan State University

in partial fulfillment of the requirement

for the degree of

DOCTOR OF PHILOSOPHY

Department of Chemistry

1996



Copyright by

Engin Deniz Yalvac

1997

ABSTRACT

REAL-TIME ANALYSIS OF LIGHT ALKENES AT ELEVATED TEMPERATURES AND PRESSURES BY FIBER OPTIC NEAR INFRARED SPECTROSCOPY

By

Engin Deniz Yalvac

This study had as its goal, the simultaneous determination of ethylene and monoalkylated light alkenes at elevated temperatures and pressures via fiber optic Fourier Transform Near Infrared (FT-NIR) spectroscopy to enable the *in situ*, real-time monitoring of these compounds. This goal was accomplished in two stages: First the simultaneous determination of ethylene and monoalkylated light alkenes at room temperature and pressure was studied. Then, the effects of elevated temperature and pressure were investigated.

Ethylene and monoalkylated light alkenes namely, propylene, 1-butene, 1-pentene, 1-hexene, 1-octene, 1-decene, were selected for the determination. Various other alkylated alkenes, i.e., 1,1 dialkylated, cis, trans dialkylated, and trialkylated alkenes were investigated to determine the effects of the molecular structure for this analysis. The first overtone of the asymmetric =CH₂ stretch of the monoalkylated alkenes was found to be unique for the light alkenes in the NIR region. This region of the spectrum was used to built a model based on Classical Least Squares (CLS) regression to demonstrate the feasibility of the determination at room temperature and pressure. Ethylene and 1-octene

solutions in Isopar E were studied as example. Concentrations of the alkenes were determined with an error less than 1 wt %.

In the second stage of the study, the effects of elevated temperature and pressure on the spectra were investigated via fiber optic FT-NIR spectroscopy. The effects of elevated pressures in the range studied (> 500 psi) on spectra are found to be insignificant for these compounds. However, the temperature effects are critical, especially for the lighter molecules such as ethylene and propylene. Therefore, the determination of these compounds at elevated temperatures (25-140 °C) requires the incorporation of the temperature effects into the calibration model. An apparatus to collect the spectra of these compounds at elevated temperatures and pressures by fiber optic FT-NIR spectroscopy was constructed. The determination of ethylene and 1-octene was evaluated. Calibration models were built using partial least-squares (PLS) regressions. Predictive ability of the model, expressed as standard error of prediction (SEP), was less than 0.5 wt % for both ethylene and 1-octene and the absolute error of determination for alkenes is expected to be less than ± 0.75 wt %.

Dedicated to my parents;
my husband, Selim;
my son, Arda...

ACKNOWLEDGMENTS

The author would like to express her gratitude to the following people and institutions who have generously contributed to the completion of this thesis.

To Professor Stanley R. Crouch for his invaluable assistance and advice throughout the course of this work. To the other members of the doctoral committee, Professor Kris Berglund, Professor George E. Leroi, Professor John L. McCracken for their interest and assistance. To Dr. L. David Rothman of the Dow Chemical Co. for his help and support as on-site advisor.

My co-workers are also an intricate part of this research, without their contributions this publication couldn't be possible. Among them I would like to thank Dr. Mary Beth Seasholtz and Dr. Randy J. Pell for their assistance with chemometric tools, Dr. M. Anne Leugers for her help with my endless questions in vibrational spectroscopy, Dr. Mark Beach for building the high temperature, pressure apparatus. All the others: Dr. J. Paul Chauvel, Dr. Del Lafavor, Dr. Mark Dittenhaffer, Dr. Bill Heeschen, Dr. Dave Albers, Dr. Mark LaPack, Mr. Robert A. Bredeweg, Mr. Jeff Larson, Dr. Richard Harner, thanks for being available for many fruitful discussions.

Finally, I would like to thank the Dow Chemical Co. as the sponsor of this research and allowing me fulfill a personal dream. "IT'S NEVER TOO LATE!"

TABLE OF CONTENTS

LIST OF TABLES.....	ix
LIST OF FIGURES.....	x
CHAPTER 1.....	1
INTRODUCTION.....	1
<i>In situ</i> Real-Time Analysis.....	1
Near-Infrared vs Mid-Infrared Analysis.....	2
Why Fourier Transform Near-IR.....	5
Historical Background.....	6
<i>In situ</i> , Real-Time Determination of Alkenes by Vibrational Spectroscopy.....	6
Determination of Alkenes in Mid IR Range Using Modified Reactors as IR Cells.....	6
Determination of Alkenes in Mid IR Range Using Internal Reflectance Crystals.....	7
Determination of Alkenes in Mid IR Range Using Attenuated Total Reflectance Element.....	8
Determination of Alkenes in Mid IR Range Using Flow-Through IR Cells.....	9
Determination of Alkenes by Near IR Spectroscopy.....	13
Chemometrics for Near-IR Spectroscopy.....	16
Goal of This Research.....	23
CHAPTER 2.....	25
THEORETICAL BACKGROUND.....	25
Effect of Temperature and Pressure on Vibrational Spectroscopy.....	25
Pressure or Temperature Induced Phase Transition.....	26
Frequency Shifts Due to Pressure and Temperature.....	28
Band Shape and Intensity Changes.....	30
Splitting of Degenerate Vibrations.....	34
Doubling of Absorption Vibrations.....	34
Sensitivity of Vibrations to Expansion of Molecular Volume.....	35
Multivariate Calibration Techniques.....	36
Classical Least Square Regression.....	36
Partial Least Square Regression.....	38

CHAPTER 3.....	42
QUANTITATIVE ANALYSIS OF LIGHT ALKENES BY FT-NIR SPECTROSCOPY: ROOM TEMPERATURE PRESSURE FEASIBILITY STUDIES.....	42
Experimental Procedures.....	43
Materials.....	43
FT-NIR System.....	45
Fiber Optic Cell Assembly.....	47
Calibration Standards.....	48
Data Analysis and Results.....	49
Interpretation of Spectra.....	49
Quantitative Determination.....	64
Summary.....	68
CHAPTER 4.....	70
<i>IN SITU</i> REAL-TIME DETERMINATION OF ALKENES BY FIBER OPTIC FT-NIR SPECTROSCOPY AT ELEVATED TEMPERATURES AND PRESSURES.....	70
Experimental Procedures.....	71
High Pressure Temperature Apparatus.....	72
Pressure Vessel.....	72
Expansion Containment Chamber.....	73
Head Space Assembly.....	73
Fiber Optic Probe-Holder Assembly.....	74
Single Sided Transmission Probe.....	74
Pressure Measurement and Control.....	75
Forced Air Oven.....	76
Temperature Measurement and Control.....	76
FT-NIR Spectrometer and the Detector.....	77
Determination of Vessel and Head Space Volume.....	79
Experimental Design.....	79
Experiments for the Determination of Pressure Effects on Spectra.....	82
FT-NIR Calibration Procedure.....	82
Data Analysis and Results.....	83
Effects of Pressure on Spectra.....	83
Effects of Temperature on Spectra.....	85
Calculation of Liquid Phase Concentration at Each Temperature Setting.....	86
Calibration Models.....	99

Determination of PLS Model Rank.....	104
Examination of Outliers.....	107
Examination of Spectral Residuals.....	110
Model Prediction Errors.....	113
Summary.....	116
CHAPTER 5.....	117
CONCLUSIONS AND RECOMMENDATIONS FOR FUTURE RESEARCH.....	117
Conclusions.....	117
Recommendations for Future Research.....	120
APPENDIX A: FT-NIR Spectra of Light Alkenes Used in the Study.....	122
APPENDIX B: Excel Spread Sheets Showing the Calculation of Liquid Phase for Each Run.....	142
APPENDIX C: Data File Names and Their Correlating Concentrations.....	182
LIST OF REFERENCES.....	185

LIST OF TABLES

Table 1: Ethylene and Monoalkylated Alkenes.....	44
Table 2: Cis and Trans Dialkylated Alkenes.....	44
Table 3: 1,1 Dialkylated Alkenes and Trialkylated Alkenes.....	45
Table 4: Characteristic IR Frequencies (cm ⁻¹) of Alkylated Ethylenes.....	59
Table 5: Shift of location of first overtone of asymmetric =CH ₂ stretch of monoalkylated alkenes.....	61
Table 6: Predicted Concentrations of 1-Octene and Ethylene.....	67
Table 7: Experimental Design Versus Actual Experiments.....	81
Table 8: Antoine Constants for 1-octene and Isopar E.....	88
Table 9: Literature Values for Constants in Temperature Dependent Density Equation	90
Table 10: Excel Spread Sheet Showing the Liquid Phase Concentration Calculations for Run # 26.....	93
Table 11: Concentrations of Liquid Phase for Standards Containing Ethylene in 1-Octene, or Isopar E.....	95
Table 12: Concentrations of Liquid Phase for Standards Containing 1-Octene in Isopar E.....	96
Table 13: Concentrations of Liquid Phase for Standards Containing Ethylene, 1-Octene, and Isopar E.....	97

LIST OF FIGURES

Figure 1: Schematic diagram of the FT-NIR Set-up.....	46
Figure 2: Schematic Diagram of the Fiber Optic Cell.....	47
Figure 3: Spectra of 98 wt %. 1-Pentene, 1-Hexene, 1-Octene, 1-Decene and Ethylene, Propylene, 1-Butene Solutions in Isopar E (monoalkylated alkenes) in 6,080 to 6,150 cm-1 Region in Overlaid Format at Room Temperature and Pressure.....	50
Figure 4: Spectra of 98 wt %. Pure Octene Isomers (cis 2-octene, cis 3-octene, cis 4-octene and trans 2-octene, trans 3-octene, trans 4-octene) (cis and trans dialkylated alkenes) in 6,080 to 6,150 cm-1 Region in Overlaid Format	51
Figure 5: Spectra of 98 wt %. Pure Trialkylated Alkenes (cis 3-methyl-3-heptene, trans 3-methyl-3-heptene) in 6,080 to 6,150 cm-1 Region in Overlaid Format	52
Figure 6: Spectrum of 98 wt %. Pure 2-Ethyl-1-Hexene (1,1 dialkylated alkene) and Octane in 6,080 to 6,150 cm-1 Region in Overlaid Format.....	53
Figure 7: Spectra of 98 wt %. 1-Pentene, 1-Hexene, 1-Octene, 1-Decene and Ethylene, Propylene, 1-Butene Solutions in Isopar E (monoalkylated alkenes) in 4,800 to 4,850 cm-1 Region in Overlaid Format.....	54
Figure 8: Spectra of 98 wt %. Pure Octene Isomers (cis 2-octene, cis 3-octene, cis 4-octene and trans 2-octene, trans 3-octene, trans 4-octene) (cis and trans dialkylated alkenes) in 4,800 to 4,850 cm-1 Region in Overlaid Format.....	55
Figure 9: Spectra of 98 wt %. Pure Trialkylated Alkenes (cis 3-methyl-3-heptene, trans 3-methyl-3-heptene) in 4,800 to 4,850 cm-1 Region in Overlaid Format..	56
Figure 10: Spectrum of 98 wt %. Pure 2-Ethyl-1-Hexene (1,1 Dialkylated alkene) and Octane in 4,800 to 4,850 cm-1 Region in Overlaid Format.....	57
Figure 11: Spectrum of 10 wt % 1-Octene, 1-2wt % Ethylene (20 times enlarged) and Pure Isopar E in 6,080 to 6,150 cm-1 Region in Overlaid Format at Room Temperature and Pressure.....	65
Figure 12: Measured and Estimated Pure Spectra for 1-Octene and Isopar E in 6,080 to 6,150 cm-1 Region in Overlaid Format at Room Temperature and Pressure.....	65

Figure 13: Schematic Diagram of the High Temperature, Pressure Apparatus.....	72
Figure 14: Schematic Diagram of the High Temperature, Pressure Vessel.....	73
Figure 15: Guided Wave Single Sided Transmission (SST) Probe.....	75
Figure 16: Schematic Diagram of the FT-NIR Set-up; Spectrometer, Detector, Fiber Optic Probe, and Probe Holder Assembly.....	78
Figure 17: Effect of Pressure on Spectra of Ethylene in Isopar E.....	85
Figure 18: Estimated Pure Ethylene, Propylene, and 1-Octene Spectra as a Function of Temperature.....	86
Figure 19: Corrected Liquid Phase Concentrations at Each Temperature for All Runs.	98
Figure 20: Full Data Used in PLS Modeling of Ethylene and 1-Octene.....	102
Figure 21: Second Derivative of the Data used in PLS Model.....	103
Figure 22: PLS Ethylene Model PRESS and SEP vs Number of Principal Component Factors.....	106
Figure 23: PLS 1-Octene Model PRESS and SEP vs Number of Principal Component Factors.....	106
Figure 24: Ethylene PLS Model Outliers.....	109
Figure 25: 1-Octene PLS Model Outliers.....	109
Figure 26: Ethylene PLS model spectral Residuals.....	111
Figure 27: 1-Octene PLS Model Spectral Residuals.....	112
Figure 28: PLS Fit Errors for Ethylene Over All Temperatures.....	114
Figure 29: PLS Fit Errors for 1-Octene Over All Temperatures.....	115

Chapter 1

INTRODUCTION

In situ, Real-Time Analysis

In situ, real-time monitoring of the chemical and physical changes that occur during processing of chemicals enables the processes to be optimized and controlled.^{1,2,3,4,5} Information collected *in situ* by sensors is transmitted in, real-time to the process control computers which compare the state of the process to the desired state and take corrective action. Chemical information obtained by chemical analyzers, is invaluable in process control along with the information obtained from physical sensors.^{6,7} Benefits of closed loop process control where chemical analyzers are used are not limited to better process control or optimum operating conditions. Closed loop process control with feedback from chemical analyzers eliminates delays and the hazards of manual sampling and analysis.^{8,9,10} An additional benefit for the environment is waste reduction or control in many instances.^{11,12,13}

Optimization studies in research and development areas also benefit from, real-time *in situ* monitoring via chemical analyzers.^{14,15} These tasks often require investigation of numerous conditions such as different process parameters or raw materials, solvents etc. *In situ* monitoring via chemical analyzers can lead to faster and fewer numbers of

experiments and thus to more rapid reaction or process optimization.^{16,17} Another area that *in situ*, real-time monitoring excels is where the reaction or the process conditions prevent the use of an alternative analysis via conventional sampling.^{18,19} Unstable intermediates or products that cannot be determined under any conditions other than the reaction conditions are good examples of these cases.²⁰ Often, the, real-time analysis required for fundamental research falls into the category of *in situ* monitoring.²¹

Various chemical analysis techniques are available for *in situ*, real-time monitoring.^{22,23,24,25} Among a host of spectroscopic, separation based, dielectric and acoustic monitoring techniques, vibrational spectroscopy represents a particularly attractive choice owing to the unparalleled breadth and wealth of the molecular level information that can be obtained.^{26,27,28,29}

Near-Infrared vs Mid-Infrared Analysis

The NIR region contains weaker overtones of the fundamental absorptions and encompasses bands that result from the harmonic overtones of fundamental and combination bands associated with hydrogen atoms. Therefore, the compounds containing O-H, N-H, and/or C-H bonds lend themselves favorably to analysis by NIR spectroscopy.

The first overtone of a fundamental stretching vibration generally appears at a location approximately equal to twice the fundamental frequency plus a relatively small shift to a

longer wavelength^{30,31} which depends on structural and/or ambient conditions.³² However, this prediction rule does not always hold.^{33,34,35} For instance, the systems characterized by the presence of more complex combination bands, where a variety of fundamental and overtone transitions occur simultaneously, are among these unpredictable cases.^{36,37,38} The vibrational spectra of liquid solutions appear as broad bands rather than the narrow lines associated with the spectra of gaseous compounds, and these bands get broader with increasing energy, leading to substantial spectral overlapping problems in the NIR region. In these instances, it is difficult to distinguish overtones of fundamental stretching and/or overtones of combination bands for a meaningful study of molecular structure or for quantitative analysis.

Due to the severe overlapping of broad bands, historically, the NIR region of the infrared spectrum was considered of little utility in molecular structure determination, and little attention has been paid to it until the last couple of decades. Only after the development of fiber optic technology and the implementation of some of the statistical tools for quantitative analysis, did NIR spectroscopy start to find more applications especially in *in situ*, real-time analysis.

One of the most important instrumental advantages of the NIR range over the MIR range is the fact that the inexpensive and readily available silica-type optical fibers can be used. The fibers, available in the MIR range are not as convenient and inexpensive as the silica-type optical fibers. They are quite brittle requiring stainless steel meshing as cladding to prevent breakage. Alternatives to optical fibers in the MIR, such as ATR (Attenuated

Total Reflectance) probes via light pipes, suffer from similar problems especially for *in situ*, real-time applications of process monitoring and control in manufacturing environments. Therefore, while MIR offers advantages in spectral interpretations, NIR is exponentially more robust.

The NIR range is characterized by lower absorptivities than the MIR range and is, hence, conducive to measurements of thicker samples or to the use of longer pathlengths. This is considered another advantage of NIR over MIR for *in situ*, real-time analysis applications since the use of small pathlengths in process analysis is troublesome. Many processes contain solid particles which cause plugging of the small pathlength (> 1 mm) IR cells.

Straightforwardness of the sample interfaces, such as fiber optic light transmission probes in the NIR region, is the reason for these devices to be commercially available at affordable prices; thus their popularity in use for *in situ*, real-time analysis. Transmission and reflectance probes are commonly used sample interfaces in the NIR region. Despite numerous designs, the principles of transmission and reflectance probes are all based on the absorption of the sample according to Beer's law. The use of these types of probes in systems where the analysis needs to be done under process conditions opened invaluable opportunities for the investigations of high temperature and pressure systems and/or systems involving reactivity or flammability hazards when sampled conventionally.

Why Fourier Transform Near-IR?

Although the superiority of FT-IR over conventional dispersive IR analyzers has been well accepted for some time, FT-NIR has a more recent history.^{39,40,41} The grating or dispersive NIR analyzers suffer less compared to their MIR counter parts due to having more sensitive detectors and more energetic light sources in the NIR region. Recently, NIR instruments have begun to be used in process analysis applications where stability and the reproducibility are critical. Vibration and temperature fluctuations in these areas are a few of the causes of instability. In order to make more stable NIR instruments manufacturers have started to move towards FT technology.

FT-NIR also benefits from Fellgett's advantage (multiplex advantage) and Jacquinot's advantage (throughput advantage) as is the case in the MIR region. Additionally, the Connes advantage (accurate frequency scale) leads to a stable wavelength axis in FT-IR or FT-NIR compared to scanning or grating instruments. All modern FT instruments employ a high accuracy laser in the interferometer where all frequencies can be mathematically related to the laser frequency leading to a very accurate frequency scale. Hence, FT-NIR instruments are advantageous over dispersive NIR instruments for *in situ*, real-time monitoring applications.

Historical Background

In situ, Real-Time Determination of Alkenes by Vibrational Spectroscopy

Historically, the use of conventional (off-line) vibrational spectroscopy to study chemical systems has been popular; recently, the use of vibrational spectroscopy for *in situ* monitoring of processes is making inroads in, real-time analysis. In the MIR range *in situ* determinations are mostly restricted to modified cells where the chemical reaction takes place and the reaction mixture is monitored in, real-time. Another alternative is to have a flow-through cell where the reaction mixture or the sample can flow through enabling, real-time monitoring. This option, while, it is pretty popular with the analysis of gaseous samples, it can be quite troublesome with liquid samples due to the possibility of having different phases (solid particles, gas bubbles) and the coating of the cell windows. Moreover, none of these cells lend themselves to use at high temperatures and pressures without extensive modifications. Regardless, they have been used in the laboratory environment, with extensive modifications, quite successfully.

Determination of Alkenes in Mid IR Range Using Modified Reactors as IR Cells

Among the applications performed in the laboratory environment, the ones pertaining to the determination of alkenes can be considered precedent to this study. For example, Karge and Bolding⁴² studied the reactions of olefins by *in situ* IR using a zeolite catalyst. An IR cell was modified which simultaneously served as the fixed-bed flow reactor. Similarly, hydroformylation of olefins were studied by a number of different groups where the IR cell functioned as the reaction chamber as well. Yin et al.⁴³ used Rh-based

supported liquid phase catalysts in heterogeneous hydroformylation of olefins at 50–150 °C by using a stainless steel tube (6 mm diameter 350 mm long) as the reactor /IR cell and monitored the reaction mixture, real-time. Chuang and Pien⁴⁴ studied hydroformylation of ethylene on rhodium/silica catalysts and monitored the reaction mixture by *in situ* IR spectroscopy. Xia et al.⁴⁵ demonstrated that the hydroformylation of olefins is faster with a rhodium-phosphine complex catalyst in 2-ethylhexanol using *in situ* IR spectroscopy. Garland and Bor⁴⁶ in another study of hydroformylation of olefins with rhodium containing catalyst used 3,3-dimethyl-1-butene, and monitored the reaction intermediates via *in situ*, real-time IR analysis. Hydroformylation of propylene was studied similarly under high temperature and high pressure (up to 17 atm) at reaction conditions by Pan et al.⁴⁷ using *in situ* IR. Cobalt catalysts were used by Mirbach et al.⁴⁸ for the hydroformylation of 1-octene in hydrocarbon solvents and the *in situ* IR spectroscopy revealed that excess 1-octene is isomerized to internal olefins under these conditions, but not hydroformylated.

Determination of Alkenes in Mid IR Range Using Internal Reflectance Crystals

A similar hydroformylation study was carried out by Moser et al.⁴⁹ However, a different cell design was used in this study to monitor 1-hexene and its conversion products. The reactor was embedded with a cylindrical internal reflectance crystal (CIR) which was coupled with the FT-IR system (CIR-FTIR). These type of reactors, embedded with the internal reflectance crystal have been popular in *in situ* monitoring of reactions where a sample can not be removed from the system. Several examples can be found in literature about their implementations in areas concerning other than olefinic compounds.^{50,51,52}

An alternative way of using an internal reflectance crystal is to install it into a probe tip or in a flow-through cell. The connection to the spectrometer and the detector is in this case accomplished by either the light pipes or the fibers that can transmit in IR region of the electromagnetic spectrum. One of the best example applications of this type of instrument design is given by Moser et al.⁵³ describing the CIR-FTIR system using chalcogenide glass optical fibers between the cylindrical internal reflectance element and the FT-IR. Remote analysis in this fashion provides more flexibility between the FT-IR and the reaction chamber. In this paper cobalt catalyzed hydroformylation of olefins described where CIR containing reaction chamber was operated under high temperature (90°C) and high pressure (750 psi) quite successfully.

Determination of Alkenes in Mid IR Using Attenuated Total Reflectance Elements

Comparable to CIR, Attenuated Total Reflectance (ATR) elements can be used embedded in either reactors, in flow-through cells or at the tip of the probes for *in situ* monitoring of various reactions. Altman and Jalkian⁵⁴ describe in a patent where an ATR element was installed in a flow-through cell to follow alkylation of olefins. A stream of olefins and a stream of isobutanes are contacted in the reactor in the presence of an HF acid catalyst. Further, the information obtained from the analyzer was used in controlling the HF, water, and sulfolane feed streams to the reactor. Rekoske and Barateau⁵⁵ used the ATR element in a probe to monitor the carbonyl coupling in liquid-solid and gas-solid reactions with reduced titanium reagents. They coupled the ATR probe with a FT-IR system and monitored the olefins formed as intermediate compounds. The signal strength

and background response are some of the concerns that both the ATR and the CIR element coupled systems encounter leading to lower signal to noise and lower sensitivity when compared with conventional IR or FT-IR instruments.

Determination of Alkenes in Mid IR Range Using Flow-Through IR Cells

Among the *in situ* IR techniques the most popular ones are where flow-through cells are used. This is especially practical with gas phase reactions. Several applications involving determination of alkenes via *in situ* IR or FT-IR coupled with flow-through cells at various pathlengths can be found in the literature. Atkinson et al.⁵⁶ monitored the gas phase reactions of alkenes with ozone by using *in situ* FT-IR. 1-pentene, 1-hexene, 1-heptene, 1-octene, 2,3-dimethyl-1-butene, cyclopentene, and 1-methylcyclohexene were investigated at room temperature and under slight vacuum (740 Torr). Intermediate compounds of the reaction was determined as well which led to defining the reaction mechanisms for these reactions. An earlier study by the same research group⁵⁷ was conducted for the gas phase reactions of a series of 1-alkenes and 1-methylcyclohexene with the OH radical in the presence of NO. 1-pentene, 1-hexene, 1-heptene, 1-octene, 2,3-dimethyl-1-butene, cyclopentene, and 1-methylcyclohexene were investigated at similar conditions using *in situ* FT-IR where this time a gas chromatograph is used to correlate and confirm the IR results.

The mechanism of the Wacker Oxidation of alkenes over Cu-Pd-Exchanged Y Zeolites was investigated by Espeel et al.⁵⁸ where an *in situ* IR analyzer is used for the determination of the effects of reactant partial pressure in the rate of oxidation. Jiang et

al.⁵⁹ used *in situ* FT-IR similarly to study the surface oxidation of light hydrocarbons on prseodymium where the reaction temperatures reached to 573 °K. They demonstrated that having a flow-through cell allows the cooling of the reaction products and that the determination of the reaction products under reaction conditions is not always necessary.

Products and the mechanism of the gas-phase reactions of alkenes and NO₃ was investigated by Cariati and Rindone⁶⁰ by using an *in situ* IR in a 480 L reactor. Products were also investigated using gas chromatography by sampling the gas mixture periodically. These authors demonstrated the value of *in situ*, real-time monitoring with almost instantaneous results over the sampling techniques with some response time. Martens and Crouset⁶¹ used an *in situ* IR as an on-line analyzer for the monitoring and control of the manufacturing of olefins and diolefins by steam cracking of hydrocarbons. The reaction mixture of the steam cracking contains paraffinic hydrocarbons, naphthenic hydrocarbons, and aromatic hydrocarbons, and the cracking temperature was controlled by the response obtained from the on-line IR analyzer based on the concentrations of naphthenic compounds which were monitored in the range of 0.8-2.6 μm.

The mechanism of selective oxidation reactions of 1-butene, 1,3-butadiene to maleic anhydride was studied by Wenig⁶² using *in situ* IR spectroscopy. In this extensive study other analytical techniques such as x-ray diffraction, laser Raman spectroscopy, SEM, X-ray energy dispersive spectroscopy were also used for the determination of the catalyst and the reactions that take place on the surface of the catalyst. Similarly, Moser⁶³ studied the selective oxidation of olefins and paraffins to maleic anhydride using *in situ* IR and *in*

situ Raman techniques. Wenig and Schrader, in earlier work,^{64,65,66} studied the same reaction at elevated temperatures (up to 300 °C) where reaction products were determined in a flow-through FT-IR cell.

Another implementation of IR or FT-IR flow-through cells has been in the area of coupling with other analytical tools such as Gas, Liquid or Super Fluid Chromatography (GC, LC, SFC). Infrared spectroscopy can be used as the detection system for these techniques; the column effluent is interfaced with the IR via a flow-through cell. Infrared spectroscopy or the FT-IR enhances the versatility of these separation techniques. Several examples of the determination of alkenes can be found in the literature as described below.

For instance Koizumi et al.⁶⁷ separated gasoline over a silica gel column (Devolisil-60, 5 µm particle size, 25 cm long, 4.6 mm ID) and determined groups of hydrocarbons (alkanes, alkenes, and aromatic hydrocarbons) by using FT-IR as the detector. Column effluent was pumped through a flow cell (24 µL with 0.3 mm path length) where the FT-IR determination was accomplished. First the alkanes then the alkenes eluted from the column and the aromatics were back-flushed in order to reduce the analysis time.

Another LC-IR determination of alkenes was accomplished by Dobrov et al.⁶⁸ for the monitoring of the phenol alkylation process by olefins. A silica gel column (particle size 0.074-0.088 mm) was used and the mobile phase was optimized for the separation of paraffinic and olefinic hydrocarbons.

In the area of GC-IR and GC/FT-IR coupling, several applications can be found concerning alkenes. Sojak and co-workers⁶⁹ combined a capillary gas chromatography with a FT-IR and a Mass Spectrometric Detector (MSD) for the identification of isomers of n-nonadecenes. A mesogenic stationary phase was found to be better than a nonmesogenic stationary phase for the separation of 17 possible isomers of n-nonadecene. Identification of compounds was confirmed both by the IR and the MSD where IR provided distinctly different spectra for the geometrical isomers. Two separate groups Listemann et al.⁷⁰ and Gurka et al.⁷¹ similarly studied number of compounds linked with environmental extracts including numerous alkenes via GC/FT-IR/MSD. In one of these studies 106 compounds were identified many of them jointly based on functional groups. FT-IR/MSD detector combination was found to be invaluable in enhancing the detection and reinforcing the identifications.

Implementation of FT-IR via a flow-through cell as the detection system in SFC has also been quite popular since the determination of high molecular weight compounds or thermally labile compounds where SFC excels has always been in need of better detection techniques. Unfortunately, many of the modifiers used in SFC interfere with the IR determination. However, there are still several IR vibrations such as the C=O or the C=C stretching that are interference free. Moreover, the use of deuterated solvents as modifiers allows the detection of C-H stretching vibrations while the use of chlorinated solvents (e.g., CCl₄) preserves the fingerprint region.⁷² However, determination of light

alkenes is not commonly investigated by SFC since less complicated alternative techniques are available.

The biggest disadvantage of flow-through cells is the fact that solids cannot be easily analyzed. Diffuse reflectance IR spectroscopy can be used for *in situ* monitoring of solid surfaces. The best examples of these type of applications pertaining to determination of alkenes are in the area of catalytic reactions of alkenes on surface of solid catalysts. For instance, using *in situ* diffuse reflectance FT-IR, Takeuchi et al.⁷³ studied the noble metal promoted (Co/SiO₂), selective vapor phase hydroformylation of ethylene and obtained strong absorption bands of linear and bridged CO species under the reaction conditions. In the course of the reaction, changes observed in these bands suggested that the linear CO species plays a major role in the CO insertion process to ethylene. Johnson et al. used diffused reflectance IR in determination of hydrocarbons for the catalytic studies of molecular sieve. Along with a gas chromatograph which was used in injections of samples collected during the course of the reaction, diffuse reflectance IR monitored the C-H stretching of the hydrocarbons that formed in the channels and pores of the molecular sieve.⁷⁴

Determination of Alkenes by Near IR Spectroscopy

Relatively fewer number of vibrational spectroscopic determinations of alkenes have been reported using the Near-IR (NIR) region and as *in situ* measurements.^{75,76,77,78,79,80,81} Maggard,⁸² in a patent describes the determination of PIANO compounds (paraffin, isoparaffin, aromatics naphthenes, and olefins) in fuel streams using NIR spectral region.

The technique uses 1672-1698 and/or 1700-1726 nm for naphthenes, 1622-1650 and/or 2064-2234 nm for olefins, 1092-1156 and/or 822-884 nm for aromatics, and 880-974 nm and/or 1152-1230, 1152-1230, 1320-1380, 1470-1578, 1614-1644, 1746-1810, 1946-1810, 1940-2000, and/or 2058-2130 nm for paraffins and isoparaffins. The statistical treatment of the data such as multiple regression has been used to help the determination of these families of hydrocarbons as well. This technique is especially designed to aid in blending of fuels such as diesel fuels. A similar fuel analysis, determination of octane number of gasoline is described by Parisi et al.⁸³ This analyzer was used on-line via fiber optic cables and the NIR cell was installed in a side stream of the process. The method checked well with the values measured by conventional techniques.

Ethylene was determined by NIR spectroscopy to monitor its polymerization reaction induced by an exciplex laser at high pressure (3200 bar), and high temperature (190-230 °C) in gas phase in a study by Breckemann et. al.⁸⁴ A kinetic scheme was presented which adequately describes the polymerization kinetics as a function of temperature, overall density, laser pulse energy, and conversion. Buback and Tups⁸⁵ in an earlier work studied the high pressure co-polymerization of ethylene and carbon monoxide via IR and NIR spectroscopy. The reaction was monitored in a stainless steel cell. Laser light was used for the photochemical initiation of the polymerization likewise.

Lysaght⁸⁶ describes a field portable fiber optic near infrared spectrometer for fuel analysis applications. This is a short wavelength (700-1100 nm) NIR instrument designed to be light weight (slightly larger than a briefcase) where the instrument is controlled by a

laptop computer. All of the components of the analyzer are chosen with this criterion in mind. A tungsten lamp was used as the light source. A thermal electric cooled 1024 element silicon photodiode array detector was used along with a holographic grating for wavelength dispersion. Volume percent ratios of aromatic and saturated compounds in fuel were determined as an example application. Chemometric data treatment was used for this determination.

All of the NIR applications discussed above are used for the general determinations of olefins as a group of compounds and that they do not distinguish among its members. In this research, an attempt to determine ethylene and the other monoalkylated light alkenes simultaneously at elevated temperatures and pressure has been attempted for the first time in the NIR spectral range.

Ethylene and monoalkylated light alkenes are industrially important compounds used in manufacturing of polyethylene and similar polymeric materials. The use of on-line, at-line and off-line vibrational spectroscopy for the control and monitoring of polyethylene solution processes has been investigated earlier. Lange et al.⁸⁷ described an on-line FT-IR analyzer for the simultaneous determination of ethylene and 1-octene in the MIR spectral range where ethylene was determined at 1909 cm⁻¹ and 1-octene at 1829 cm⁻¹. The information obtained from the analyzer is used in control of the feed addition to the polyethylene solution process. Other on-line measurements such as density, viscosity, melt index, and gas chromatography have also been studied for monitor and control of polyethylene manufacturing processes.^{88,89}

Chemometrics for Near-IR Spectroscopy

The application of multivariate statistical calibration and prediction methods to quantitative FT-NIR spectroscopy has been one of the most important reasons for its popularity today. Chemometrics can be broadly defined as the application of statistical and mathematical methods for the design or optimization of chemical experiments and for the efficient extraction of information from chemical data.⁹⁰ Multivariate data analysis has been shown to improve precision, accuracy, reliability and applicability of infrared spectral analysis relative to conventional univariate methods of data analysis.

Multivariate methods drive their power from the simultaneous use of multiple intensities (i.e. multiple variables) in each spectrum. Thus, the problem of spectral interferences can be eliminated with the use of any one of a number of multivariate calibration and prediction methods.^{91,92} These methods include classical least squares (CLS), inverse least squares (ILS), q-matrix, partial least squares (PLS), and principal component regression (PCR). Correlation and Kalman filter methods have received less attention in the infrared spectroscopy therefore, and will not be described here. PLS and PCR exhibit the greatest range of applicability and are attracting the most attention in the NIR applications.

In spectroscopy, CLS is a multivariate least-squares procedure based directly on Beer's law. Infrared spectroscopists have sometimes referred to this method as the K-matrix method.^{93,94} The CLS model accounts for errors in the spectral measurements. CLS can accommodate spectral intensities at all frequencies for all calibration samples. In general,

all overlapping spectral components should be known for optimal performance of CLS. By being a full-spectrum method, CLS has the ability to achieve improved precision since there is a signal averaging effect when many or all the spectral intensities are included in the analysis.⁹⁵

The ILS method is a least-squares method [sometimes called P-matrix, or multiple-linear regression (MLR) when applied to near-infrared]. It uses the inverse of the Beer's law as its model. That is, concentration is modeled as a linear combination of absorbances. The ILS model accounts for errors in the reference concentrations. The ILS technique is a frequency-limited method and, therefore, is not capable of the precision improvements of CLS from signal averaging of multiple intensities. However, ILS can often be a useful method even if only one component is known for the calibration samples.⁹⁶

The factor analysis methods of PLS and PCR are capable of being full-spectrum methods. Like ILS, PLS and PCR can be employed even when only one component is known in the calibration samples. Both PLS and PCR methods factor the spectral data calibration matrix into the product of two smaller matrices. This amounts to a data compression step where the intensities at all frequencies used in the analysis are compressed to a small number of intensities in a new full-spectrum coordinate system. This new coordinate system is composed of loading vectors that can be used to represent the original spectral data. The intensities in the new full-spectrum coordinate system (called scores) are then used in a model where concentration is presumed to be a linear function of these intensities. Thus, PLS and PCR are methods that are concerned with modeling both

spectra and concentrations during calibration. PCR performs the factoring of the spectral data matrix without using information about the concentrations. Therefore, there is no guarantee that the full-spectrum basis vectors that are associated with PCR are relevant for concentration prediction. PLS, on the other hand, performs the spectral factoring trying to account for the spectral variation while assuring that the new basis vectors relate to the calibration concentrations. Thus, PLS sacrifices some fit of the spectral data relative to PCR in order to achieve better correlation to concentrations during predictions.⁹⁷

The diversity of multivariate methods available for application to quantitative spectroscopy can create problems in terms of which one to use. The choice of multivariate method for NIR spectroscopy often depends on the particular data set. Therefore, the spectroscopist usually is faced with comparing the predictive ability of a couple of different algorithms. However, lately more significant comparisons of these methods from a statistical point of view have been made and methods were compared. One of the best examples of this kind of comparison was made by Thomas et al.⁹⁸ The quantitative prediction ability of the four most heavily used multivariate calibration methods in infrared spectroscopy (CLS, ILS, PLS, and PCR) have been compared by using extensive Monte Carlo simulations. The simulations were performed assuming that Beer's law holds and that spectral measurement errors and concentration errors associated with the reference method are normally distributed. Eight different factors that could affect the relative performance of the calibration methods were varied in a two-level,

eight-factor experimental design in order to evaluate their effect on the prediction abilities of the four methods.

It was found that each of the three full spectrum methods has its range of superior performance. The frequency-limited ILS method was never the best method, although in the presence of relatively large concentration errors it sometime yields comparable analysis precision to the full-spectrum methods for the major spectral component. Among the full-spectrum methods, PCR and PLS were found to be very similar. The major difference between these two methods was that PLS seems to predict better than PCR in the cases when there are random linear baselines or independently varying major spectral components which overlap with the spectral features of the analyte. This result was not surprising when one considers the fact that the PCR decomposition is based entirely on spectral variation without regard to component concentrations while the PLS decomposition is dependent on the component concentrations. Because the spectral variations caused by the presence of a random linear base line or major spectral components can be reasonably large, the PCR decomposition is significantly influenced by variations which have no relevance to the analyte concentrations. Therefore, PCR is not able to predict as well as PLS in these situations.

It was also found that the differences between CLS and PLS are more numerous and complex, but are also affected by the algorithms used in the analysis. The PLS method was the optimal performer or close to optimal over the wide range of conditions considered in this study. Unlike CLS, all overlapping spectral components do not have to

be known, nor does the spectral base line have to be explicitly modeled. It seems that the only inherent dangers of using PLS result from over- or underfitting by an inappropriate number of factors.

It is important to realize that factors other than prediction ability often need to be considered when choosing a calibration method. For example, the estimated pure-component spectra generated by CLS contain significant qualitative information which is very useful for the determination. The PLS method can also yield qualitative information of better quality than is generally possible with PCR, but of poorer quality than CLS. However, it should be noted that this study assumed that Beer's law holds. The biggest problem comes in real-life applications where the concentrations of the components are high enough to be outside the linear range of Beer's law. In these instances the choice is usually PLS.

It seems that there are certain applications that CLS will be preferable not because its predictive ability is superior, but it can provide quick, qualitative information. One example of such a case can be a feasibility study in the laboratory environment where several different chemical systems are being screened. The advantage of CLS in this case would be the number of standards needed to build the model, since in CLS, one can built a reasonable model by only using the pure spectra of the components.

However, robust models to be implemented in process analysis applications would always have to be built with a sufficient number of standards drawn from careful

experimental design schemes representing the concentration ranges used in the application. These types of models also need to be cross validated before they can be implemented in process analysis applications which will require preparation of an adequate number of standards. Therefore, for such process analysis application CLS would lose its advantage in terms of a lower number of standards.

Numerous applications have appeared in the literature in last five years that compared CLS and PLS. The PLS method has been the choice, overwhelmingly, for applications in process analysis due to its robustness and ability to deal with possible sample matrix changes from chemical interferences or temperature effects along with non-linearities from Beer's law. For instance: Marjoniemi and Mantysalo⁹⁹ compared PLS, PCR, ILS and CLS to measure dye components in the visible region and PLS gave the best results. Lin and Brown¹⁰⁰ measured the salinity of sea water in NIR (680-1230 nm) again PLS calibration produced a better predictive model. Ortho and metha cresol in water was determined for an array of four piezoelectric crystals by Wei.¹⁰¹ et al. PLS performed better than CLS because there was some co-linearity problem with the data. In another study, PLS gave somewhat better results than CLS in the determination of ascorbic acid in pharmaceutical preparations, but only in the more complex samples.¹⁰² Slightly better results for PLS were also obtained in a NIR tobacco analysis investigation,¹⁰³ a visible absorption measurement of myoglobin oxygen saturation,¹⁰⁴ and in on-line analysis of sugars in a fermentation process.¹⁰⁵ The PLS method was said to offer a more workable approach than CLS in the analysis of mixtures, due to the mixture constraint.¹⁰⁶ It was also claimed that PLS could take nonlinear effects into account better than CLS.¹⁰⁷

Ni,¹⁰⁸ has studied the reaction of the trace metals Co, Ni, Cu, Zn, and Fe with a chromogenic reagent in the visible region with multivariate calibration methods. He found that PLS performed better than CLS. Van de Voort and co-workers¹⁰⁹ used FT-IR for the analysis of milk and found a viable technique for this purpose when it was used with PLS. Miller in a NIR study combined the first overtone and the second overtone regions with the multivariate methods of PLS and CLS for the analysis of EPDM (ethylene-propylene-dien monomers) polymers. The PLS coefficient spectra and the CLS reconstructed spectra obtained from the calibrations were used to determine the sources of the unknown spectral effects. Results indicated that the combination, first overtone, and second overtone regions of the spectrum can be used to determine ethylene and propylene concentrations in the terpolymers, and the combination region can be used to determine diene concentrations. Because the unknown interaction effects are present in the spectra of these materials, the PLS calibration method gives more accurate calibrations than CLS.¹¹⁰

On the other hand, some studies indicated that CLS and PLS results were equivalent for their sample sets, which included the determination of cadmium by inductively coupled plasma mass spectrometry,¹¹¹ the determination of aromatics and saturates in aviation fuel by NIR,¹¹² and the estimation of crude lipid content in trout by NIR.¹¹³

Goal of This Research

The overall goal of this study was to find distinguishable features for ethylene and monoalkylated light alkenes in the NIR region, so that fiber optic probes could be used for the simultaneous, *in situ*, *real-time* determinations of these compounds at elevated temperatures and pressures. The first part of this research is involved with measurements made at room temperature and pressure to establish the feasibility of the analysis. The *in situ* measurements for the determination of the effects of the temperature and pressure on this analysis was done in a separate system where a high pressure, temperature apparatus was coupled with the fiber optic FT-NIR spectrometer.

An FT-NIR instrument incorporating a sample cell via fiber optic cables was used for the feasibility study. Ethylene and monoalkylated light alkenes namely propylene, 1-butene, 1-pentene, 1-hexene, 1-octene, and 1-decene were used in this determination. Various other alkylated alkenes (e.g., 1,1 dialkylated, cis, trans dialkylated, and trialkylated alkenes) were investigated to determine the effects of molecular structure on this determination.

The first overtone of the asymmetric $=\text{CH}_2$ stretch of the monoalkylated alkenes (6,080- $6,150 \text{ cm}^{-1}$) was found to be unique for alkenes, and was used to build a model based on Classical Least Squares (CLS) regression. A mixture of ethylene and 1-octene was taken as the example mixture to prove feasibility at room temperature and pressure. The

reliability of the results was tested using the residual spectra which were obtained by subtracting the estimated spectra from the measured spectra.

In the second part of this research the effects of elevated temperature and pressure for the determination of light alkenes were investigated, and calibration models were developed using high pressure, temperature apparatus. The ethylene and 1-octene system, evaluated during the feasibility study was investigated at elevated temperatures and pressures to provide continuity from the feasibility study.

Considerable difficulties are involved in preparing well-known mixtures of the components to build calibration models for accurate quantitative determination at elevated temperatures and pressures. Consequently, for this particular work, *in situ* fiber optic probe technology was essential. A special apparatus was built to obtain the spectra of known concentration mixtures at varying temperatures and pressures. A high pressure vessel was modified to incorporate a fiber optic probe which was coupled to the FT-NIR spectrometer. The high pressure vessel was placed in an oven. Calibration standards were prepared gravimetrically and the concentration of the liquid phase was corrected for each temperature setting. Calibration models were built using partial least-squares (PLS) regression to predict the concentrations of these compounds at varying temperatures and pressures.

Chapter 2

THEORETICAL BACKGROUND

Effects Of Temperature And Pressure On Vibrational Spectroscopy

The effects of temperature and pressure on electronic and vibrational spectroscopy have been studied in solids more than other phases since these effects can be investigated over a wide temperature and pressure range without observing too many phase changes.^{114,115,116}

Effects of either high pressure or temperature on vibrational modes are mostly due to changes relative to spin states, oxidation states, and changes in geometry.^{117,118} However, all the general changes in vibrational spectroscopy can be listed as follows:

1. Pressure or temperature induced phase transitions,
2. Frequency shifts due to pressure and temperature,
3. Band shape and intensity changes,
4. Splitting of degenerate vibrations,
5. Doubling of absorption vibrations,
6. Sensitivity of vibrations to expansion of molecular volume.

Other effects of pressure, such as the effects on hydrogen-bonded systems and mode softening, will not be discussed here. Additionally, the effects of temperature and pressure on the vibrational spectroscopy of liquids and dissolved gases in liquids are the focus rather than gas phase (only) or solid phase (only) systems. However, where there are similarities no differentiation will be made. For instance, some of the effects are either the same or very similar for solids and liquids. Similarly, effects can be the same for gaseous compounds and their solutions in liquids.

Pressure or Temperature Induced Phase Transitions

If the applied pressure or the temperature causes a phase change, substantial differences can be observed in the vibrational spectra. This is a consequence of the differences between the selection rules for the two different phases.^{119,120} A change in the molecular symmetry of the compound would be the most important reason for substantial changes in spectra. However, spectral changes occur during phase changes where there are no known changes in the molecular symmetry of the molecule. These changes are due to a change in the distance between molecules in going from gas to liquid and to solid phase. When the molecules are closer together more molecular interactions occur which may effect the vibrational energy levels of the molecule.

The molecular interactions may be in the form of collisions. Two types of collisions are described in literature: adiabatic and diabatic. After an adiabatic collision the molecule is left in the same energy level that it had before the collision. With diabatic collisions,

there is a change in the energy level of the molecule. This type of energy changes which may be caused by temperature or pressure changes will influence the vibrational energy levels of the molecule since $\Delta E = hc\bar{v}$ and may cause frequency shifts, intensity changes, and band broadening.^{121,122}

Mixtures behaves similar to the pure compounds when there is a phase transfer from vapor to liquid phase. Additional intermolecular interactions are expected between the compound and the solvent molecules which will affect the vibrational spectra. A good example was reported by Morin and co-workers¹²³ using supercritical carbon dioxide and liquid carbon dioxide as solvent. Spectra of numerous compounds were collected in the gas phase, in supercritical carbon dioxide, and in the liquid carbon dioxide. Substantial frequency shifts were observed for the (C-H), (C=C), (C-H out of plain), (C-H), and (C=O) vibrations studied. The frequency shifts from gas phase to solutions of the compounds of interest in the supercritical phase observed were 1-3 cm⁻¹ less than the shifts observed from supercritical fluid to liquid phase (3-23 cm⁻¹). This illustrates the temperature, pressure induced phase changes on spectral shifts due to the increased molecular interactions.

Another example of intensity and band shape changes and frequency shifts in vibrational spectroscopy because of phase changes is given by Taha and Tossen.¹²⁴ The intensity and frequency of N-O stretching mode of crystalline Ba(NO₃)₂ was monitored. When the phase changed from ordered (I) to disordered (II) between 25-400°C, changes in band shape, intensity and frequency shifts were observed. These spectral changes due to phase

change were explained similarly by density changes of the compound which affect intermolecular interactions.

The light alkenes investigated in this study mostly remain in one phase under the experimental conditions used. Thus, no phase shift transitions are expected to be observed for these compounds.

Frequency Shifts Due to Pressure and Temperature

Pressure and temperature can induce other changes in the geometric configuration of the compounds, (e.g., conformational changes, isomerizations,¹²⁵ deformation,^{126,127} and reorientations).¹²⁸ When this happens substantial changes can occur in vibrational frequencies. There are numerous studies that indicate conformational changes and related IR or Raman frequency shifts in liquids,^{129,130} gases,¹³¹ and lately with biochemical compounds such as proteins.¹³² One of these applications given by Kato et al.¹³³ investigates the temperature, pressure and solvent effects on the 1,3 dichloropropane conformational equilibrium between the trans-gauche and gauche-gauche conformations and provides a correlation between enthalpy differences due to pressure and temperature changes and the frequency shifts of the C-Cl stretching mode.

Other frequency shifts due to temperature occur with the thermochromic compounds.¹³⁴ The cause of this type of effect is usually associated with the intramolecular proton or electron transfer. One case is described by Hoshino et. al.¹³⁵ where they studied the thermally induced proton transfer in N,N'-bis(salicylidene)-p-phenylenediamine crystals.

The O-H vibrational stretch was monitored in the IR region showing considerable broadening and a frequency shift toward lower energy.

For molecules that are not undergoing a phase transition or a conformational change, the normal coordinates of the vibration remain unchanged. Since the masses also remain unchanged, any frequency shifts are due to changes in force constants.^{136,137}

Sherman has developed a model to determine the effect of pressure on force constants and thus, frequencies.¹³⁸ According to this model, a molecule can be described by a potential

$$V = A - Br^{-n} + Cr^{-m} \quad [1]$$

where A, B, C, n, and m are constants and r is the interatomic distance. The rate of change of the force constant k with r is given by

$$\frac{dk}{dr} = -(n + m + 3) k_0 / r_0 \quad [2]$$

where k_0 and r_0 are the ambient pressure values of k and r. A Lennard-Jones potential shows a force constant change of

$$\frac{dk}{k_0} = -21 \frac{dr}{r_0} \quad [3]$$

which amounts to a 21% increase in k for 1% decrease in r.

Pressure effects for solids cause changes for both inter- and intramolecular interactions.

This is illustrated by the examination of the equation

$$\frac{k_E}{dr_E} = \frac{k_I}{dr_I} \quad [4]$$

where k_E is the external force constant and k_I is the internal force constant. The values r_E and r_I represent the respective compression. The order of frequency shifts with pressure is $1\text{-}3 \text{ cm}^{-1} \text{ kbar}^{-1}$ for external modes. For internal bond-stretching modes, the range is $0.3\text{-}1 \text{ cm}^{-1} \text{ kbar}^{-1}$. Bond-bending modes are less affected and are on the order of $0.1\text{-}0.3 \text{ cm}^{-1} \text{ kbar}^{-1}$. These estimates are for average behavior and there are exceptions which do not follow the general trends.

Since the pressures required for these types of effects ($\sim 14,000$ psi) are much higher than those employed in this study (max experimental pressure < 750 psi), no frequency shifts are expected for the first overtone of the asymmetric $=\text{CH}_2$ stretch of ethylene and the monoalkylated alkenes.

Band Shape And Intensity Changes

It is known that band shape and intensity changes occur as well as frequency shifts due to temperature changes in vibrational spectroscopy. These changes can be described by the Boltzmann distribution function.^{139,140} The relative populations of the various energy levels are calculated by:

$$\frac{n_i}{n_0} = e^{-(E_i - E_0)/kT} \quad [5]$$

Where n_i and n_0 are the numbers of molecules in the i^{th} and zero energy levels, $(E_i - E_0)$ is the energy difference between the levels, k is Boltzmann's constant and T is the absolute temperature. For vibrational spectroscopy, the lowest possible energy level is where $v=0$. If we substitute the energy term $\Delta E = hc\bar{v}$ into equation [5], we obtain

$$\frac{n_i}{n_0} = e^{-hc\bar{v}/kT} \quad [6]$$

As can be seen from this equation at higher temperatures the number of molecules at zero energy level will decrease since a fraction of the molecules will be at $v=1$, and a smaller fraction in $v=2$, etc. This will result in a decrease in the absorbance since the absorbance is proportional to the population of molecules in the $v=0$ level according to the Beer's law.

In the liquid phase, a general broadening in the shape of the band occurs along with a decreased intensity of the band when temperature is increased. Several different studies relate the shape of the band to experimentally measurable physical parameters such as temperature, area or height of the absorbance band. One of these techniques is called the correlation-function approach.^{141,142} According to the correlation-function calculations the shape of a spectral band can, in general be defined by band moments $M(n)$.

$$M(n) = \int_{-\infty}^{+\infty} (\omega - \omega_0)^n \hat{I}(\omega) d\omega \quad [7]$$

where $n = 0, 1, 2, \dots$, $\omega = 2\pi\nu$, $\hat{I}(\omega)$ is the height of the band at the angular frequency ω of the vibration (for instance $\hat{I} = (\omega_0)$ is the height of the band at the center). These band moments can be expanded in a Taylor-series. However, only the first few moments can be evaluated experimentally and related to temperature changes.¹⁴³ For example $M(2) = 2kT/I$ where T is the absolute temperature, and I is the moment of inertia of the linear solute molecule for two atomic molecules such as HCl or DCl.

Other methods correlating the band shape to the experimentally measurable parameters use mostly least-squares fitting via computer programs.¹⁴⁴ The cause of band shape changes can be explained by population changes in the rotation-vibrational energy levels. The temperature changes are similar to those observed with vibrational energy levels and can be explained by Boltzmann statistics too.

The light source in vibrational spectroscopy causes an excitation of the rotational energy levels along with the vibrational excitation levels. The fine structure of the rotational vibrations are more visible in the vibrational spectra of gas phase compounds. In the liquid phase or with solutions of gases in liquids, the rotational energy levels between the vibrational energy levels are closer together, and often the rotational fine structure is lost.

In the liquid phase, a general broadening in the shape of the band occurs along with a decreased intensity of the band maximum. Several studies relate the shape of the band to physical parameters such as temperature.^{145,146} Band shape changes can be explained by a population change in the rotation-vibrational energy levels which are influenced by temperature similarly to the vibrational energy levels. The radiation source in vibrational spectroscopy causes excitation of the rotation-vibrational energy levels as well. This rotation-vibrational fine structure is more visible in the spectra of gas phase compounds.

In the liquid phase or with solutions of gases in liquids, the rotation-vibrational levels are effected more than gases due to collisions between the molecules. In the liquid phase, the distance between the molecules get smaller leading to increased number of collisions. Therefore, in condensed phase, the rotational structure is blurred by frequent molecular collisions and IR vibrational bands are broad with no rotational structure.¹⁴⁷ Solutions of small molecules carries the characteristics of the gas phase more than the liquid phase. Thus, For solutions of small gas molecules such as ethylene and propylene, fewer collisions occur compared to the condensed phase. Therefore, more pronounced population change in the rotation-vibrational energy levels is observed compared to the condensed phase which will lead to more significant broadening in the band due to the temperature change. This is why a more pronounced temperature effect can be seen in the vibrational spectra of solutions of ethylene and the other gas members of monoalkylated light alkenes (propylene, 1-butene) compare to the liquid members. Overall, the increased temperature tends to decrease the band intensity and increase the width of the band.

Splitting of Degenerate Vibrations

A loss in the degeneracy of E- or F- type vibrations with pressure is also possible. In some cases, this may be due to a lowering of the symmetry of the molecule where a compound may have two or more molecules per unit cell. It is possible that the vibrations in the unit cell might couple, causing a factor-group splitting, or Davydov splitting.^{148,149} Davydov splitting (also known as crystal field splitting) is observed in solids with a crystalline structure. Wu C.K. et al.¹⁵⁰ studied the infrared active rocking modes of crystalline polymethylenes in orthorhombic and monoclinic structures. Also, instances are possible whereby unallowed vibrations may become allowed by application of pressure.¹⁵¹ No such observations are expected for ethylene and the monoalkylated alkenes since no symmetry changes are predicted to be induced under the experimental conditions used and these compounds are not crystalline.

Doubling of Absorption Vibrations

In the course of various studies it is observed that a doubling of bands can occur with pressure or temperature.^{152,153} This may be due to a lowered site symmetry. Alternatively, two accidentally overlapping vibrations may occur at the same frequency. These may be induced to separate because of a difference in the pressure dependencies manifested by the two vibrations, or separate due to factor-group splitting.¹⁵⁴ Fermi resonance can also cause some band doubling as the pressure is increased.¹⁵⁵

It is also possible that at high pressure and temperature, normally forbidden modes might become allowed (in a lower site symmetry) due to structural interconversions.¹⁵⁶

No such observations are predicted for ethylene and monoalkylated alkenes due to changes in pressure and temperature, since no site symmetry changes are expected to be induced under the experimental conditions employed.

Sensitivity of Vibrations to Expansion of Molecular Volume

Generally, for complexes, molecular expansion is expected to affect the molecular symmetry which can lead to different vibrations and the disappearance of some and appearance of others.¹⁵⁷ Additional changes are observed due to molecular volume changes caused by bond distance changes. The bond distance changes that do not affect the molecular symmetry will shift the vibrational bands to higher energy.¹⁵⁸ A correlation between the vibrational energy levels and the molecular volume changes due to temperature or pressure can be given in the following equations.^{159,160}

$$\Delta V = RTn_0 / P \quad [8]$$

Substituting n_0 from the Boltzmann equation

$$\Delta V = RTn_i / Pe^{-hc\bar{v}/kT} \quad [9]$$

No frequency changes for the first overtone of the asymmetric $=\text{CH}_2$ stretch caused by structural interconversions due to temperature and pressure are predicted for ethylene and the monoalkylated alkenes under the experimental conditions employed.

Multivariate Calibration Techniques

Classical Least Square Regression

Classical Least Squares (CLS) regression in general describes the procedure where the calibration model represents the physical law which relates the variation in the spectra with composition, i.e., Beer's law where spectral absorbance is represented as a linear function of component concentration.¹⁶¹ Since CLS explicitly uses a Beer's law model, it is referred as a hard model or explicit model method.¹⁶² Although the CLS method is less flexible than soft modeling methods such as PLS and PCR, it provides greater qualitative information in the range that it is defined.¹⁶³ However, lack of fit can occur due to deviations from Beer's law such as curvature in the absorbance versus concentration plot, or the existence of interactions between components in a mixture.¹⁶⁴

CLS assumes that the mixture spectrum is a linear combination of the pure component spectra. Therefore, a mixture spectrum \mathbf{A} , based on Beer's law can be written as a combination of all pure-component spectra, \mathbf{K} .¹⁶⁵

$$\mathbf{A} = \mathbf{C}\mathbf{K} + \mathbf{E}$$

[10]

where \mathbf{A} is the m by n matrix consisting of the absorbances of each of the m samples at n frequencies. \mathbf{C} is the m by l matrix of the l component concentrations in the m samples, and \mathbf{K} represents the l by n matrix of pure-component spectra. \mathbf{E} is the m by n matrix of spectral noise or model error present in the spectra.

During calibration, the least-squares solution for the pure-component spectra \mathbf{K} is:

$$\hat{\mathbf{K}} = (\mathbf{C}'\mathbf{C})^{-1}\mathbf{C}'\mathbf{A} \quad [11]$$

Where $\hat{\mathbf{K}}$ is used to represent the least-squares estimate of the matrix \mathbf{K} that minimizes the sum of squared spectral errors in equation [10]. \mathbf{C}' is the transpose of matrix \mathbf{C} .

During prediction, the unknown sample spectrum vector \mathbf{a} is equal to:

$$\mathbf{a} = \mathbf{K}'\mathbf{c} + \mathbf{e} \quad [12]$$

where \mathbf{c} is the unknown concentration vector and \mathbf{e} is the error vector and \mathbf{K}' is the transpose of matrix \mathbf{K} . Note the order of matrix multiplication is reversed from that of equation [10] since vectors are being represented as column vectors.

The least-squares solution for the component concentrations of the unknown is obtained by using $\hat{\mathbf{K}}$ from equation [11].

$$\mathbf{c} = (\hat{\mathbf{K}} \hat{\mathbf{K}}')^{-1} \hat{\mathbf{K}} \mathbf{a} \quad [13]$$

where $\hat{\mathbf{K}}'$ is the transpose of matrix $\hat{\mathbf{K}}$.

Similarly by using least-squares regression an estimate of the error in the predicted concentrations can be calculated. This error is equal to noise when the set of calibration spectra chosen for the analysis fit exactly with the sample spectrum. The fit will degrade when nonlinearities are experienced or when the chemical impurities exist but are not accounted for in the modeling.^{166,167,168}

In CLS, the absorbance of the spectrum at a given wavelength is assumed to be an additive function of the concentration of the constituents. Hence, the CLS technique can only be applied to systems where the make up of the sample has to have exactly the same components as the standards. In other words, if there is an additional compound (impurity) in the sample CLS will still assume that the sample is the mixture of the components used in the training set. CLS also assumes that no other spectral variation exist and effects the data.

Partial Least Square Regression

The theoretical background of partial least squares lies in factor-based regression which is outside of the scope of this research. Only a brief description of the mechanics will be provided here to be able to interpret the results of the PLS algorithm.

Partial least squares is a decomposition technique which consolidates the variation in spectra. The spectral variations are due to mostly, the concentration variations of the constituents, the inter-constituent interactions i.e. solvent effects, instrument variations such as detector noise, temperature effects, density changes etc. PLS uses those variations as partial spectra which are often called eigenvectors, (or spectral loadings, or loading factors or principal components or simply factors) to construct the unknown spectra. Presumably, these eigenvectors can be used to reconstruct the spectrum of a sample by multiplying each one by a different constant scaling factor and adding the results together until the new spectrum closely matches the unknown spectrum. These scaling constants used to reconstruct the spectra are generally known as scores.¹⁶⁹

In PLS both the spectral data and the concentration data are decomposed into their respective most common variations. This generates two sets of eigenvectors and two sets of corresponding scores: one set for the spectral data, and the other for the constituent concentrations. These two sets of scores are related to each other through some type of regression which constructs the calibration model. PLS performs the decomposition on both the spectral and concentration data simultaneously. As each new factor is calculated for the model, the scores are "swapped" before the contribution of the factor is removed from the data. The newly reduced data matrices are then used to calculate the next factor, and the process is repeated until the desired number of factors is calculated.¹⁶⁹

The eigenvector that represents the common variations in the spectral data is called the spectral "loading" and the eigenvector that represents the changes in the spectra corresponding to the regression constituents is called the spectral weight.

Correspondingly, there are two sets of scores: one for the spectral data and another for the concentration data. The mechanics of the calculation require, a weighting score to be taken as the starting value, and through the regression the convergence of the calculation is expected. After setting an initial value for the weighting scores, a spectral weighting vector is calculated, which in the next step is normalized to unit length. In the following step, the spectral scores are obtained.¹⁶⁹

Calculations of concentration loading vectors is done next and normalized to the unit length. After this step, new weighting scores are calculated and convergence is checked by new scores to the previous pass. If the scores are effectively the same, the PLS cross product is calculated which then followed by the obtaining the spectral loading vector. This spectral loading vector is normalized by the spectral scores and its contribution is removed from the spectral data and also from the concentration data. After this point the vector counter is increased by one and the steps are repeated until all desired factors are calculated.¹⁶⁹

One of the difficult tasks in PLS is determining the correct number of loading factors to use to model the data. The earlier factors in the model are most likely to be the ones related to the concentration of the constituents, while later factors generally have less information that is useful for predicting concentration. In fact these factors will

eventually begin to model the system noise (which usually provides the smallest contribution to the data). However, if too few vectors are used to construct the model, the prediction accuracy for unknown samples will suffer since not enough terms are being used to model all the spectral variations that compose the constituents of interest. Therefore, it is very important to define a model that contains enough vectors to properly model the components of interest without adding too much contribution from the noise. Models that include noise vectors or more vectors than are actually necessary to predict the concentrations are called overfit. Models that do not have enough factors in them are known as underfit.¹⁶⁹

PLS can account for the compound of interest accurately if there are impurities in the sample that were not accounted for during the calibration.

Chapter 3

QUANTITATIVE ANALYSIS OF LIGHT ALKENES BY FT-NIR SPECTROSCOPY: ROOM TEMPERATURE PRESSURE FEASIBILITY STUDIES

To find distinguishable features for ethylene and monoalkylated light alkenes in the NIR region, and to achieve their simultaneous, *in situ*, *real-time* determination at elevated temperatures and pressures, a feasibility study was performed at room temperature and pressure. The *in situ* measurements for the determination of the effects of the temperature and pressure on this analysis were done in a separate system where a high pressure/temperature apparatus was coupled with the fiber optic FT-NIR spectrometer (see Chapter 4).

For the feasibility study, an FT-NIR instrument incorporating a sample cell via fiber optic cables was used. Ethylene and monoalkylated light alkenes, namely propylene, 1-butene, 1-pentene, 1-hexene, 1-octene, and 1-decene, were used in this determination. Various other alkylated alkenes (e.g., 1,1 dialkylated, cis, trans dialkylated, and trialkylated alkenes) were investigated to determine the effects of molecular structure.

The first overtone of the asymmetric $=\text{CH}_2$ stretch of the monoalkylated alkenes (6,080- σ , 150 cm^{-1}) was found to be unique for alkenes, and was used to build a model based on classical least squares (CLS) regression (multiple linear regression). A mixture of

ethylene and 1-octene was taken as the mixture to prove feasibility at room temperature and pressure. The reliability of the results was tested by means of residual spectra which were obtained by subtracting the estimated spectra from the measured spectra.

Experimental Procedures

Materials

The light alkenes investigated during the feasibility study were ethylene and monoalkylated ethylenes namely propylene, 1-butene, 1-pentene, 1-hexene, 1-heptene, 1-octene and 1-decene (Table 1). Additionally, cis and trans-dialkylated alkenes, 1,1 dialkylated alkenes and trialkylated alkenes were investigated to determine the effects of the molecular structure on the quantitative analysis of these compounds. Most of the cis and trans dialkylated alkenes were isomers of octene. These were cis 2-octene, cis 3-octene, cis 4-octene and trans 2-octene, trans 3-octene, and trans 4-octene (Table 2). Cis- and trans-3-methyl-3-heptenes were the trialkylated alkenes used in the study. The compound 2-ethyl-1-hexene was used as an example of a 1,1 dialkylated alkene. Table 3 shows the formula for 1,1 dialkylated alkenes, trialkylated alkenes and n-octane.

Isopar E, a liquid cut of saturated hydrocarbon distillation (Exxon Company, U.S.A), was used as a solvent during these experiments. Isopar E contains about 60 volume % iso-octane and a variety of other saturated hydrocarbons.

Table 1: Ethylene and Monoalkylated Alkenes

Compounds	Formulae
1. Ethylene	$\text{CH}_2=\text{CH}_2$
2. Monoalkylated Alkenes	
2.1. Propylene	$\text{CH}_2=\text{CH}=\text{CH}_3$
2.2. 1-Butene	$\text{CH}_2=\text{CH}=\text{CH}_2=\text{CH}_3$
2.3. 1-Pentene	$\text{CH}_2=\text{CH}=\text{CH}_2=\text{CH}_2=\text{CH}_3$
2.4. 1-Hexene	$\text{CH}_2=\text{CH}=\text{CH}_2=\text{CH}_2=\text{CH}_2=\text{CH}_3$
2.5. 1-Octene	$\text{CH}_2=\text{CH}=\text{CH}_2=\text{CH}_2=\text{CH}_2=\text{CH}_2=\text{CH}_2=\text{CH}_3$
2.6. 1-Decene	$\text{CH}_2=\text{CH}=\text{CH}_2=\text{CH}_2=\text{CH}_2=\text{CH}_2=\text{CH}_2=\text{CH}_2=\text{CH}_2=\text{CH}_3$ 3

Table 2: Cis and Trans Dialkylated Alkenes.

Compounds	Formulae
Cis-2-Octene	$\text{CH}(\text{CH}_3)=\text{CH}(\text{=CH}_2=\text{CH}_2=\text{CH}_2=\text{CH}_2=\text{CH}_3)$
Trans-2-Octene	$\text{CH}(\text{CH}_3)=\text{C}(\text{CH}_2=\text{CH}_2=\text{CH}_2=\text{CH}_2=\text{CH}_3)\text{H}$
Cis-3-Octene	$\text{CH}(\text{CH}_2=\text{CH}_3)=\text{CH}(\text{=CH}_2=\text{CH}_2=\text{CH}_2=\text{CH}_3)$
Trans-3-Octene	$\text{CH}(\text{CH}_2=\text{CH}_3)=\text{C}(\text{CH}_2=\text{CH}_2=\text{CH}_2=\text{CH}_3)\text{H}$
Cis-4-Octene	$\text{CH}(\text{CH}_2=\text{CH}_2=\text{CH}_3)=\text{CH}(\text{=CH}_2=\text{CH}_2=\text{CH}_3)$
Trans-4-Octene	$\text{CH}(\text{CH}_2=\text{CH}_2=\text{CH}_3)=\text{C}(\text{CH}_2=\text{CH}_2=\text{CH}_3)\text{H}$

Table 3: 1,1 Dialkylated Alkenes and Trialkylated Alkenes

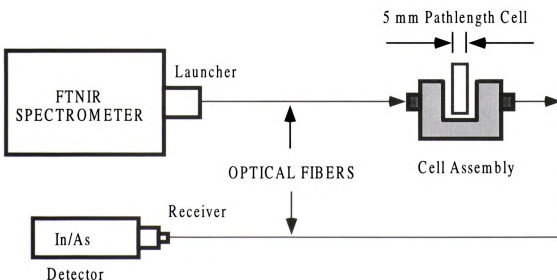
Compounds	Formulae
1. Trialkylated Alkenes	
(1.1) Cis-3-Methyl-3-Heptene	$\text{CH}_3(\text{CH}_3=\text{CH}_2)\text{C}=\text{C}(\text{CH}_2=\text{CH}_2=\text{CH}_3)\text{H}$
(1.2) Trans-3-Methyl-3-Heptene	$(\text{CH}_3=\text{CH}_2)\text{CH}_3\text{C}=\text{C}(\text{CH}_2=\text{CH}_2=\text{CH}_3)\text{H}$
2. 1,1 Dialkylated Alkenes	
2-Ethyl-1-Hexene	$\text{CH}_2=\text{C}(\text{CH}_2=\text{CH}_3)(\text{CH}_2=\text{CH}_2=\text{CH}_2=\text{CH}_3)$
Octane	$\text{CH}_3=\text{CH}_2=\text{CH}_2=\text{CH}_2=\text{CH}_2=\text{CH}_2=\text{CH}_2=\text{CH}_3$

FT-NIR System

A Diamond 20 model FT-NIR spectrometer manufactured by KVB/Analect (Pasadena, CA) was used in these experiments. The spectrometer was coupled with a cell assembly via optical fibers as illustrated in Figure 1. The Diamond 20 FT-NIR system has a 1.5 cm^{-1} transect IV hermetically sealed interferometer. Calcium fluoride optics were used for the 12,000 to 1,200 cm^{-1} region. The spectrometer includes an internal source and all optical control electronics. It is controlled by a 66 MHz 486 based data system operated under MS DOS/Windows 3.1. The spectrometer and the data station were interfaced with a LAN interface card provided by the manufacturer. The system includes the manufacturer's FX-70, DOS based software program, and FX-80, Windows 3.1 based software for the control and operation of the analyzer.

The spectrometer was coupled with a three stage, Indium-Arsenide (InAs), SP-2426 model detector repackaged and sold by KVB/Analect as well. The detector was cooled with a thermoelectric cooler. The light from the spectrometer to the sample cell and back from the sample cell to the detector were carried with fiber optic cables. A fiber optic receiving module was used at the interferometer outlet and at the detector inlet.

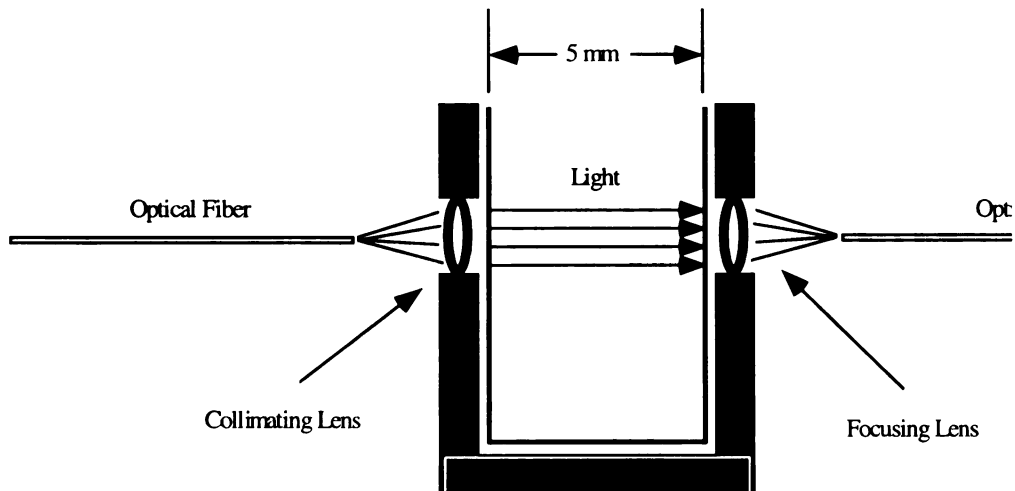
Figure 1: Schematic diagram of the FT-NIR Set-up.



Fiber Optic Cell Assembly

A cell holder was designed as illustrated in Figure 2 to interface the optical fibers with an optical cell. Plano-convex lenses (5 mm in diameter) were used to collimate and focus the light as shown. A removable cell was used in the middle of the holder. A set screw was used to keep the cell from moving once in its place.

Figure 2: Schematic Diagram of the Fiber Optic Cell.



A 5 mm path length cell was used in this study to obtain about 0.3 absorbance units (a.u.) for the first overtone ($6,120 \text{ cm}^{-1}$) of the asymmetric $=\text{CH}_2$ stretch of 1-octene at a concentration of 10% by weight. Background spectra were obtained with empty clean optical cells for all of the absorbance measurements.

The fiber optic cables were 550 μm , low OH content fibers supplied by SpecTran Specialty Optics (Avon, CT). The cable was purchased as bulk fiber, and the fiber optic connectors were installed by using a termination kit supplied by SpecTran, at the end of the fibers, after cutting to the required length. About 20 feet of fiber optic cable was used to connect the cell assembly and the spectrometer/detector.

Calibration Standards

The spectra of the most of the monoalkylated ethylenes and di and tri alkylated alkenes were collected in pure form (98% or more purity) and in solutions using Isopar E as solvent. All solutions were prepared at room temperature and pressure except for the ethylene and propylene solutions in Isopar E which were prepared at 4 °C. For this purpose, the gas (ethylene or propylene) was bubbled into Isopar E in a small vial placed in an ice bath. This solution was quickly weighed and transferred to the optical cell where the spectrum was obtained immediately. The 1-butene solution in Isopar E was prepared at room temperature due to the higher solubility of 1-butene in Isopar E.

Additionally, mixtures of 2%, 4%, 6%, and 10% by weight of 1-octene and the other alkenes were prepared. The spectra obtained from these mixtures were used in checking the validity of the calibration model. The spectra of all of these compounds were obtained at 4 cm^{-1} resolution and as an average of 64 scans from 4,000 to 12,000 cm^{-1} .

Data Analysis and Results

Interpretation of the Spectra

Despite the immense amount of information in the literature for assigning the fundamentals of alkenes in the mid-IR region,^{170,171,172,173,174,175} there is comparatively little information for the assignments of the first overtones in the NIR region. Therefore, to be able to find distinct bands that can be related to alkenes in the NIR range, the overtones of the fundamentals had to be estimated.

A coarse inspection of the NIR spectra obtained from mono, di and trialkylated alkenes reveals that there are two main regions where differences in spectra occur. These are the $6,100\text{ cm}^{-1}$ region and the $4,750\text{ cm}^{-1}$ region. Figures 3 through 6 show the $6,100\text{ cm}^{-1}$ region of the spectra, for ethylene and monoalkylated alkenes (Figure 3), cis and trans dialkylated alkenes (Figure 4), trialkylated alkenes (Figure 5), and 1,1 dialkylated alkenes (Figure 6) in overlaid mode. The $4,750\text{ cm}^{-1}$ region of the spectra for these groups of compounds, similarly, are shown in Figure 7, Figure 8, Figure 9, and Figure 10.

Additionally the full NIR spectra of all compounds used in the study are given in the Appendix A Figures A1 through A17.

Figure 3: Spectra of 98 wt %, 1-Pentene, 1-Hexene, 1-Octene, 1-Decene and Ethylene, Propylene, 1-Butene Solutions in Isopar E (monoalkylated alkenes) in 6,080 to 6,150 cm^{-1} Region in Overlaid Format at Room Temperature and Pressure.

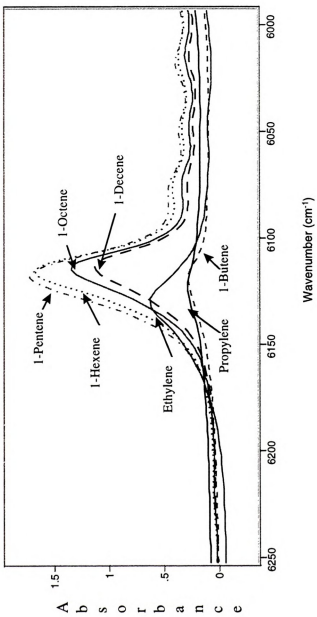


Figure 4: Spectra of 98 wt %. Pure Octene Isomers (cis 2-octene, cis 3-octene, cis 4-octene, trans 4-octene) (cis and trans dialkylated alkenes) in 6,080 to 6,150 cm^{-1} Region in Overlaid Format at Room Temperature and Pressure.

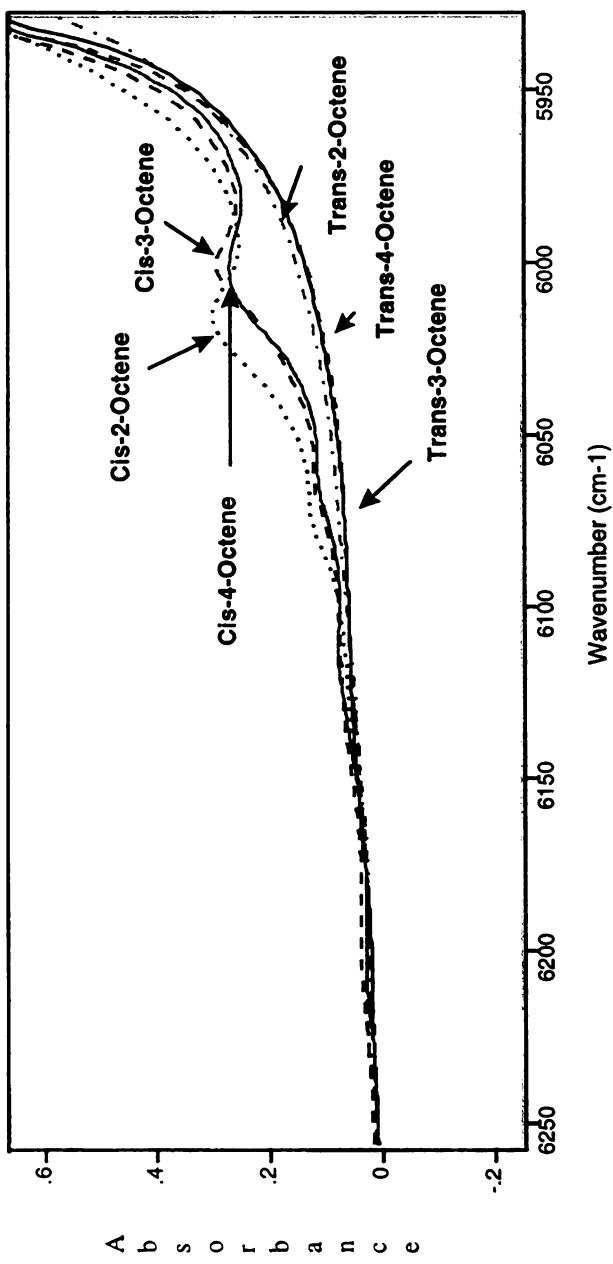


Figure 5: Spectra of 98 wt %. Pure Trialkylated Alkenes (cis 3-methyl-3-heptene, trans 3-methyl-3-heptene) in 6,080 to 6,150 cm^{-1} Region in Overlaid Format at Room Temperature and Pressure.

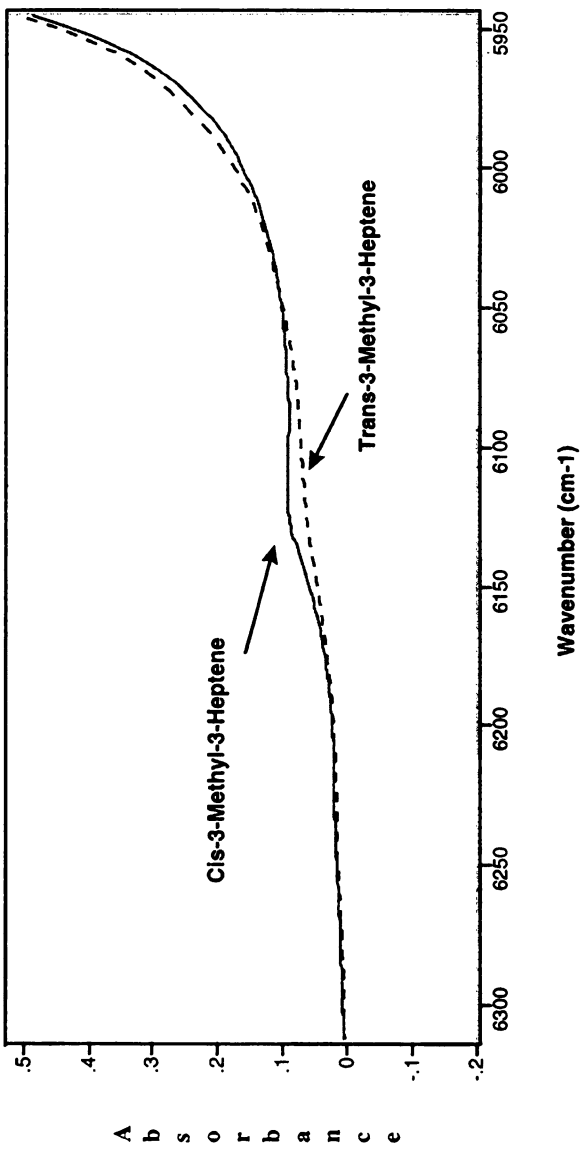


Figure 6: Spectrum of 98 wt %. Pure 2-Ethyl-1-Hexene (1,1 dialkylated alkene) and Octane in 6,080 to 6,150 cm^{-1} Region in Overlaid Format at Room Temperature and Pressure.

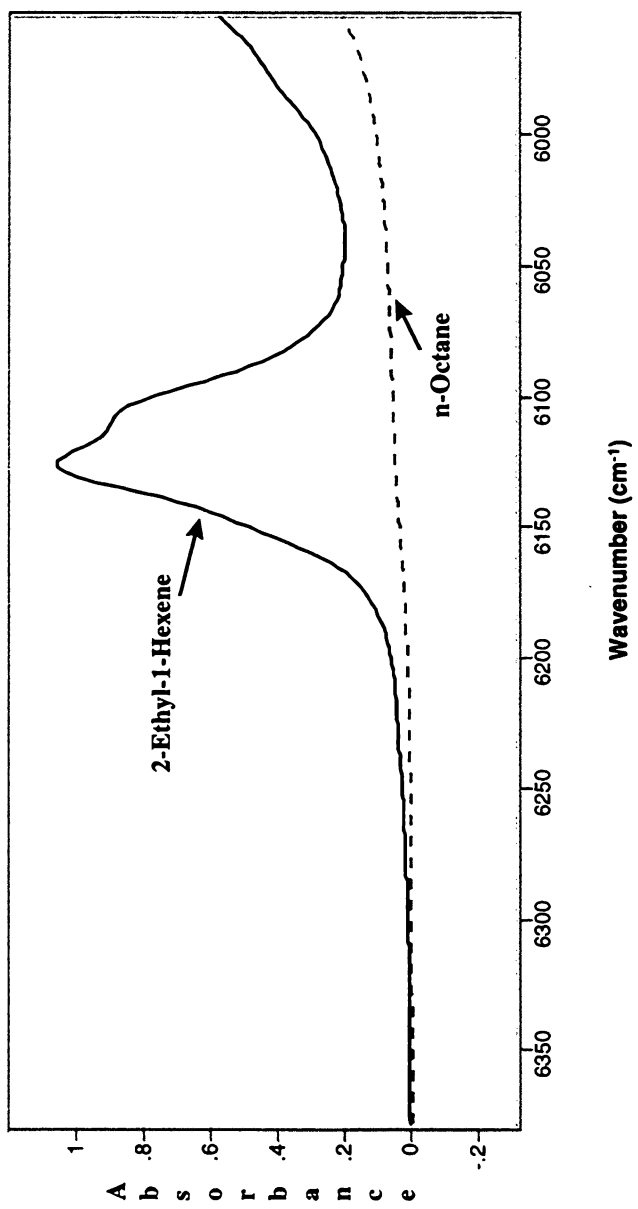


Figure 7: Spectra of 98 wt %, 1-Pentene, 1-Hexene, 1-Octene, 1-Decene and Ethylene, Propylene, 1-Butene Solutions in Isopar E (monoalkylated alkenes) in 4,800 to 4,850 cm^{-1} Region in Overlaid Format at Room Temperature and Pressure.

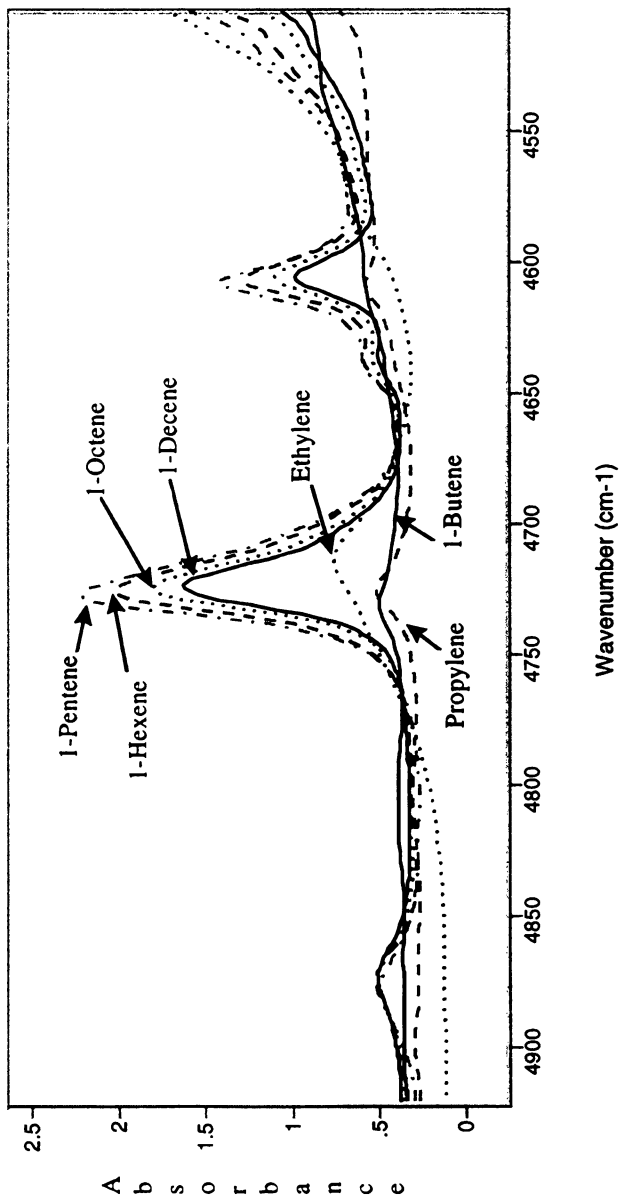


Figure 8: Spectra of 98 wt %. Pure Octene Isomers (cis 2-octene, cis 3-octene, cis 4-octene, trans 2-octene, trans 3-octene, trans 4-octene) (cis and trans dialkylated alkenes) in 4,800 to 4,850 cm^{-1} Region in Overlaid Format at Room Temperature and Pressure.

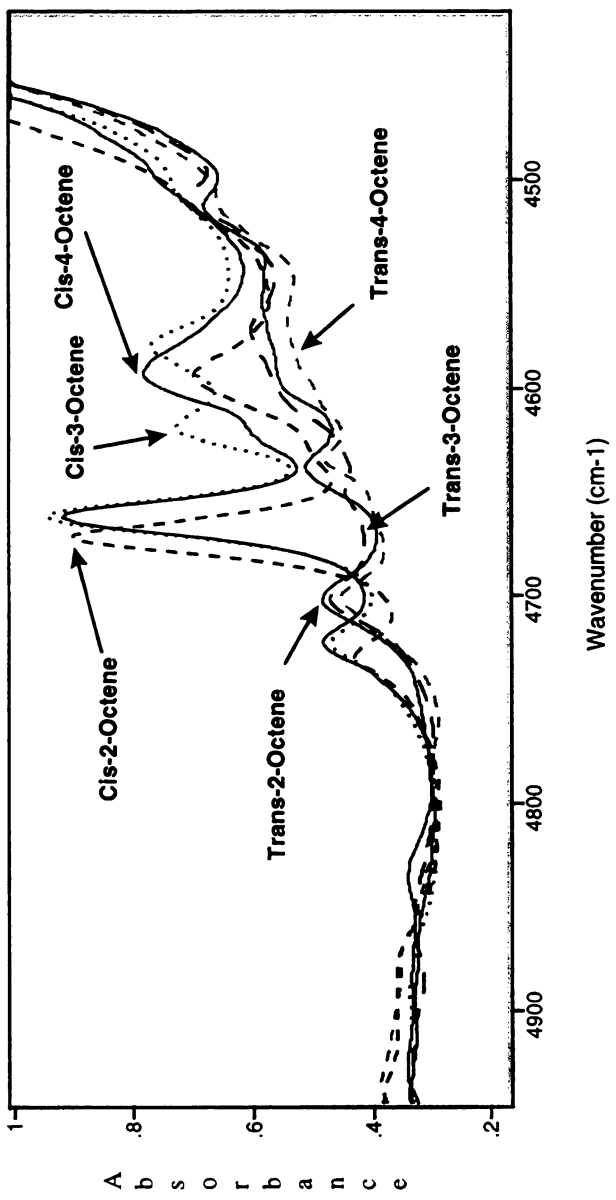


Figure 9: Spectra of 98 wt %. Pure Trialkylated Alkenes (cis 3-methyl-3-heptene, trans 3-methyl-3-heptene) in 4,800 to 4,850 cm^{-1} Region in Overlaid Format at Room Temperature and Pressure.

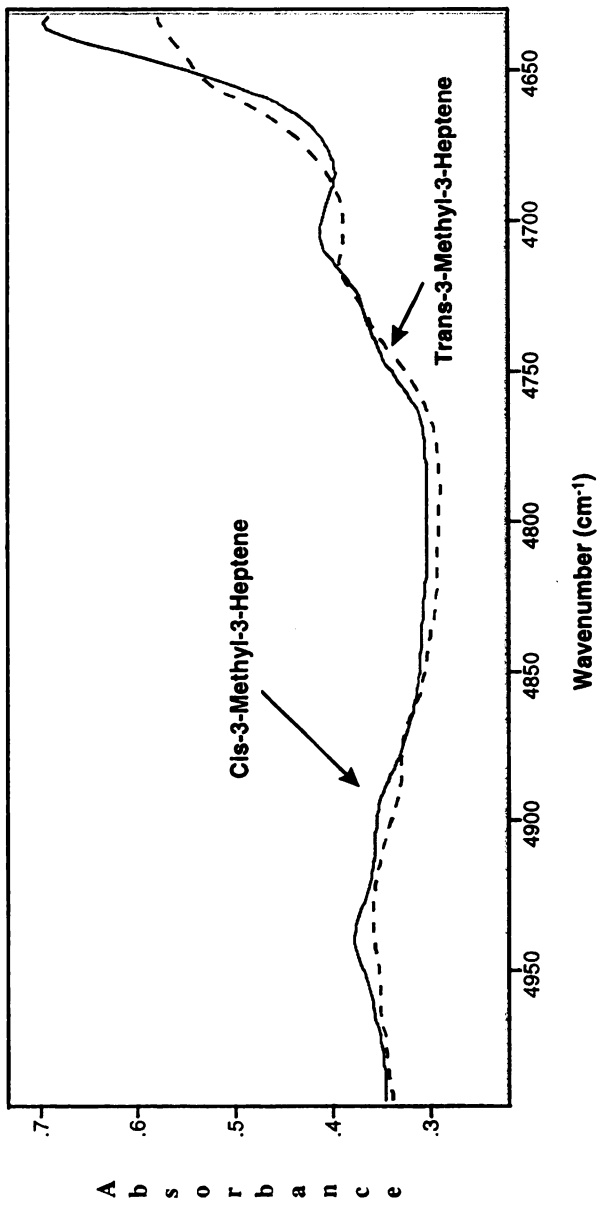
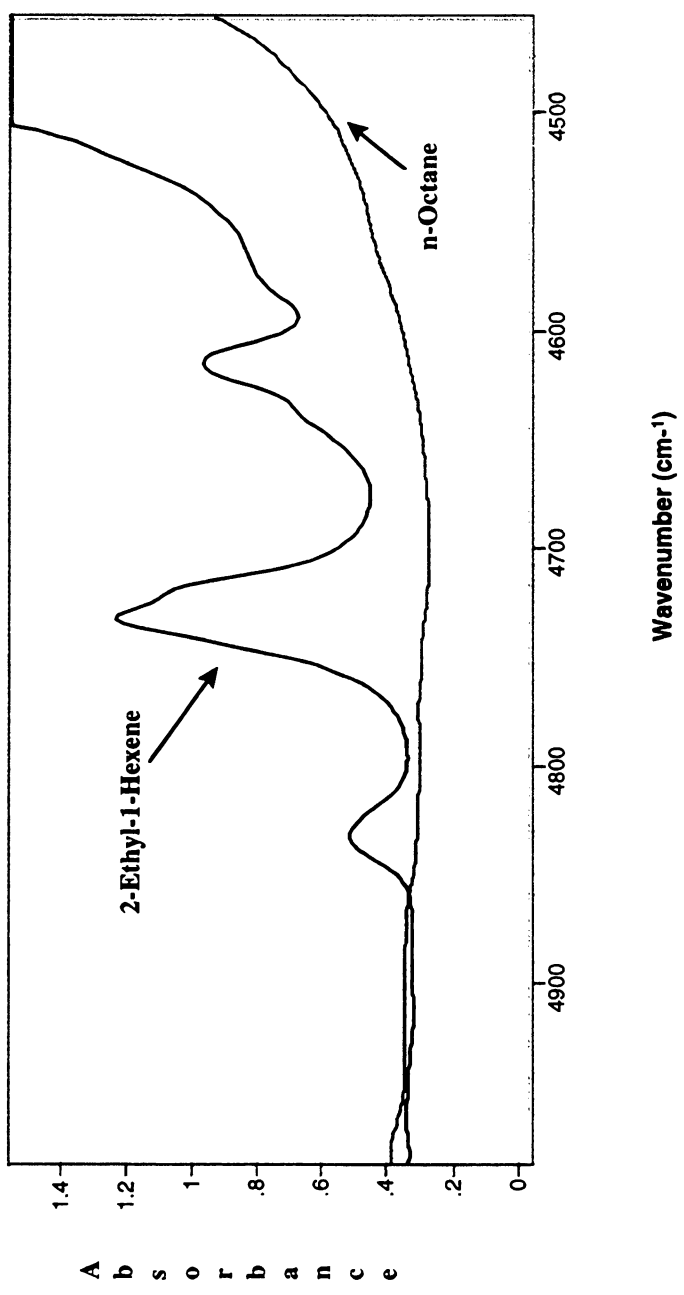


Figure 10: Spectrum of 98 wt %. Pure 2-Ethyl-1-Hexene (1,1 Dialkylated alkene) and Octane in 4,800 to 4,850 cm^{-1} Region in Overlaid Format at Room Temperature and Pressure.



A closer look at these regions indicates that the differences in the 6,100 cm⁻¹ are more significant comparatively. Therefore, this region was taken during the study to build the CLS calibration model for the determination of ethylene and the monoalkylated alkenes. To be able to interpret the differences in spectra in this region the fundamentals of the C-H stretches in the MID-IR region have been inspected.

Table 4 shows the characteristic frequencies of alkylated ethylenes.¹⁷⁶ Three important vibrational stretching bands (fundamental bands in mid-IR) for the alkenes have the potential for an overtone band in the NIR region.^{177,178,179, 180,181} These are: the =CH₂ asymmetric stretch (3,090-3,075 cm⁻¹), the =CH stretch (3,020-2,995 cm⁻¹) and the in phase (symmetric) stretch of =CH₂ (3,000-2,980 cm⁻¹). Other fundamentals, for instance the C=C stretch, the CH₂ wagging, the CH₂ deformation and the CH₂ rocking are at longer wavelength; thus, their first overtones should not be in the NIR region. The second or the third overtones of these bands in the NIR region would be too weak to be significant.

Table 4: Characteristic IR Frequencies (cm^{-1}) of Alkylated Ethylenes.

Group	cm^{-1}	IR	R	Assignment
 Monoalkyl (vinyl)	3090-3075	m	m	CH_2 asym. str.
	3020-2995	w	s, p	CH str.
	3000-2980	m	w	CH_2 sym. str.
	1840-1805	w	—	$2 \times 910 \text{ cm}^{-1}$
	1650-1638	ms	vs, p	C=C str.
	1420-1412	mw	s, p	CH_2 scis. def.
	1309-1288	w	s, p	CH rock
	995-985	vs	w	trans CH in-phase wag
	910-905	vs	w	CH_2 wag
	688-611	w	w	cis CH in-phase wag
 1,1-Dialkyl (vinylidene)	3090-3075	m	w	CH_2 asym. str.
	3000-3075	m	s, p	CH_2 sym. str.
	1810-1770	w	—	$2 \times 890 \text{ cm}^{-1}$
	1660-1640	ms	vs, p	C=C str.
	1420-1400	w	m, p	CH_2 scis. def.
	900-885	vs	w	CH_2 wag
 cis-Dialkyl	3020-2995	m	m	CH str.
	1662-1631	mw	vs, p	C=C str.
	1429-1397	m	—	cis CH asym. rock
	1270-1250	w	s	cis CH sym. rock
	730-650	ms	vw	cis CH wag
 trans-Dialkyl	3010-2995	m	m	CH str.
	1676-1665	vw	vs, p	C=C str.
	1325-1300	vs	s	trans CH sym. rock
	ca. 1295	mw	—	trans CH asym. rock
	980-965	vs	vw	trans CH wag
 Trialkyl	3040-3020	w	m	CH str.
	1680-1664	w	vs, p	C=C str.
	1360-1322	—	w	CH rock
	840-790	m	vw	CH wag
 Tetraalkyl	1680-1665	—	vs, p	C=C str.

A thorough investigation of this table and the NIR spectra of the alkenes used in these experiments shows that the band observed around $6,120\text{ cm}^{-1}$ is unique to monoalkylated alkenes and 1,1 dialkylated alkenes both of which contain a fundamental $=\text{CH}_2$ stretch in the mid-IR. Cis and trans octenes are cis and trans dialkylated alkenes and do not contain a $=\text{CH}_2$ group; thus, no overtone of either the symmetric or asymmetric stretch of this group is expected. Experimentally, no overtones are observed experimentally in the $6,100\text{ cm}^{-1}$ region which confirms the prediction. None of the trialkylated alkenes (cis and trans 3-methyl-3-heptenes) containing a single $=\text{CH}$ stretch have any bands in this region. Therefore, the band observed at $6,120\text{ cm}^{-1}$ cannot be due to the first overtone of the $=\text{CH}$ stretch. Similarly, the symmetric $=\text{CH}_2$ stretch can be eliminated since the location of the fundamental is at lower energy to meet the energy level of $6,120\text{ cm}^{-1}$ region. Therefore, the band that is observed at $6,120\text{ cm}^{-1}$ region is more likely to be the first overtone of the asymmetric $=\text{CH}_2$ stretch of alkylated ethylenes.

The anharmonic oscillator approximation can be used to estimate the location of the first overtone of the asymmetric $=\text{CH}_2$ stretch ($3,090\text{-}3,075\text{ cm}^{-1}$).^{182,183,184}

The energy levels (cm^{-1}) of the anharmonic oscillator are given by

$$E_{\text{vib}} = \bar{\nu}_e(v + 1/2) - x_e \bar{\nu}_e(v + 1/2)^2 \quad [14]$$

where $\bar{\nu}_e$ is the fundamental (cm^{-1}), v is the vibrational quantum number and x_e is the anharmonicity constant.

For the first overtone $v = 2$ to $v = 0$

$$\Delta E_{vib} = 2\bar{\nu}_e - 6\bar{\nu}_e x_e \quad [15]$$

For a typical value of $\chi_e = 0.0025$,^{185,186} the calculated wavenumber of the first overtone using a fundamental of 3090 cm^{-1} is $\Delta E_{vib} = 6180 - 46 = 6134 \text{ cm}^{-1}$ while the observed value is 6129.8 cm^{-1} . Hence, it was concluded that the observed band is the first overtone of the asymmetric $=\text{CH}_2$ stretch.

The spectra of ethylene, propylene, 1-butene, 1-pentene, 1-hexene, 1-octene and 1-decene are shown in Figure 3 in overlaid mode, in the first overtone of the asymmetric $=\text{CH}_2$ stretch region. Careful examination of this region of the spectra indicates that the first overtone of the asymmetric $=\text{CH}_2$ stretch in $6,080$ to $6,160 \text{ cm}^{-1}$ region shifts towards longer wavelengths or towards lower energy with increasing chain length. Table 5 lists these shifts among the members of the monoalkylated alkenes. The shift decreases with an increasing number of carbon atoms in the molecule. Among 1-pentene, 1-hexene, 1-octene and 1-decene this shift is about only a couple of wavenumbers.



Table 5: Shift of location of first overtone of asymmetric $=\text{CH}_2$ stretch of monoalkylated alkenes.

Alkene	Number of C atoms	Max of the band location (cm^{-1})	ΔC_i	$\Delta(C_2 \cdot C_i)$
Ethylene	C ₂	6,129.8		
Propylene	C ₃	6,123.1	6.7	6.7
1-Butene	C ₄	6,119.5	3.6	10.3
1-Pentene	C ₅	6,118.2	1.3	11.6
1-Hexene	C ₆	6,116.1	2.1	13.7
1-Octene	C ₇	6,114.3	1.8	15.5
1-Decene	C ₈	6,113.6	0.7	16.2

In addition to the decrease in the frequency of the first overtone of the asymmetric $=\text{CH}_2$ stretch, a decrease in the intensity of the band with the increasing chain length was also observed. The decrease in the dipole moment derivative of the molecule due to the increased chain length is known to be the cause of a decrease in the integrated area of the bands in vibrational spectroscopy.¹⁸⁷

Furthermore, the spectrum of 2-ethyl-1-hexene (a 1,1-dialkylated alkene) shown in Figure 6, clearly presents two overlapped bands that can be interpreted similarly. The band observed at $6,126 \text{ cm}^{-1}$ is due to the asymmetric stretch of $=\text{CH}_2$ and the adjacent band is due to the symmetric stretch of $=\text{CH}_2$ ($6,109 \text{ cm}^{-1}$).

This interpretation can be used in developing quantitative determinations of these compounds by NIR spectroscopy. For instance, simultaneous determination of mixtures of monoalkylated alkenes starting from 1-pentene to 1-decene would be difficult because the first overtones of the asymmetric $=\text{CH}_2$ stretching vibrations overlap severely. However, since a more significant shift is observed between the first overtone of the asymmetric $=\text{CH}_2$ stretching vibration from ethylene to 1-butene, the simultaneous determination of these light members of the monoalkylated alkenes is possible.

Additionally, the determination of pairs consisting of small and larger molecules should also be more feasible than the determination of adjacent pairs. For instance, the determination of the ethylene and 1-octene pair separation should be more feasible than the determination of the 1-octene and 1-decene (0.7 cm^{-1}) pair or the 1-butene and 1-pentene pair (1.3 cm^{-1}).

Moreover, the determination of mixtures containing more than 2 compounds, may be challenging as well. Therefore, for demonstrating the feasibility of the quantitative analysis of these compounds, the readily distinguishable, ethylene and 1-octene mixture was taken as an example.

Quantitative Determinations:

For the ethylene/1-octene example, the 6,080-6,160 cm⁻¹ region (the asymmetric stretch of =CH₂) was used instead of whole spectrum since this region was found to be sufficient to allow quantitative determination. Thorough examination of the FT-NIR spectra of 1-octene, Isopar E and ethylene in this region revealed a small interference from Isopar E (see Figure 11).

Additionally, the compounds that absorb in this region such as 1-pentene through 1-decene and 2-ethyl-1-hexene will interfere with the determination and bias both the ethylene and 1-octene estimates for the reasons described earlier. Therefore, this determination is limited to mixtures where there is no 1-pentene, 1-hexene, 1-heptene, 1-octene, and longer chain members. However, 2-Ethyl-1-hexene has a unique band in 4,800-4,600 cm⁻¹ region as shown on Figure 10. Therefore, if both regions are used 2-ethyl-1-hexene will not bias the ethylene or 1-octene results.

It was found that using the spectrum of 1-octene measured from pure 1-octene gave biased results, attributed to deviations from Beer's law. Therefore, a pure spectrum of 1-octene in the presence of Isopar E was estimated from spectra of samples containing Isopar E and 1-octene at concentrations of 10 to 20 wt % levels. The measured and estimated pure spectra for 1-octene and Isopar E are shown in Figure 12, in overlaid mode. The 1-octene spectrum in the presence of Isopar E appears to be shifted to higher wave numbers.

Figure 11: Spectrum of 10 wt % 1-Octene, 1-2wt % Ethylene (20 times enlarged) and Pure Isopar E in 6,080 to 6,150 cm^{-1} Region in Overlaid Format at Room Temperature and Pressure.

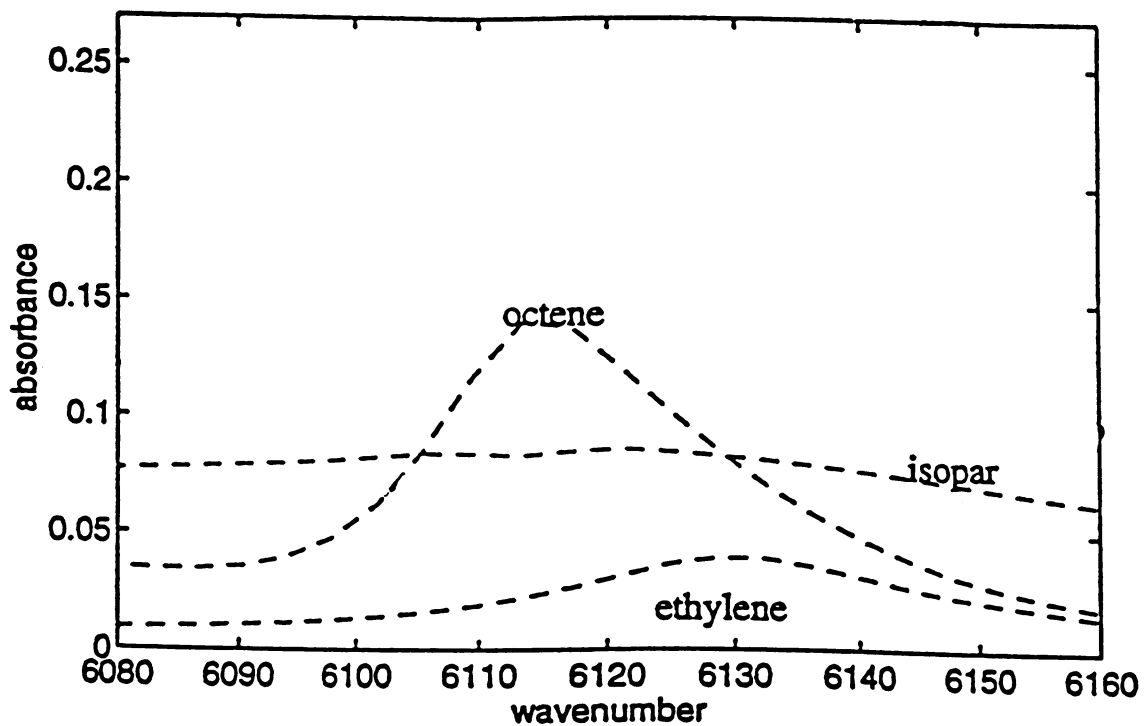
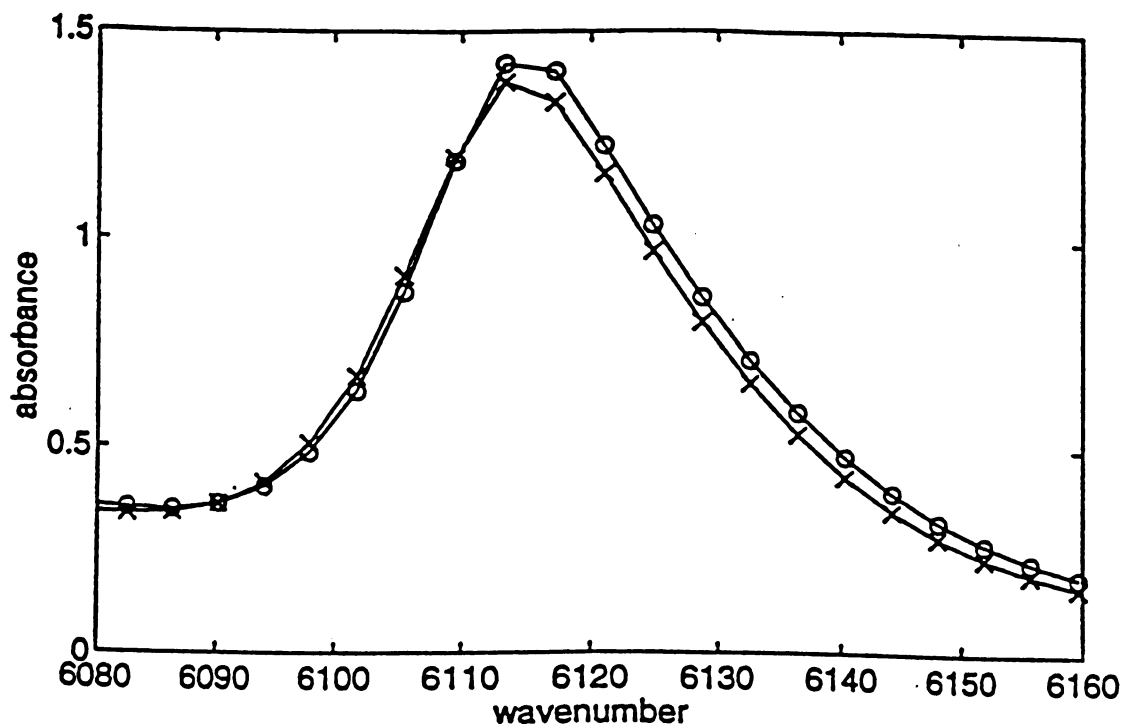


Figure 12: Measured and Estimated Pure Spectra for 1-Octene and Isopar E in 6,080 to 6,150 cm^{-1} Region in Overlaid Format at Room Temperature and Pressure.



Since an appropriate instrumental arrangement to obtain the pure spectra of ethylene and propylene was not available during the first part of the study, the ethylene spectrum was estimated by subtracting the Isopar E spectrum from the spectrum of the mixture. The error in estimation of this concentration could be as large as 1 wt % absolute. However, obtaining high accuracy was not one of the goals of the study at this stage.

Concentrations of standard mixtures were estimated using the CLS model. The CLS was chosen among the available linear regression techniques due to its simplicity (see discussion on comparison of multivariate calibration techniques in Chapter 2).

Numerical results for the analysis of multiple samples are given in Table 6 . The table provides the sample number, the true and predicted values of octene and ethylene, as well as the uncertainties associated with these predictions. The uncertainties are from the regression analysis, and increase as the noise in the data increases, or as the fit degrades. The samples indicated by an asterisk are the samples that were used to estimate the 1-octene and Isopar E spectra. For samples 12-19, the absolute errors in the 1-octene prediction ranged from -0.2 to 0.1%, with 1-octene levels ranging from 4.8 to 20%. The errors in the ethylene prediction were impossible to ascertain accurately, as there were large errors in the true amount of ethylene in the samples.

The uncertainties shown in Table 6 are a result of the least squares calculation and represent the confidence in the predicted concentrations. The uncertainties increase dramatically for the prediction of the 100% 1-octene samples, as these are not well described by the estimated spectra, due to deviations from Beer's law.

Table 6: Predicted Concentrations of 1-Octene and Ethylene.

#	True 1-Octene	Predicted 1-Octene	Delta (Difference)	True Ethylene	Predicted Ethylene	Delta (Difference)	Uncertainty in 1-Octene	Uncertainty in Ethylene
1	0	-0.3	0.3	0	0.0	0.0	0.1	0.0
2	0	-0.2	0.2	0	0.0	0.0	0.1	0.0
3	0	-0.3	0.3	0	0.1	-0.1	0.1	0.0
4	100	98.5	1.5	0	-2.3	2.3	1.5	0.7
5	100	98.0	2.0	0	-2.6	2.6	1.3	0.6
6	100	101.6	-1.6	0	-4.0	4.0	1.6	0.7
7	100	101.2	-1.2	0	-4.3	4.3	1.4	0.6
8‡	0	0.0	0.0	x	1.0	?	0.0	0.0
9	0	-0.2	0.2	x	1.0	?	0.1	0.0
10	0	-0.2	0.2	x	0.7	?	0.1	0.0
11	0	-0.3	0.3	x	1.3	?	0.1	0.0
12*	10	9.9	0.1	0	0.0	0.0	0.1	0.0
13*	20	20.1	-0.1	0	0.1	-0.1	0.0	0.0
14*	4.8	5.0	-0.2	0	0.0	0.0	0.0	0.0
15*	9.9	9.8	0.1	0	0.0	0.0	0.0	0.0
16*	15.4	15.4	0.0	0	-0.1	0.1	0.1	0.0
17	4.8	5.0	-0.2	x	1.1	?	0.0	0.0
18	9.9	9.9	0.0	x	1.2	?	0.0	0.0
19	15.4	15.5	-0.1	x	1.1	?	0.1	0.0

x True ethylene concentration around $1.5 \pm 1\% \text{ wt}$ ‡ Ethylene concentration defined to be 1.0 % wt. This was the pure spectrum used for ethylene. The true concentration is around $1.5 \pm 1\% \text{ wt}$. All ethylene predictions are relative to this.

? = Unknown value

* Samples used to estimate 1-octene and Isopar E spectra

Data shown in this table was generated by Mary Beth Seasholtz using MATLAB (Trademark of the Mathworks Inc.)

The calibration model is expected to change from room temperature and pressure conditions, to elevated temperature and pressure conditions, since the spectra of all of these compounds will be slightly different at elevated temperature and pressure. Therefore, this model is limited to room temperature and pressure conditions.

Summary

Distinguishable features for light alkenes in NIR region were established at room temperature and pressure. Light alkenes ranging from ethylene to 1-decene were selected for the determination and to study the effect of molecular structure. It was found that the first overtone of the asymmetric stretch of $=\text{CH}_2$ for light monoalkylated alkenes i.e. ethylene, propylene, 1-butene, shifts toward the lower energy which may be enough to distinguish and determine these compounds simultaneously in a mixture.

Additionally, the determination of mixtures containing small and larger molecules such as ethylene and 1-octene, ethylene and 1-hexene, or ethylene and 1-decene should be possible as was demonstrated with ethylene and 1-octene mixture in this study. Among the heavier members of the monoalkylated alkenes, the addition of a carbon atom to the molecule causes a slight shift in location of the first overtone of the asymmetric $=\text{CH}_2$ stretch towards lower energy. Therefore, this method may not be suitable to determine 1-pentene through 1-decene in a mixture simultaneously. Other alkylated light alkenes such as 1,1 dialkylated, cis and trans-dialkylated and trialkylated alkenes were evaluated to make sure that the technique is unique for the determination of the monoalkylated alkenes. 1,1 dialkylated alkenes were found to be an interference in the region of the

asymmetric $=\text{CH}_2$ stretch; however, they can be resolved if desired, by the use of the $4,750 \text{ cm}^{-1}$ region in the model. Cis, trans dialkylated and trialkylated alkenes do not interfere with the determination.

The first overtone of the asymmetric $=\text{CH}_2$ stretch of the monoalkyl group was used to build a model based on CLS regression. The reliability of the results was checked from the residual spectrum for the ethylene/1-octene example, obtained by subtracting the estimated spectrum from the measured spectrum. Determination error was expressed as predicted minus measured and, was less than 1% for the ethylene/1-octene analysis.

Chapter 4

IN SITU REAL-TIME DETERMINATION OF ALKENES BY FIBER OPTIC FT-NIR SPECTROSCOPY AT ELEVATED TEMPERATURES AND PRESSURES

In the second part of this research the effects of elevated temperature and pressure for the determination of light alkenes were investigated and calibration models were developed using high pressure, temperature apparatus. The ethylene and 1-octene system, evaluated during the feasibility study was investigated at elevated temperatures and pressures to provide continuity.

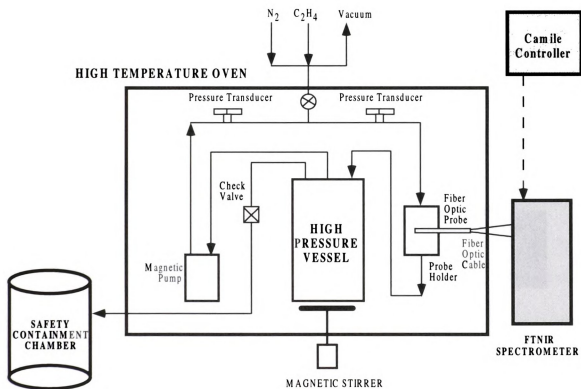
Considerable difficulties are involved in preparing well-known mixtures of the components to build calibration models for accurate quantitative determination at elevated temperatures and pressures. Consequently, for this particular work, *in situ* fiber optic probe technology was essential. A special apparatus was built to obtain the spectra of known concentration mixtures at varying temperatures and pressures. A high pressure vessel was modified to incorporate a fiber optic probe which was coupled to the FT-NIR spectrometer. The high pressure vessel was placed in an oven. Calibration standards were prepared gravimetrically and the concentration of the liquid phase was corrected for each temperature setting. Calibration models were built using partial least-squares (PLS) regression to predict the concentrations of these compounds at varying temperatures and pressures.

Experimental Procedures

A high pressure, temperature apparatus was constructed to obtain spectra of light alkenes in Isopar E at elevated temperatures and pressures. A block diagram of the set up illustrating the components of the system is given in Figure 13. The apparatus consists of a pressure vessel, and a circulation loop which incorporates the fiber optic probe holder assembly and a variety of pressure transducers. The circulation loop employs a magnetic circulation pump to recycle the contents of the vessel through the loop. Thus, the liquid phase is circulated through the fiber optic probe holder where the sample and spectrometer interface is provided. A magnetic stirrer is used for agitation within the vessel. The vessel and the circulation loop assembly, including the fiber optic probe holder, are placed inside a forced air oven.

The apparatus is controlled and data acquired by a Camile (Segion, Midland, MI) brand name data acquisition and control system. Camile is used in controlling the temperature set points of the oven, the operation of the circulation pump, and the speed of the agitator. Additionally, it is used to record all the experimental conditions.

Figure 13: Schematic Diagram of the High Temperature, Pressure Apparatus.



High Pressure, Temperature Apparatus

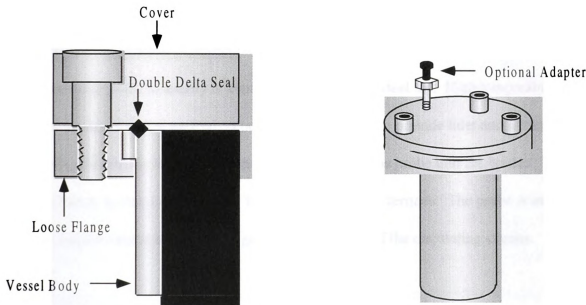
Pressure Vessel:

The apparatus incorporates an Autoclave Engineers (Erie, PA) Eze-Seal model 100 mL volume high pressure vessel ($P_{Limit} = 3000$ psig, $T_{Limit} = 315^{\circ}\text{C}$). The vessel consists of two parts: a top (cover) and the body. These two parts of the vessel are sealed together with a metal gasket (double delta seal) as shown in Figure 14. The top portion of the vessel provides several inlets and exits via dip pipes and other connections incorporating either high temperature and high pressure valves. All of these high temperature, pressure

connectors were welded to the line and a metal gasket was used for a seal between them.

Each time the vessel is removed from the system, these metal gaskets were replaced.

Figure 14: Schematic Diagram of the High Temperature, Pressure Vessel.



Expansion Containment Chamber

The high pressure vessel contains a safety relief valve rated at 2000 psi which is connected to a six liter, high pressure, stainless steel vessel (rated at 3000 psi). In case of an unexpected temperature increase or an unexpected reaction which would increase the pressure of the vessel above 2000 psi, the expansion would be contained in this chamber.

Head Space Assembly

The high pressure vessel is connected to a circulation loop consisting of a probe/holder assembly, circulation pump, and a variety of pressure transducers. The circulation loop

employs a Ruska brand name (Model 2330-802) magnetic circulation pump to recycle the contents of the vessel through the loop where the sample and spectrometer interface is located. The head space is also connected to a vacuum pump to evacuate the system when needed, and to a distributor assembly to discharge nitrogen and ethylene into the system.

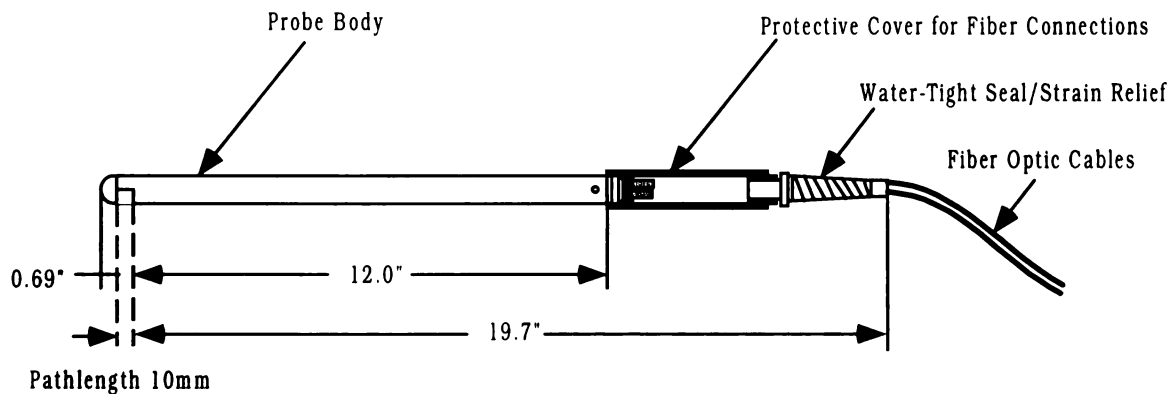
Fiber Optic Probe-Holder Assembly

The fiber optic probe assembly is a modified $\frac{3}{4}$ " stainless steel tee. High temperature, pressure connections are welded on both sides of the Tee to provide inlet and outlet ports; a $\frac{3}{4}$ " Swagelok fitting is welded on the third side to seal the probe into the holder. The probe attaches to this assembly with $\frac{3}{4}$ " Swagelok nut and ferrules. The probe is inserted into the holder such that the sample gap is in the middle of the circulating stream.

Single Sided Transmission Probe:

The Single Sided Transmission (SST) probe is manufactured by UOP/Guided Wave (El Dorado Hills, CA). It is a Visible/NIR transmission probe with the transmission slit on the side as shown in Figure 15. The probe internally contains a pair of 500 μm in diameter fibers to provide the light interface at the windows. All of the optics are installed in a $\frac{3}{4}$ inch O.D., 15 inch long 316 stainless steel body. Two sapphire windows, sealed by gold brazing, provide the sample interface. Two fiber optic connectors at the end of the probe connect the probe to the spectrometer and the detector via fiber optic cables.

Figure 15: Guided Wave Single Sided Transmission (SST) Probe.



The Guided Wave SST probe is available from the manufacturer in 2 mm, 5 mm, 10 mm and 20 mm fixed pathlengths. The optimum probe pathlength for the experimental concentrations of ethylene and 1-octene is chosen as 10 mm, deduced from the feasibility study. The fiber optic cables used to connect the SST probe to the interferometer and to the detector are 500 μm , low hydroxyl fibers supplied by SpecTran Specialty Optics. About 20 feet of fiber optic cable is used to connect the SST fiber optic probe and the spectrometer/detector set up. The fiber optic cable carries the light from the spectrometer to the probe and from the probe to the detector.

Pressure Measurement and Control

Pressure measurements are done with one of the following pressure transducers depending on the pressure of the system (Maximum 750 psi): MKS Model 315BA-

25,000 (0.1% accuracy), and GP:50 Model 331-RM-GP/GJ/GX (0.25% accuracy), or Setra C206 (0.13 % accuracy). Each transducer is calibrated against a digital pressure gauge with an accuracy of 0.01%. Pressure calibrations are performed at several pressures at each temperature set point. Before performing a calibration the pressure transducers are allowed to equilibrate for at least two hours at each temperature setting.

Forced Air Oven

A Hotpack (Philadelphia, PA) model 212034 forced-air oven is used with a 9.5 cubic feet internal volume. Oven walls are modified to establish several external connections such as vacuum lines, pressure transducer signal lines, magnetic stirring driver. This floor stand type oven has a 25"×22"×30" door which enables the removal of the pressure vessel conveniently and easy operations and modifications of the system. The solid-state electronics with multi-mode control option provides a remote access set point with an accuracy of $\pm 2^{\circ}\text{C}$ from the Camile data acquisition and control system. The internal oven temperature gradient below 200 °C is less than 0.9 °C. The Hotpack model 212034 oven contains a 4.4 watt 230V heating element with a 3 °C per min heating rate.

Temperature Measurement and Control

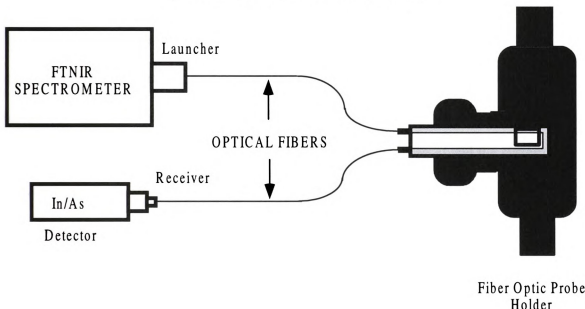
Temperature measurements are made with a Burns 12092 Platinum Resistance Thermometer (PRT) connected to a Hewlett-Packard HP34401A digital multimeter. This PRT is calibrated against another calibrated Fluke Model 2189A platinum resistance thermometer. Several PRT's are installed in the system to obtain the temperature of the head space, liquid phase and different locations of the oven.

|

FT-NIR Spectrometer and the detector:

The Diamond 20 model FT-NIR spectrometer manufactured by KVB/Analect (Pasadena, CA) is used in these experiments. The spectrometer is coupled with a Single Sided Transmission (SST) fiber optic probe manufactured by UOP Guided Wave via optical fibers as illustrated in Figure 16. The Diamond 20 FT-NIR system has a 1.5 cm^{-1} transect IV hermetically sealed interferometer. NIR CaF₂ optics are used for the 12,000 to 1,200 cm^{-1} region. The spectrometer includes an internal source and all optical control electronics. It is controlled by a 66 MHz 486 based data system operated under MS DOS/Windows 3.1. The spectrometer and the data station are interfaced with an interface card provided by the manufacturer. The system includes the manufacturer's FX-70, DOS based software program, and FX-80, Windows 3.1 based software for the control and operation of the analyzer.

Figure 16: Schematic Diagram of the FT-NIR Set-up; Spectrometer, Detector, Fiber Optic Probe, and Probe Holder Assembly.



The spectrometer is coupled with a three stage, Indium-Arsenide (InAS), SP-2426 model detector repackaged and sold by KVB/Analect. The detector is cooled with a thermoelectric cooler. Radiation is carried from the spectrometer to the fiber optic probe and back to the detector with fiber optic cables. A fiber optic receiving module is used at the interferometer outlet and at the detector inlet.

The spectrometer is coupled to the Camile process control computer by an input/output (I/O) hardware. Via this connection, the data collection by the FT-NIR spectrometer is triggered whenever the system reaches equilibrium under the desired conditions. An analog signal (4-20 ma) from Camile is sent to the FT-NIR PC to initiate the data collection.

Determination of Vessel and Head Space Volume

In order to determine the total volume of the apparatus (vessel plus the head space) a calibration vessel with a volume of 144.37 ml is used. This calibration vessel is connected to the system and to the pressure transducers via a specially designed valve assembly. The calibration vessel is pressurized and its pressure is measured at constant temperature. By opening the valve connecting the calibration vessel and the system, the entire system is pressurized and the new pressure is measured. Since the initial volume and the pressure are known and the second pressure is measured, the second volume is calculated from: $V_2 = P_1 V_1 / P_2$ at constant temperature. During the course of the experiments several modifications were made to the head space assembly which required the determination of the system volume each time. The system volume used in the experiments ranged from 249 ml to 264 ml.

Experimental Design

The number of standards needed to develop a representative calibration model for multivariate calibration techniques is an important factor in experimental design. The concentration range of the standards and the similarity of the standards to the unknown sample matrix are also factors that contribute to the accuracy of the model. The concentration range of ethylene was chosen as 0.5 to 7.5 percent weight in solution, and the range of 1-octene was selected as 2 to 30 percent weight in Isopar E for these experiments. PLS models require the number of standards to be higher than the number of variables in the system. However, the more data , the higher the confidence in the

analysis and in the statistics. Since the concentration range of 1-octene was at least twice the concentration range of ethylene, a rectangular two factorial experimental design was used to represent the concentration range of the each component. For 1-octene a 4 level, and for ethylene a 3 level concentration design was configured. Thus, the experiments consisted of three concentration levels of ethylene and four concentration levels of 1-octene. Each run was performed at five different temperature (25, 60, 85, 110, 140 °C) since the temperature constitutes another factor in the experimental design. Table 7 shows the experimental design layout and the target concentrations for each run. The same table also lists the actual concentrations (liquid plus gas phase) and temperatures. The experimental difficulties in addition of ethylene into the system resulted in slightly different concentrations for the components than the targeted concentrations. However, achieving actual concentrations around the targeted concentrations was sufficient for the calibration purposes. Several runs were aborted due to experimental or equipment problems. Ten to twelve spectra were collected for every run at each temperature once equilibrium is established

Table 7: Experimental Design Versus Actual Experiments

EXPERIMENTAL DESIGN			ACTUAL EXPERIMENTS				
TARGETED CONCENTRATIONS*			ACTUAL CONCENTRATIONS				
RUN#	1-OCTENE	ETHYLENE	TEMPERATURES °C	RUN#	1-OCTENE	ETHYLENE	TEMPER. °C
WT %	WT %	(T1,T2,T3,T4,T5)		WT %	WT %	WT %	(T1,T2,T3,T4,T5)
1	0.00%	0.00%	25, 60, 85, 110, 140	7	0.00%	6.69%	85,110,140
2	0.00%	0.50%	25, 60, 85, 110, 140	08A	0.00%	1.38%	85,110,140
3	0.00%	3.00%	25, 60, 85, 110, 140	08B	0.00%	10.08%	85,110,140
4	0.00%	10.00%	25, 60, 85, 110, 140	9	2.00%	0.00%	85,110,140
5	2.00%	0.00%	25, 60, 85, 110, 140	10	7.00%	0.00%	85,110,140
6	8.00%	0.00%	25, 60, 85, 110, 140	11	15.00%	0.00%	60, 85, 110, 140
7	16.00%	0.00%	25, 60, 85, 110, 140	12	30.00%	0.00%	60, 85, 110, 140
8	30.00%	0.00%	25, 60, 85, 110, 140	13	1.98%	1.23%	60, 85, 110, 140
9	2.00%	0.50%	25, 60, 85, 110, 140	14	1.92%	3.90%	25, 60, 85, 110, 140
10	2.00%	3.00%	25, 60, 85, 110, 140	15	1.84%	7.95%	25, 60, 85, 110, 140
11	2.00%	10.00%	25, 60, 85, 110, 140	16	6.72%	4.01%	25, 60, 85, 110, 140
12	8.00%	0.50%	25, 60, 85, 110, 140	17	6.89%	1.64%	25, 60, 85, 110, 140
13	8.00%	3.00%	25, 60, 85, 110, 140	18	6.50%	7.13%	25, 60, 85, 110, 140
14	8.00%	10.00%	25, 60, 85, 110, 140	21	17.07%	5.17%	25, 60, 85, 110, 140
15	16.00%	0.50%	25, 60, 85, 110, 140	22	17.79%	1.19%	25, 60, 85, 110, 140
16	16.00%	3.00%	25, 60, 85, 110, 140	23	17.23%	4.26%	25, 60, 85, 110, 140
17	16.00%	10.00%	25, 60, 85, 110, 140	24	26.03%	13.23%	25, 60, 85, 110, 140
18	16.00%	0.50%	25, 60, 85, 110, 140	25	29.52%	1.58%	25, 60, 85, 110, 140
19	30.00%	3.00%	25, 60, 85, 110, 140	26	28.22%	5.93%	25, 60, 85, 110, 140
20	30.00%	10.00%	25, 60, 85, 110, 140	27	0.00%	8.64%	25, 60, 85, 110, 140
				28	98.53%	1.47%	25, 60, 85, 110, 140

* Balance is Isopar E

Experiments for the Determination of Pressure Effects on Spectra

Since the experiments are run at as high as 140 °C, the system pressure is expected to reach several hundred psi due to the vapor pressure of ethylene, with the exact pressure dependent on the ethylene concentration in the solution. Preliminary experiments were conducted to determine the effects of pressure on the spectroscopic bands of interest. Separate runs were prepared with 1-octene in Isobar E and ethylene in Isobar E at constant temperature where the system was pressurized with nitrogen at several different pressures (300 psi, 400 psi, 485 psi). Spectra were collected under each set of conditions.

FT-NIR Calibration Procedure

Several standards were prepared for the ethylene, 1-octene system targeting the experimental design. The actual ethylene concentrations ranged from 0.5 wt % to 13 wt % and 1-octene ranging from 0.5 wt % to 30 wt %. These standards were prepared gravimetrically in the high pressure vessel at room temperature. The amount of each component added was determined by mass difference. The vessel was first evacuated via the vacuum pump, valves were closed and disconnected from the apparatus. After weighing the empty vessel, the 1-octene/Isopar E mixture, prepared in advance, was loaded into the vessel using a 100 ml glass syringe. A 15 gauge syringe needle was modified to fit to the high temperature, pressure connector of the vessel inlet. The vessel was weighed again after degassing it under vacuum for several minutes. Next ethylene was charged into the vessel, from a small (5 lb) cylinder via a distribution system allowing the evacuation of the lines from cylinder to the vessel. After the ethylene addition, the vessel was weighed and reconnected to the apparatus.

The apparatus was heated and allowed to equilibrate at the required temperature set point.

When temperature equilibrium was reached, the vessel pressure remained constant. At each temperature set point, 10-12 spectra were obtained of the liquid phase. The system pressure and temperature at equilibrium were recorded in order to calculate the vapor phase composition, which was used to correct the liquid phase concentration of each component.

Data Analysis and Results

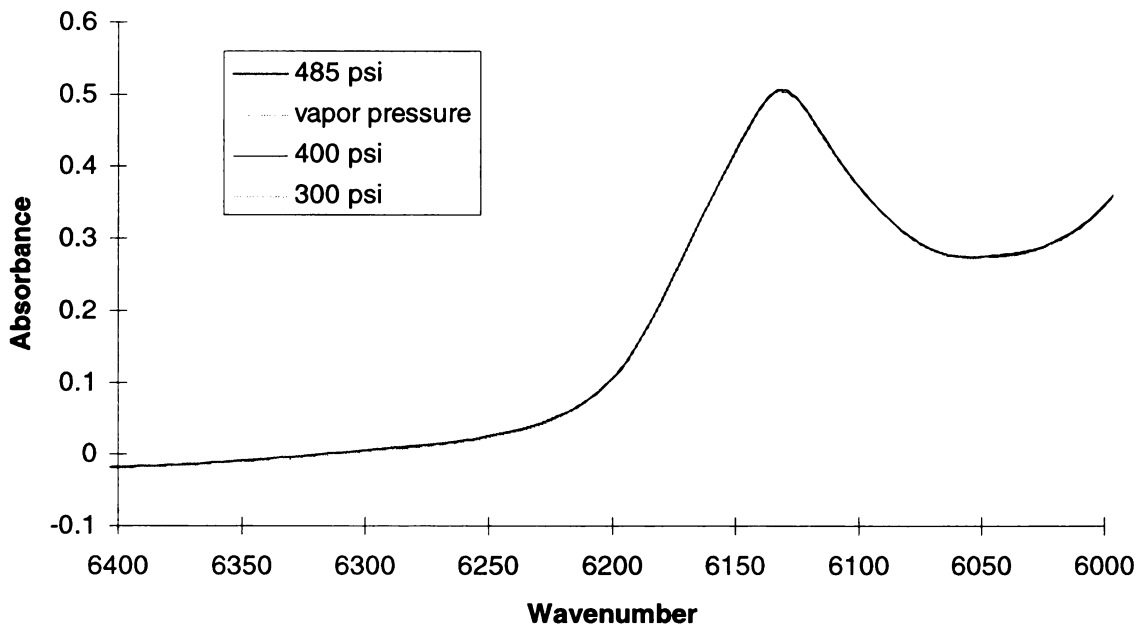
Effects of Pressure on Spectra

According to theory, the effects of pressure in vibrational spectroscopy are significant when there is a phase change and/or a change in the symmetry group of the compound due to the applied pressure. Either situation requires application of significant amounts of pressure. The experimental conditions used during this study did not cause phase changes or lead to a change in the symmetry group. The system pressure originates from the vapor pressure of ethylene at the set-point temperature. At the highest concentrations of ethylene (13 wt % at room temperature) and the highest temperature set-points (140 °C), the vapor pressure of the system is less than 750 psi. The supercritical temperature (T_c) and pressure (P_c) of ethylene are 10 °C and 52.2 atm (762 psi), respectively. Since all experimental temperatures are above the supercritical temperature of ethylene, ethylene is in the supercritical phase in this matrix. Furthermore, monoalkylated alkenes, under the experimental conditions used, are in the liquid phase and, thus, no phase

transitions are expected. Also, according to theory, high pressures (~14,000 psi) are necessary before starting to change the symmetry group of molecules. Hence, no change in the first overtone of the asymmetric $=\text{CH}_2$ stretch of the monoalkylated alkenes is predicted.

Results of the experiments correlate well with predictions. Figure 17 shows the spectra of 6.31 wt % ethylene in Isobar E (at room temperature) in the 6100 cm^{-1} region at several different pressures. If any effects of pressure on band shape or frequency shifts do occur in this system it would be most observable for ethylene. As seen in Figure 17, spectra of ethylene solutions collected at different pressures showed no difference from each other in the region where the first overtone of the asymmetric stretch of $=\text{CH}_2$ is monitored. Pressures above the vapor pressure of ethylene were obtained by pressuring the system with nitrogen at constant temperature. After these experiments, the remainder of the calibration was carried out at system pressure.

Figure 17: Effect of Pressure on Spectra of Ethylene in Isopar E.

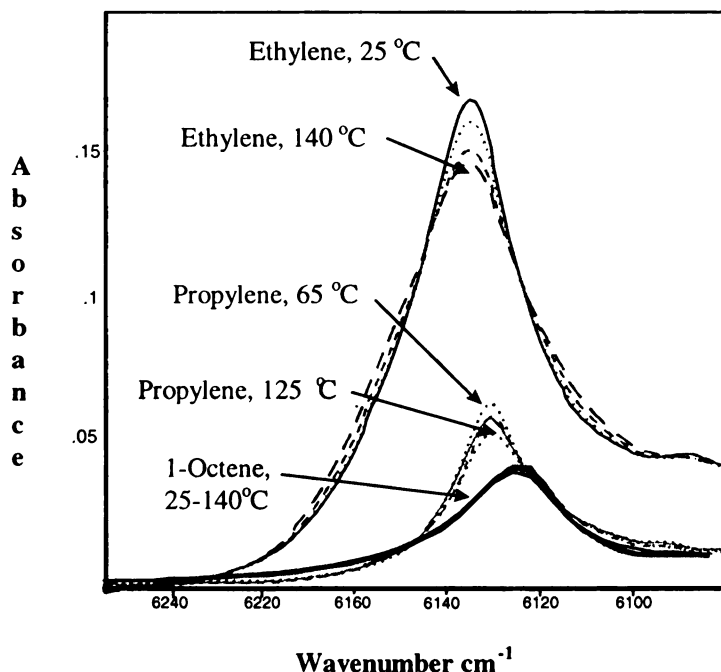


Effects of Temperature on Spectra

The determination of the effect of temperature on the C-H stretch in NIR range for ethylene and monoalkylated ethylenes was accomplished by varying the temperature from room temperature to 140°C (25°C, 60°C, 85°C, 110°C, 140°C) for ethylene, propylene and 1-octene. A known concentration of ethylene in Isobar E was prepared and spectra were collected at these 5 different temperatures. The spectra were corrected for concentration changes due to the temperature/density changes. When these bands of interest were overlaid, significant differences were observed on band shape. Mainly, bands become broader and showed decreased peak intensity at elevated temperatures. Similar experiments were done with propylene and 1-octene in Isobar E. The effect

observed on the band of interest by temperature gets smaller and becomes less significant with increasing chain length. The effect on band shape is much more significant for ethylene than is for 1-octene. These effects are shown in Figure 18 for ethylene, propylene and 1-octene for the first overtone of the asymmetric stretch of $=\text{CH}_2$.

Figure 18: Estimated Pure Ethylene, Propylene, and 1-Octene Spectra as a Function of Temperature.



Calculation of Liquid Phase Concentration at Each Temperature Setting

Due to thermal expansion, a volume for expansion of the liquid needs to be left in the vessel where the liquid is heated. If the head space volume is significant relative to the total volume, the partitioning of the compounds between the liquid and the gas phase will

be important affecting the concentration of the liquid phase. When the vessel is heated to higher temperatures, there will be more number of molecules in the gas phase than there are at lower temperatures. Consequently, the concentration of the liquid phase will be changed at each temperature setting. This is particularly significant with volatile compounds such as ethylene.

In order to account for this change, and to be able to calculate the liquid phase concentrations accurately, the concentration of the gas phase was estimated using experimental parameters such as temperature and the pressure of the head space and the vapor pressures of the compounds from physical property tables. Then, the calculated vapor phase amount was subtracted from the initial concentration of the liquid.

The accuracy of the calibration model will directly be related to the accuracy of the standards and the accuracy of the experiments. In order to calculate the head space concentration, head space volume had to be calculated. This requires an estimation of the liquid volume and the solution density at each temperature set point since

$$V_{\text{vapor phase}} = V_{\text{total}} - V_{\text{liquid}}$$

Vapor phase concentration is calculated according to the Ideal Gas Law by using each component's partial pressure. The number of moles of each component in the vapor phase is (n_i^V):

$$n_i^v = \frac{P_i^v V^v}{RT} \quad [16]$$

The partial pressure of the components in the vapor phase (P_i^v) for 1-octene and Isobar E are determined from the pure component vapor pressure of the compound (P_i^o) at that temperature, by using the Raoult's Law. Since the total vapor phase pressure is measured and known, ethylene's partial pressure can be determined from the difference according to the following equation.

$$P_{C2} = P_{Meas}^{Tot} - P_{C8} - P_{IsoparE} \quad [17]$$

Pure component vapor pressures of 1-octene and Isobar E at room temperature were obtained from physical property tables and corrected for temperature by using the Antoine equation.^{188,189}

$$\log(P) = A - \frac{B}{T + C} \quad [18]$$

Antoine constants are given in the following Table 8 for 1-octene and Isobar E.¹⁸⁸

Table 8: Antoine Constants for 1-octene and Isopar E

	A	B	C
Isopar E	3.40926	1185.31	222.048
1-octene	4.05935	1358.21	213.311

Using the pure component vapor pressure, the partial pressures of 1-octene and Isopar E are given by Raoult's Law:

$$P_i = x_i P_i^{\circ} \quad [19]$$

where x_i = the liquid mole fraction of component i.

In addition, the vapor or head space volume is required (V^V) in equation [16]. This is determined by subtracting the liquid volume which is sum of the volume of each liquid component, V_i^L , from the total vessel volume, V^T .

$$V^V = V^T - \sum n_i^L V_i^L \quad [20]$$

Where V_i = the molar volume of component i in cc/mol (or partial molal volume for ethylene),

In order to find the liquid volume at each temperature set point, the liquid phase solution density must be calculated. An overall solution density is obtained by dividing the total molar mass of the material by the overall molar volume. The overall molar volume of the solution is the sum of the molar volumes of each component, the latter are calculated by

dividing the masses of each component (number of moles of each component times their molecular weight) by their pure component densities. The pure component density is calculated at each set point temperature by equation [21]:

$$\rho_i = A_i + B_i T \quad [21]$$

where

ρ_i = the density of component i in g/cc,

T = the temperature in degrees °C.

A_i = Experimental constants (literature values) for component i.

B_i = Experimental constants (literature values) for component i.

Literature values of A_i , B_i and M_i (molecular weight for component i) are given in Table 9 for 1-octene, Isobar E and ethylene:^{188,189}

Table 9: Literature Values for Constants in Temperature Dependent Density Equation

	M_i	A_i	B_i
Isopar E	123.00	0.73468	-8.245E-4
1-octene	112.215	0.73502	-9.167E-4
Ethylene	28.054	0.46757	0

After obtaining the overall molar volume, an overall density can be calculated by dividing the overall mass by the overall molar volume. This density can be used for calculation of the liquid volume by dividing the total mass originally loaded in the vessel by the overall density (assuming that all the components are in the liquid phase). After calculating this approximate liquid phase volume, the volume of the vapor phase and the number of

moles in the vapor phase can be calculated according to equations [16] and [21]. The number of the moles in liquid phase is equal to the difference between the total number of moles (n_i^T) and the number of moles in the vapor phase (n_i^V).

$$n_i^L = n_i^{Tot} - n_i^V \quad [22]$$

from this the mole fraction of the solution can be calculated by equation [23]:

$$x_i^L = \frac{n_i^L}{\sum n_i^L} \quad [23]$$

This calculation process summarized in Eq. [16]-[23] is repeated until the calculated system pressure (P_i^{Tot}) which is equal to:

$$P_i^{Tot} = P_{C2} + P_{C8} + P_{IsoparE} \quad [24]$$

converges with the measured system pressure (P_{Meas}^{Tot}). It was found that the iteration converged after one pass. An example of this calculation for one of the runs of the experiment is shown in Table 10. For this calculation process, the system is assumed to exhibit ideal behavior (fugacity is equal to the partial pressure).

Table 10: Excel Spread Sheet Showing the Liquid Phase Concentration Calculations for Run # 26

RUN#26		CORR	C8	ISOPAR	C2	SUM	DENSITY	VOLUME	VOLUME	VAPOR	VAPOR	C8	ISOPAR	C2	
P15SET	MKSPT1	TYES1	P_ATM	VP_ATM	P0_ATM	Po_ATM	V	g/mL	V_L	V_L	v_MOL	v_MOL	v_MOL	v_MOL	
110.82	117.05	22.27	117.1	7.97	0.0197	0.0361	0.0050	0.0194	7.95	144.4	0.6940	0.1150	0.1493	0.0003	
116.81	122.61	26.37	122.6	8.34	0.0247	0.0434	0.0062	0.0233	8.31	145.0	0.6909	0.1155	0.1488	0.0004	
164.07	167.10	59.80	166.1	11.30	0.1220	0.1599	0.0307	0.0857	11.18	150.5	0.6656	0.1199	0.1444	0.0016	
164.07	167.23	59.86	166.2	11.31	0.1223	0.1602	0.0308	0.0859	11.19	150.5	0.6655	0.1200	0.1444	0.0016	
164.07	167.35	59.91	166.3	11.32	0.1225	0.1605	0.0309	0.0861	11.20	150.6	0.6655	0.1200	0.1444	0.0016	
200.02	201.32	84.08	199.1	13.55	0.3106	0.3446	0.0783	0.1848	13.29	154.8	0.6470	0.1234	0.1409	0.0009	
200.35	201.44	84.24	199.2	13.56	0.3124	0.3462	0.0787	0.1857	13.29	154.9	0.6469	0.1234	0.1409	0.0009	
200.35	201.44	84.25	199.2	13.56	0.3126	0.3464	0.0788	0.1858	13.29	154.9	0.6469	0.1234	0.1409	0.0009	
238.62	237.24	108.06	233.5	15.89	0.6809	0.6886	0.1716	0.3583	15.36	159.4	0.6287	0.1270	0.1373	0.00075	
238.62	237.24	108.45	233.6	15.90	0.6870	0.6895	0.1731	0.3559	15.37	159.4	0.6284	0.1270	0.1373	0.00075	
238.62	237.24	108.45	233.5	15.89	0.6889	0.6889	0.1736	0.3567	15.36	159.4	0.6284	0.1270	0.1373	0.00076	
297.53	280.89	136.86	274.8	18.70	1.5160	1.2787	0.3820	0.6859	17.63	165.2	0.6065	0.1316	0.1327	0.00151	
296.53	279.92	137.01	273.9	18.64	1.5216	1.2826	0.3834	0.6880	17.57	165.2	0.6064	0.1317	0.1327	0.00151	
															0.06924
<i>P15SET is the readout of the first pressure transducer</i>															
<i>TYES1 is the readout of the second pressure transducer</i>															
<i>CORR P, PSA is corrected pressure according to the calibration of the pressure transducer (y=mx+n) x=readout of MKSPT1</i>															
<i>P_ATM is corrected pressure in units of atm.</i>															
<i>C8 VP_ATM is the vapor pressure of C8 at the set point temperature calculated by using Antoine Constants according to Log(p)=A-B/(T+C)</i>															
<i>ANTOINE CONSTANTS ATM, C, for IsoparE and 1-Octene are:</i>															
<i>ISOPARE VP_ATM is the vapor pressure of IsoparE calculated similar to C8</i>															
<i>C8 Po_ATM is the partial pressure of C8 =(vp of C8)/partial pressure of IsoparE</i>															
<i>ISOPARE Po_ATM is the partial pressure of IsoparE = (vp of IsoparE)/partial pressure of IsoparE</i>															
<i>C2 Po_ATM is the partial pressure of C2. It is equal to Partial pressure of C8/(partial pressure of IsoparE)</i>															
<i>SUM of the molar volume of the components (C2,C8, IsoparE) obtained from sum of the each components molar mass devided by its density</i>															
<i>DENSITY of the mixture obtained by the molar mass devided by the total molar volume</i>															
<i>VOLUME of the liquid phase (Liter) = total mass of the original liquid divided by density</i>															
<i>VAPOR C8 MOL is the # of moles of 1-octene in vap. phase obtained by using state of the gas equation (par. pres. of the C8 + vap. phase volume)/0.8206°TK)</i>															
<i>VAPOR ISOPAR MOL is the # of moles of IsoparE in vap. phase obtained by using state of the gas equation (par. pres. of the IsoparE vap. phase volume)/0.8206°TK)</i>															
<i>VAPOR C2 MOL is the # of moles of C2 in vap. phase obtained by using state of the gas equation (partial pressure of the C2* vap. phase volume)/0.8206°TK)</i>															
<i>For the density equation D=A+B/T</i>															
MASS, g	WT%							MOLES	MOLE FRACTION						
C8/ISOPA	75.1	30.00	C2	5.93%	4.73			0.1686	0.2116	B					
C2	4.73	0.00	C8	28.22%	22.53			0.2008	0.2220	28.2764					
			ISOPAR E	65.85%	52.57			0.4274	0.5364	65.9782	C8	0.73502	-8.25E-04		
VESSEL VOLUME	264.32ml		TOTAL	100.00%	79.83			0.7988	1.0000	100.1910	C2	0.46757	-9.17E-04		

Table 10 (Cont.): Excel Spread Sheet Showing the Liquid Phase Concentration Calculation for Run#26

The results of the calculations for each run are tabulated and the corrected liquid phase concentrations (in mole fraction) for each component are given in Table 11 (standards containing ethylene and Isopar E), in Table 12 (standards containing 1-octene and Isopar E), and in Table 13 (standards containing all three components). Additionally, calculated liquid phase concentrations are plotted at each temperature and shown in **Figure 19**.

The Excel spreadsheets showing the calculations of liquid phase concentrations of each run are given in Appendix B Tables B1 through B20.

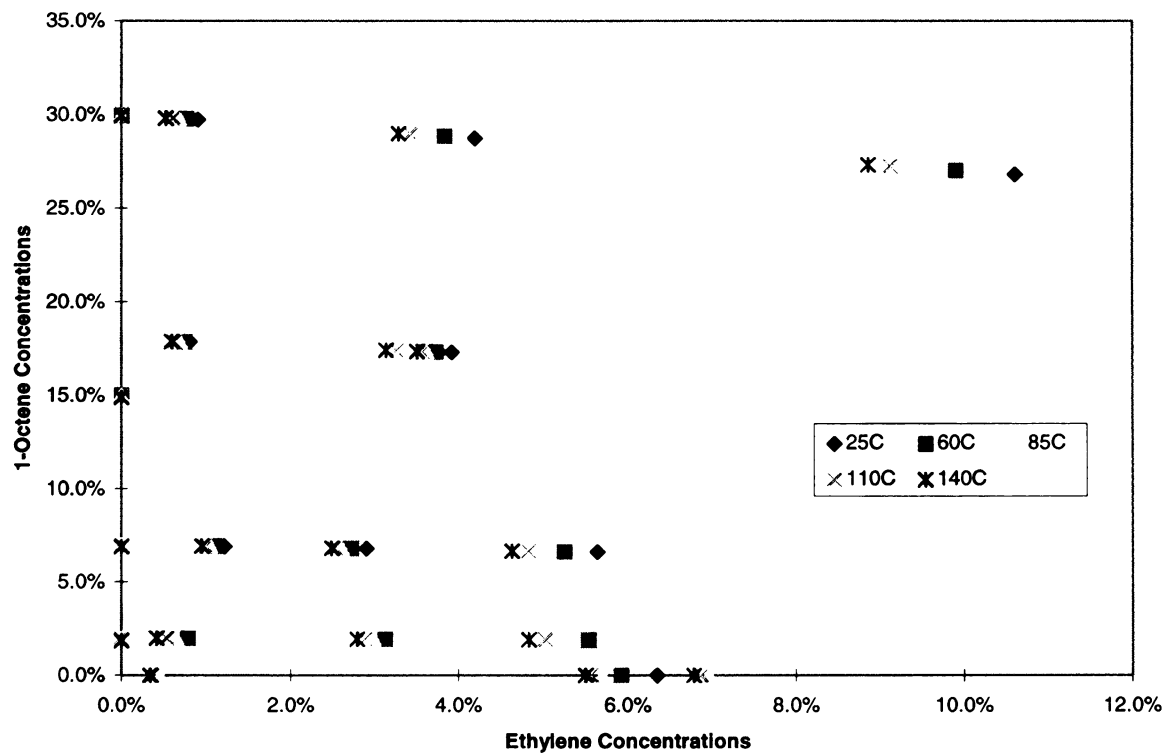
Table 11: Concentrations of Liquid Phase for Standards Containing Ethylene in 1-Octene, or Isopar E

Table 12: Concentrations of Liquid Phase for Standards Containing 1-Octene in Isopar E

Table 13: Concentrations of Liquid Phase for Standards Containing Ethylene, 1-Octene, and Isopar E.

SUMMARY OF C2 IN OCTENE/ISOPAR STUDIES												
FILE	T C	P, PSIA	ORIGINAL			EQUILIBRIUM			EQUILIBRIUM			MOL F
			Liquid	C8	ISOPAR	Liquid	C2	C8	ISOPAR	Liquid	C2	C8
			C2	C8	ISOPAR	C2	C8	ISOPAR	C2	C8	ISOPAR	MOL F
RUN#13	59.94	37	1.23%	1.98%	96.80%	0.78%	1.98%	97.23%	0.0334	0.0212	0.9454	
RUN#13	84.65	54	1.23%	1.98%	96.80%	0.65%	1.98%	97.38%	0.0278	0.0213	0.9509	
RUN#13	108.86	72	1.23%	1.98%	96.80%	0.53%	1.98%	97.48%	0.0229	0.0214	0.9557	
RUN#13	137.68	97	1.23%	1.98%	96.80%	0.41%	1.98%	97.60%	0.0179	0.0215	0.9607	
RUN#14	59.92	66	3.90%	1.92%	94.18%	3.12%	1.94%	94.94%	0.1236	0.0192	0.8573	
RUN#14	84.64	87	3.90%	1.92%	94.18%	2.98%	1.94%	95.07%	0.1187	0.0193	0.8620	
RUN#14	108.73	110	3.90%	1.92%	94.18%	2.88%	1.94%	95.18%	0.1150	0.0194	0.8657	
RUN#14	137.36	140	3.90%	1.92%	94.18%	2.79%	1.94%	95.27%	0.1116	0.0194	0.8690	
RUN#15	59.92	239	7.95%	1.84%	90.21%	5.54%	1.89%	92.57%	0.2041	0.0174	0.7785	
RUN#15	84.68	269	7.95%	1.84%	90.21%	5.26%	1.90%	92.85%	0.1953	0.0176	0.7871	
RUN#15	109.08	338	7.95%	1.84%	90.21%	5.03%	1.90%	93.07%	0.1881	0.0178	0.7942	
RUN#15	137.54	395	7.95%	1.84%	90.21%	4.83%	1.90%	93.27%	0.1818	0.0179	0.8004	
RUN#16	29.12	89	4.01%	6.72%	89.28%	2.90%	6.80%	90.30%	0.1152	0.0674	0.8173	
RUN#16	59.99	118	4.01%	6.72%	89.28%	2.72%	6.81%	90.47%	0.1085	0.0680	0.8235	
RUN#16	84.87	144	4.01%	6.72%	89.28%	2.61%	6.82%	90.57%	0.1044	0.0683	0.8273	
RUN#16	109.20	171	4.01%	6.72%	89.28%	2.53%	6.82%	90.65%	0.1016	0.0685	0.8299	
RUN#16	138.02	205	4.01%	6.72%	89.28%	2.49%	6.82%	90.69%	0.1000	0.0685	0.8315	
RUN#17	25.78	33	1.64%	6.89%	91.48%	1.22%	6.92%	91.87%	0.0509	0.0723	0.8767	
RUN#17	59.89	48	1.64%	6.89%	91.48%	1.11%	6.92%	91.98%	0.0467	0.0727	0.8806	
RUN#17	84.66	60	1.64%	6.89%	91.48%	1.05%	6.93%	92.02%	0.0441	0.0729	0.8831	
RUN#17	109.02	75	1.64%	6.89%	91.48%	0.98%	6.93%	92.09%	0.0415	0.0730	0.8854	
RUN#17	137.86	94	1.64%	6.89%	91.48%	0.95%	6.92%	92.13%	0.0399	0.0731	0.8870	
RUN#18	25.71	157	7.13%	6.50%	86.37%	5.64%	6.61%	87.75%	0.2065	0.0605	0.7330	
RUN#18	59.87	222	7.13%	6.50%	86.37%	5.25%	6.63%	88.12%	0.1944	0.0614	0.7441	
RUN#18	84.72	270	7.13%	6.50%	86.37%	5.02%	6.65%	88.33%	0.1872	0.0620	0.7508	
RUN#18	108.88	319	7.13%	6.50%	86.37%	4.83%	6.67%	88.51%	0.1809	0.0624	0.7557	
RUN#18	137.73	380	7.13%	6.50%	86.37%	4.63%	6.67%	88.70%	0.1746	0.0629	0.7626	
RUN#21	24.77	117	5.17%	17.07%	77.76%	3.92%	17.30%	78.78%	0.1495	0.1650	0.6655	
RUN#21	59.92	166	5.17%	17.07%	77.76%	3.60%	17.36%	79.05%	0.1385	0.1671	0.6944	
RUN#21	84.67	201	5.17%	17.07%	77.76%	3.41%	17.39%	79.20%	0.1322	0.1683	0.6985	
RUN#21	108.69	238	5.17%	17.07%	77.76%	3.28%	17.41%	79.33%	0.1268	0.1683	0.7039	
RUN#21	137.47	281	5.17%	17.07%	77.76%	3.13%	17.42%	79.45%	0.1222	0.1701	0.7077	
RUN#22	37.59	33	1.19%	17.79%	81.02%	0.81%	17.86%	81.34%	0.0339	0.1874	0.7787	
RUN#22	59.88	43	1.19%	17.79%	81.02%	0.74%	17.87%	81.39%	0.0313	0.1879	0.7808	
RUN#22	84.35	54	1.19%	17.79%	81.02%	0.69%	17.88%	81.43%	0.0290	0.1883	0.7826	
RUN#22	108.64	68	1.19%	17.79%	81.02%	0.63%	17.88%	81.48%	0.0267	0.1888	0.7846	
RUN#22	137.24	86	1.19%	17.79%	81.02%	0.59%	17.87%	81.53%	0.0251	0.1889	0.7860	
RUN#23	25.74	42.9	4.28%	17.23%	78.51%	3.77%	17.32%	78.91%	0.1444	0.1660	0.6896	
RUN#23	60.02	58.4	4.28%	17.23%	78.51%	3.68%	17.34%	78.98%	0.1412	0.1666	0.6922	
RUN#23	84.49	71.4	4.28%	17.23%	78.51%	3.62%	17.35%	79.03%	0.1393	0.1670	0.6938	
RUN#23	108.81	86.8	4.28%	17.23%	78.51%	3.57%	17.36%	79.08%	0.1374	0.1673	0.6953	
RUN#23	137.33	109.6	4.28%	17.23%	78.51%	3.50%	17.35%	79.14%	0.1353	0.1675	0.6971	
RUN#24	26.78	277	13.23%	26.03%	60.74%	10.60%	26.82%	62.58%	0.3368	0.2123	0.4519	
RUN#24	59.89	390	13.23%	26.03%	60.74%	9.90%	27.03%	63.07%	0.3189	0.2177	0.4634	
RUN#24	84.55	476	13.23%	26.03%	60.74%	9.46%	27.16%	63.37%	0.3081	0.2212	0.4707	
RUN#24	108.59	556	13.23%	26.03%	60.74%	9.13%	27.26%	63.61%	0.2997	0.2238	0.4765	
RUN#24	137.33	644	13.23%	26.03%	60.74%	8.88%	27.33%	63.81%	0.2990	0.2258	0.4812	
RUN#25	25.74	42.5	1.58%	29.52%	68.89%	0.90%	29.73%	69.37%	0.0373	0.3077	0.6550	
RUN#25	60.02	58.0	1.58%	29.52%	68.89%	0.77%	29.78%	69.46%	0.0319	0.3095	0.6586	
RUN#25	84.49	71.0	1.58%	29.52%	68.89%	0.68%	29.80%	69.52%	0.0286	0.3105	0.6609	
RUN#25	108.81	86.4	1.58%	29.52%	68.89%	0.61%	29.81%	69.59%	0.0254	0.3115	0.6631	
RUN#25	137.33	109.2	1.58%	29.52%	68.89%	0.52%	29.81%	69.67%	0.0219	0.3123	0.6659	
RUN#26	26.37	122.6	5.93%	28.22%	66.85%	4.20%	28.74%	67.08%	0.1574	0.2693	0.5733	
RUN#26	59.91	166.3	5.93%	28.22%	66.85%	3.83%	28.86%	67.31%	0.1452	0.2733	0.5816	
RUN#26	84.25	199.2	5.93%	28.22%	66.85%	3.61%	28.92%	67.47%	0.1378	0.2756	0.5866	

Figure 19: Corrected Liquid Phase Concentrations at Each Temperature for All Runs.



Calibration Models

The most popular chemometrics method for quantitative analysis, partial (PLS) least squares regression has been investigated for the determination of light alkenes at elevated temperatures and pressures. The classical least squares has been the choice earlier in proving the feasibility of the work due to its simplicity. However, partial least squares is needed for modeling the data obtained at elevated temperatures (see discussions on multivariate calibration techniques in Chapter 2). The goal in this regression technique is to find a mathematical relation between two data sets. In spectroscopy one of these data sets represents concentrations and the other the spectra. The spectra and the known composition concentrations of the standards form the calibration set (also known as the training set) from which the calibration equations (calibration model) are built. Once the calibration equations or the model is created, predictions of the concentration values from measuring the spectrum of the unknown can be accomplished.

During the initial study, CLS was chosen to investigate the feasibility of the analysis, and the goal was not to develop highly accurate models but provide qualitative analysis. However, for the second part of the study the goal was to be able to do the analysis accurately at elevated temperatures and pressures. All of the chemometric techniques were screened for this purpose and PLS was chosen as the most promising technique. Models were developed using this technique for ethylene and 1-octene separately.

Extensive investigation of the spectra and the spectral features of the light alkenes in the NIR region was reported in Chapter 3. Unique bands (first overtone of asymmetric

stretch of $=\text{CH}_2$) were classified for the identification of these compounds. Using this unique region (6268 to 6071cm^{-1}) of the spectrum with the regression techniques produces accurate models. For many of the chemometric techniques (e.g., CLS and PLS), the whole spectrum can be and sometimes should be utilized in the model in order to obtain information about the impurities.^{190,191} However, in other cases, as is the case with light alkenes, utilizing the whole spectrum does not produce the best model.¹⁹² For instance, in the NIR spectrum of these compounds highly absorbing bands in the C-H stretching region are observed due to the high concentration of paraffinic hydrocarbons. Therefore, in the multivariate data modeling in this study, only the 6,268 to $6,071\text{cm}^{-1}$ spectral region is included. The spectra are baseline corrected at $7,650\text{cm}^{-1}$ during these studies by subtracting the absorbance at $7,650\text{cm}^{-1}$.

One way to validate the predictive ability of the calibration model is to perform a cross validation. One of the popular methods of cross validation is done by leaving one-sample or a selected small group of samples out of the model, building a new model, and predicting the concentration of the left out sample or samples. For the PLS cross validation, the models are estimated by leave-one sample out cross validation technique as well.

PLS models for the ethylene and 1-octene system was accomplished by using Pirouette (Trademark of Infometrix, Inc.) software. Two separate PLS models were built for prediction of ethylene and 1-octene. Additionally models that excluded some outlier data were also generated and the best predictive model was chosen.

A mean centering preprocessing technique was used in modeling via Pirouette software.

Mean centering involves subtraction of the mean of the column in a data matrix from each entry in the column. This technique helps take care of the intercept term in the regression model and helps stabilize the regression. It is recommended that mean centering should always be performed as the preprocessing technique for PLS.¹⁸⁹

Figure 20 shows the full data set used in building this model. Also in Appendix C the data file numbers and correlating concentrations used in construction of the PLS model for both ethylene and 1-octene are given in Table C1

The second derivative of the data is used as the smoothing/transformation technique in building the PLS model. Figure 21 shows the second derivative of the full data used in the model.

Figure 20: Full Data Used in PLS Modeling of Ethylene and 1-Octene

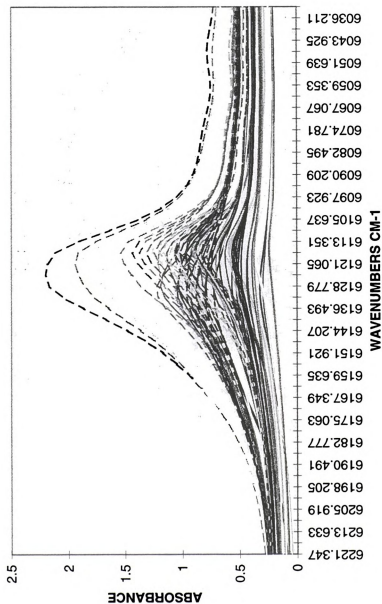
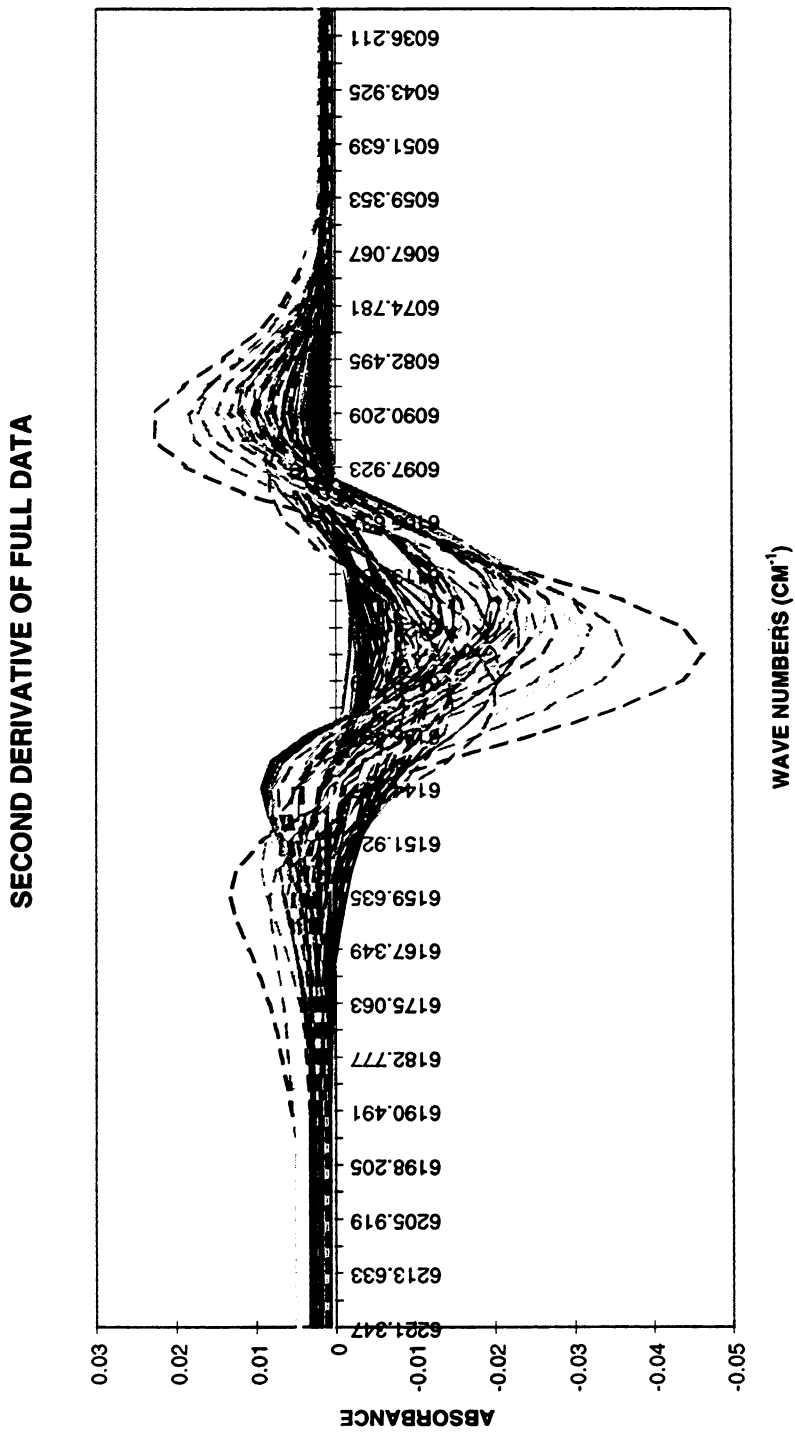


Figure 21: Second Derivative of the Data used in PLS Model



Determination of PLS Model Rank

As it was discussed in Chapter 2, one of the difficult tasks in PLS is determining the correct number of loading factors to model the data. One of the most effective ways of determining these factors and the predictive ability of the model is to calculate the Prediction Residual Error Sum of Squares (PRESS) for every possible factor.^{193,194} The PRESS is calculated by building a calibration model with a number of factors, then predicting some samples of known concentration (usually the "leave one out cross validation" method for PLS) against the model.^{195,196,197} The sum of the squared difference between the predicted and known concentrations give the PRESS value for that model.^{169,198,199}

$$\text{PRESS} = \sum_{i=1}^n \sum_{j=1}^m (C_{p,i,j} - C_{i,j})^2 \quad [25]$$

Where **n** is the number of samples in the training set, and **m** is the number of constituents. **C_p** is the matrix of predicted sample concentrations from the model, and **C** is the matrix of known concentrations of the samples. The smaller the PRESS value, the better the model is able to predict the concentrations of the calibrated constituents.

Another useful tool in determining the prediction ability of the model and the number of factors in PLS is the standard error of prediction SEP.

$$\text{SEP} = \left[\frac{\sum_{i=1}^N (c_i - \hat{c}_i)^2}{N - 1} \right]^{\frac{1}{2}} \quad [26]$$

where \hat{c}_i is the predicted concentration of analyte in sample i with the use of a calibration model that excludes sample i , c_i is the known concentration, and N is the number of calibration samples.^{200,201,202}

Both SEP and PRESS values were calculated using the “leave one sample out” cross validation technique for ethylene and 1-octene separately. Figure 22 and Figure 23 show the error prediction of the model (both SEP and PRESS) versus the number of loading factors (principle components) for ethylene and 1-octene models. As can be seen for the ethylene model, the error prediction after the 3rd principle component of the variance remains practically unchanged. Hence, this number was taking as the rank of the ethylene model. In the same way, rank of 6 was chosen for the 1-octene model

Figure 22: PLS Ethylene Model PRESS and SEP vs Number of Principal Component Factors.

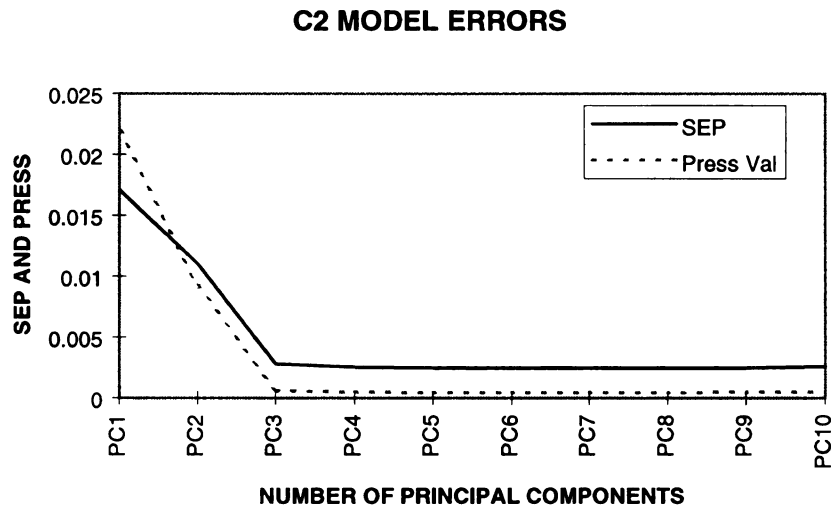
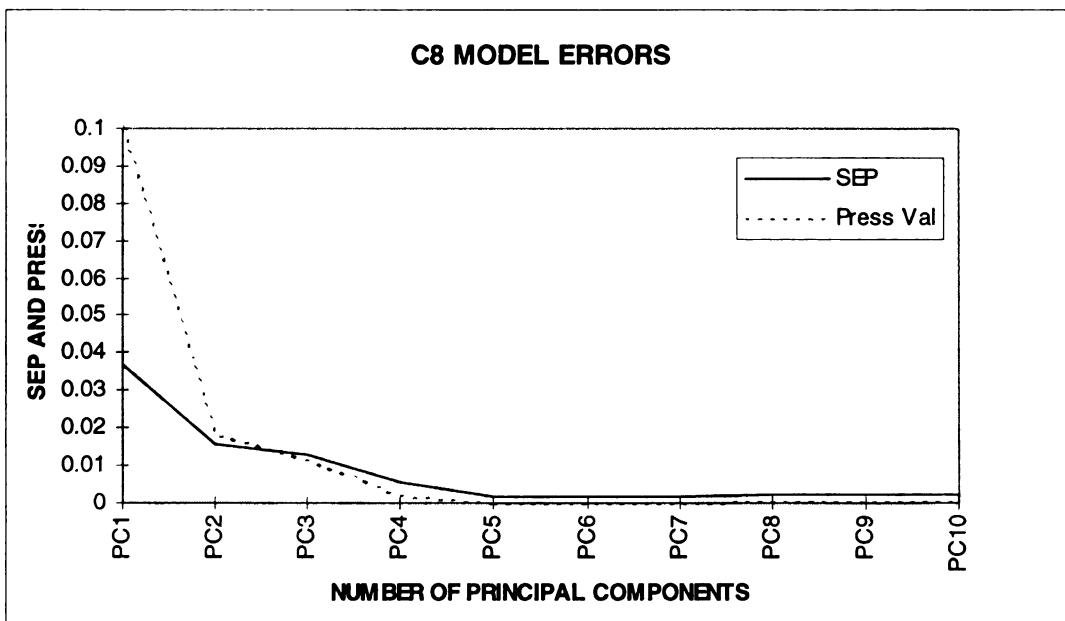


Figure 23: PLS 1-Octene Model PRESS and SEP vs Number of Principal Component Factors.



Examination of Outliers

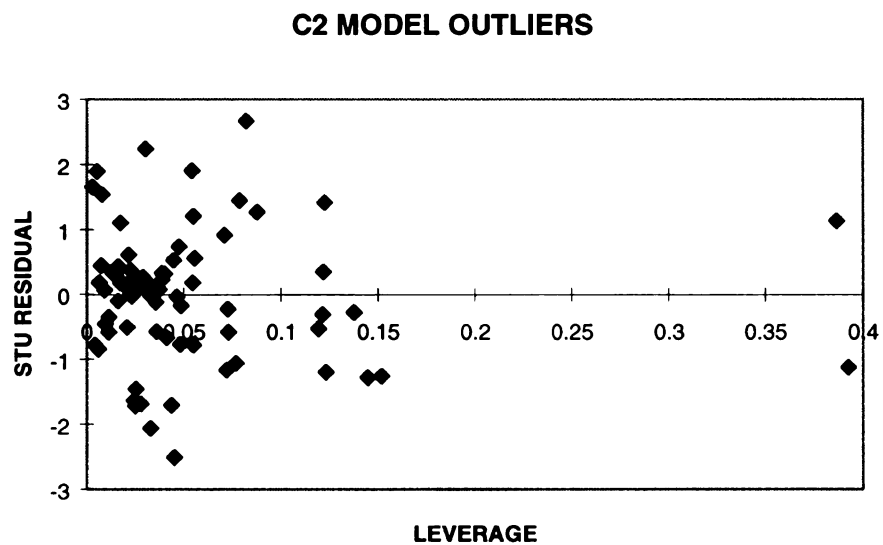
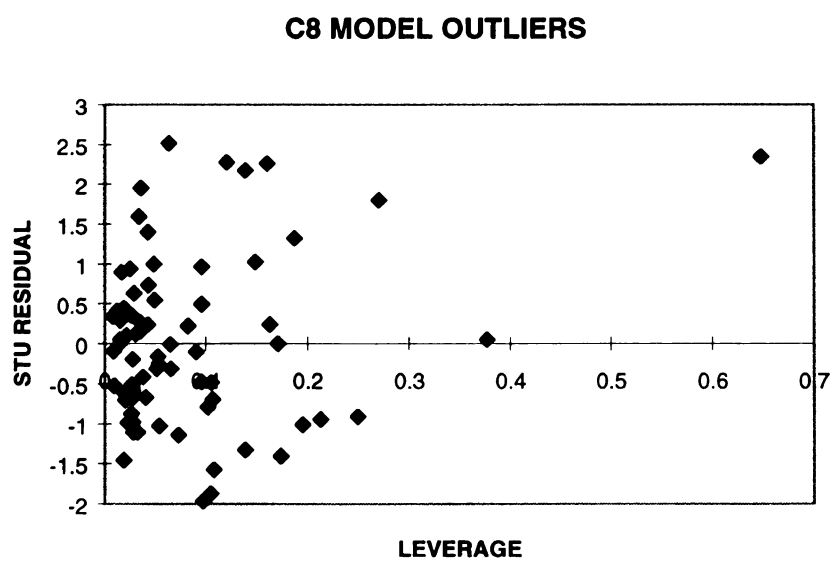
A number of different aspects in PLS can also shed light into the selection of the proper rank for the model. Pirouette offers outlier plots. Monitoring the spread of outliers within the concentration space is a good way of providing confidence in the model. If an unusual spread of data is observed, it can indicate an improper rank choice or there might be problems with the data which may require pretreatment. However, the latter is not expected in this study since these are synthetic samples which were prepared based on an experimental design.

Pirouette provides outlier plots showing the leverage of the sample against the residual distances. Influential or high leverage samples are of particular interest in model development. If a sample's profile differs greatly from the average training set profile, it will have a great influence on the model, drawing the model closer to its location in factor space. A sample's influence is quantified by its leverage, which represents a sample's distance from the centroid of the training set. As the model size grows, the leverage increases until all samples have equal influence on the model.

However, influential samples are not always outliers. If a sample lies a large distance from the center of the training set because it has an extreme value of the dependent variable, it contributes important information to the model. In examining outliers the leverage is usually plotted against studentized residuals instead of Y-residuals since studentized residuals takes leverage into account. The studentized residuals weigh the value of the residuals by taking into account the greater precision near the middle of the

data set versus the extremes. The studentized residuals tend to be distributed according to the student t distribution. Therefore, when eliminating outliers a good reason associated with the outlier needs to be present. Only three samples were eliminated from this model. These were the samples with very low ethylene concentration in which the errors involved with their preparation were significant due to the lower limit of the balance used. Measurement of a small amount of ethylene (less than 0.5 g) was not accurate enough.

Figure 24 and Figure 25 show the outliers for ethylene and the 1-octene models with no apparent outliers. Two samples in the ethylene model and one sample in the 1-octene model appearing far out on the leverage axis are not outliers. They are the samples with extreme concentrations.

Figure 24: Ethylene PLS Model Outliers**Figure 25:** 1-Octene PLS Model Outliers

Examination of Spectral Residuals

Examining the spectral residuals also provides information about the model. For instance, if the spectral residuals present a spectrum looking structure it indicates problems with the model, since they should look like random noise if the model is adequate.

Figure 26 and Figure 27 show the enlarged spectral residuals with no particular spectra structure.

Figure 26: Ethylene PLS model spectral Residuals

C2 MODEL RESIDUALS

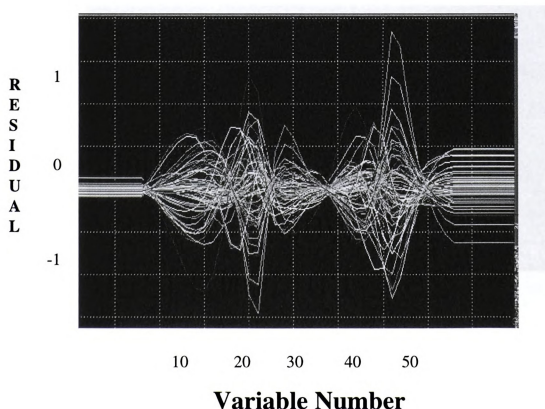
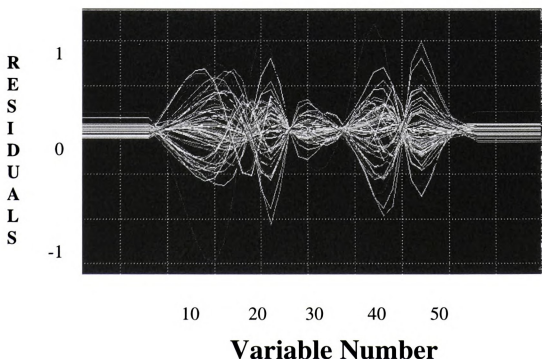


Figure 27: 1-Octene PLS Model Spectral Residuals

C8 MODEL RESIDUALS



Model Prediction Errors

Obtaining the correlation between the calculated versus measured concentrations is the ultimate indication of the model's predictive ability. Usually measured values (actual values) are plotted against the difference between the predicted and the measured (predicted-measured) values. These plots are given for ethylene and 1-octene in Figure 28 and Figure 29.

As it can be clearly seen from these plots, the absolute errors in the PLS model for both ethylene and 1-octene were less than ± 0.5 wt %., and ± 0.75 wt % (absolute) respectively.

As a result the predictions of both (ethylene and 1-octene) models were found satisfactory when tested using the training set (cross validation). PLS will be a robust model for the real-life samples as well since it can tolerate the existence of impurities and/or changes in the Isobar E composition. Additionally, since PLS includes the temperature and density effects in the model, it will not necessitate the measurement of the sample temperature.

Figure 28: PLS Fit Errors for Ethylene Over All Temperatures.

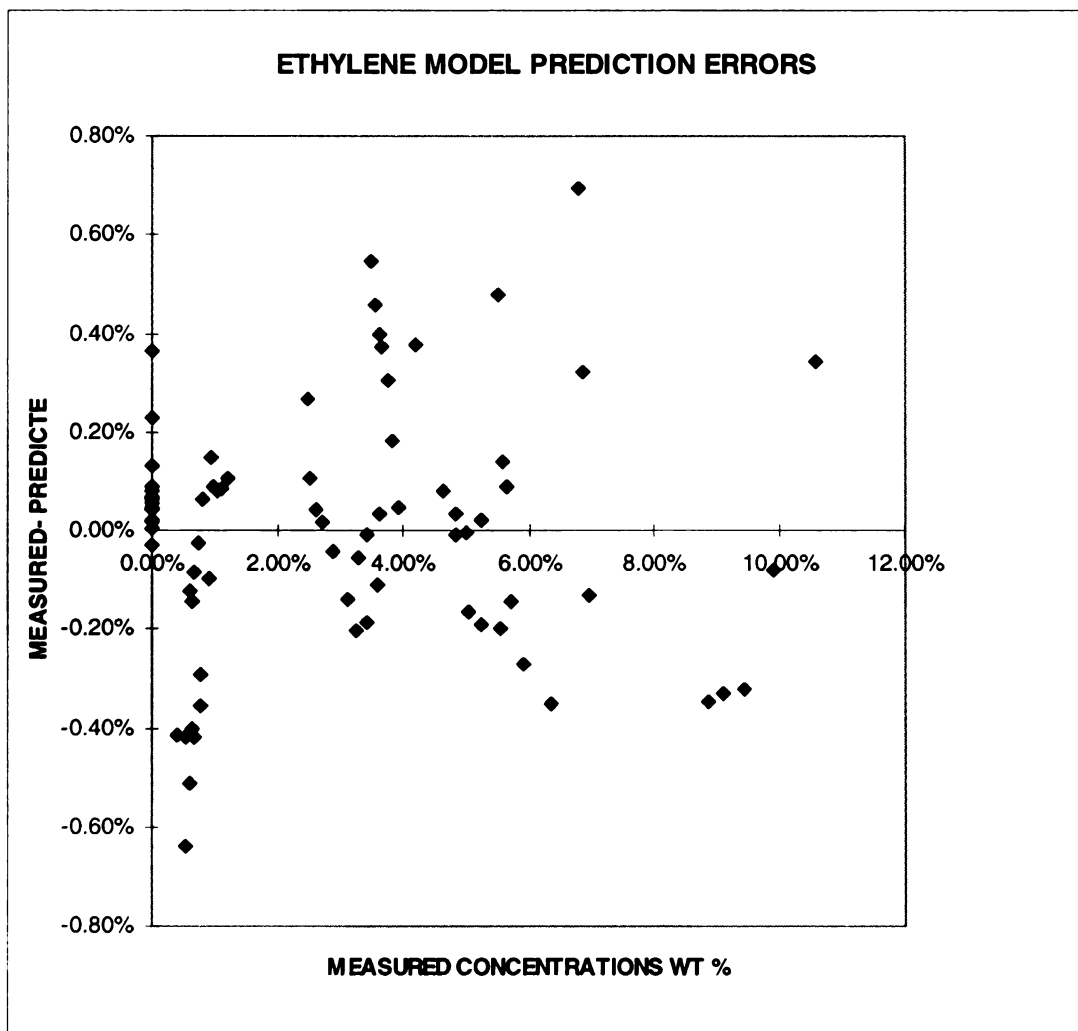
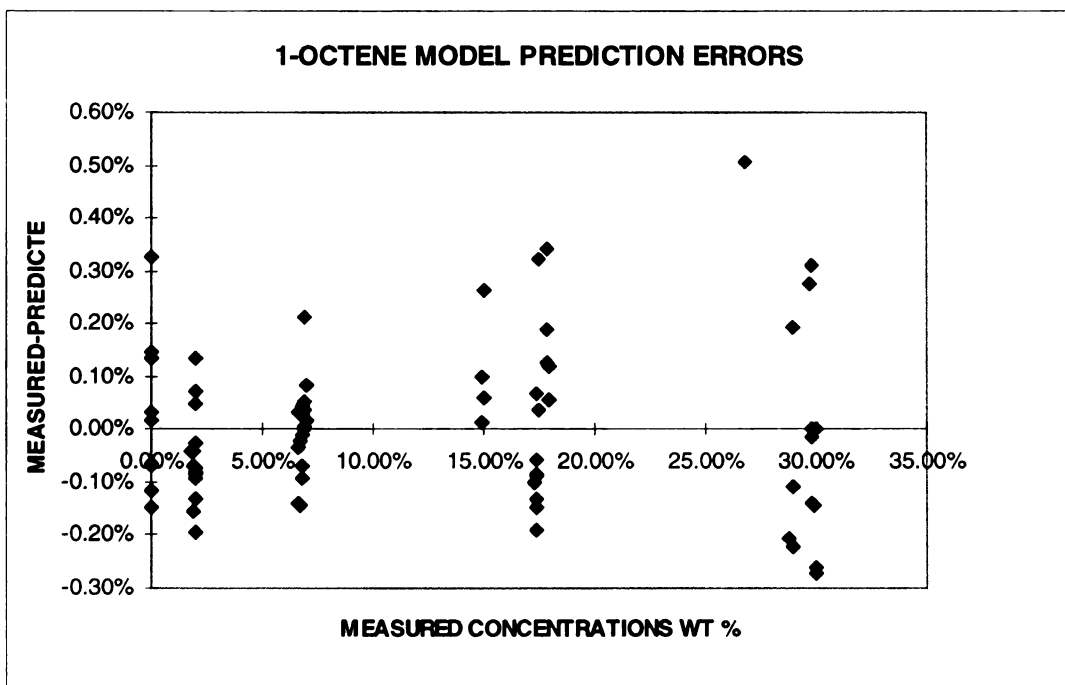


Figure 29: PLS Fit Errors for 1-Octene Over All Temperatures.



Summary

Determination of light alkenes via fiber optic FT-NIR spectroscopy at elevated temperature (140 °C) and pressure (500 psi) has been demonstrated. The effects of elevated pressures on spectra were found to be insignificant for these compounds. However, the temperature effects are critical, especially for the lighter molecules such as ethylene and propylene. Temperature effects on spectra decrease with increasing chain length among the light members of monoalkylated alkenes. Calibration models were constructed incorporating the temperature effects. Calibration standards were prepared and spectra obtained at elevated temperatures and pressures. An apparatus for this purpose was built and used for the collection of spectra. The determination of ethylene and 1-octene was used as the example system. Partial least-squares regression was investigated for both ethylene and 1-octene. The calibration covered the range of about 1-13 wt % ethylene, and 2-30 wt % 1-octene over the temperature range of 25 to 140 °C. Absolute prediction errors are expected to be less than ± 0.75 wt % for both ethylene and 1-octene.

CHAPTER 5

CONCLUSIONS AND RECOMMENDATIONS FOR FUTURE RESEARCH

A viable method has been developed to achieve the simultaneous determination of ethylene and monoalkylated light alkenes at elevated temperatures and pressures via fiber optic Fourier Transform Near Infrared (FT-NIR) spectroscopy for *in situ, real-time* monitoring of these compounds.

An additional goal of the study, to evaluate the effects of molecular structure of the monoalkylated light alkenes on this determination, has also been accomplished. In addition, the effects of elevated temperature and pressure on the vibrational spectroscopy of the light alkenes in the NIR region were investigated.

Conclusions

By far the most important result of this investigation is the development of a method for the simultaneous determination of ethylene and monoalkylated light alkenes at elevated temperatures and pressures via FT-NIR spectroscopy for *in situ, real-time* monitoring of these compounds. Also, the effects of molecular structure on this determination have been shown along with the effects of elevated temperatures and pressures. Other conclusions drawn from this study are summarized below:

1. NIR spectroscopy is a viable tool for *in situ*, real-time monitoring of systems both in the laboratory environment and in process analysis.
2. Coupling NIR spectroscopy with fiber optic probes enables the *in situ*, real-time monitoring of systems especially for process analysis applications.
3. FT-NIR spectroscopy is more stable and a more reliable tool than conventional NIR spectroscopy.
4. NIR has many advantages over MIR for *in situ*, real-time monitoring.
5. The first overtone of the asymmetric stretch of $=\text{CH}_2$ is unique to ethylene and monoalkylated light alkenes. Thus, the simultaneous determination of several light alkenes in presence of di and tri alkylated alkenes is possible in the NIR region.
6. The first overtone of the asymmetric stretch of $=\text{CH}_2$ for ethylene and the monoalkylated light alkenes shifts towards lower energy with an increasing number of carbon atoms in the molecule. This shift is significant enough to allow for the simultaneous determination of these compounds in the NIR region.
7. The intensity of the first overtone of the asymmetric stretch of $=\text{CH}_2$ for monoalkylated light alkenes decreases with increasing molecular weight.
8. Simultaneous determinations of ethylene and monoalkylated light alkenes are more feasible for those compounds with the biggest shift difference between them. For instance, the determination of ethylene and any other monoalkylated light alkene in a mixture is possible. However, determination of 1-pentene through 1-decene in a mixture may be difficult with this technique due to the spectral overlap.

9. Additional features other than the first overtone of the asymmetric stretch of $=\text{CH}_2$ (use of different regions of NIR spectrum such as $4,800 \text{ cm}^{-1}$ region) can be an aid for determination of these compounds in presence of interferences such as that from 2-ethyl-1-hexene in this determination.
10. Multivariate data analysis is necessary in NIR studies.
11. Classical least square regression is an adequate tool to use as a multivariate data analysis tool in NIR spectroscopy. Its simplicity makes it the preferred tool for qualitative laboratory feasibility studies.
12. Pressure in the range used in this study (less than 750 psi) has no effect on vibrational spectroscopy of the light alkenes in terms of absorption intensity, band shape changes, or the vibrational frequency.
13. Temperature effects are significant for the gas phase molecules or their solutions in liquids. The smaller members of the light alkenes (ethylene, propylene, and 1-butene) are more influenced than the heavier members of the light alkenes. Within the temperature range ($25\text{-}140^\circ\text{C}$) implemented in this study the effects of temperature are enough to influence the determination of light alkenes at elevated temperatures.
14. Temperature effects on the first overtone of the asymmetric stretch of the $=\text{CH}_2$ decrease with increasing molecular weight among the light alkenes.
15. Temperature effects in the range studied ($25\text{-}140^\circ\text{C}$) for the light alkenes are in the form of decreased intensity and broadened absorption bands for the first overtone of the asymmetric stretch of the $=\text{CH}_2$.
16. The effects of temperature on the intensity of the absorption band for the first overtone of the asymmetric stretch of $=\text{CH}_2$ can be explained by the population

changes in the energy levels. With increased temperature the population of the molecules at ground vibrational energy level decreases since some of the molecules are elevated to the first vibrational energy level.

17. The effects of temperature on the shape of the absorption band for the first overtone of the asymmetric stretch of $=\text{CH}_2$ can be explained by a change in the energy distribution among the rotational energy levels which are located between the vibrational energy levels. Since rotation vibrational energy levels are also excited by the radiation. A similar redistribution of the population of the rotational energy levels will influences the shape of the band.

18. Partial least squares regression can be used for modeling the training set for the simultaneous determination of light alkenes in NIR region. The absolute errors predicted by this model are less than ± 0.75 wt % for ethylene and 1-octene

Recommendations for Future Research

The feasibility of simultaneous determination of light alkenes *in situ*, real-time at elevated temperatures and pressures opens several areas of investigation. First of all via this technique even higher temperatures and pressures can be studied to determine their effects on the vibrational spectroscopy of these molecules. Secondly, ethylene as a supercritical fluid at the elevated temperatures and pressure can be investigated in terms of its supercritical properties such as its solvation power or its intermolecular interactions.

The development of this type of *in situ, real-time* analysis technique via fiber optic probes can be implemented in other systems with distinguishable features in NIR. For instance the similar hydrocarbons (paraffinic, olefinic, aromatic) can be investigated. Expansion of this determination to simultaneous determination of similar compounds along with light alkenes, such as the determination of di or trialkylated light alkenes should also be feasible.

The possibilities of using this tool in process analysis in similar applications for process optimization and control will benefit the control of manufacturing chemicals in industry. Thus, further research should seek to implement NIR spectroscopy for process analysis of many other compounds.

APPENDICES

APPENDIX A

APPENDIX A

This appendix contains the FT-NIR spectra (2,500-12,000 cm^{-1}) of ethylene, mono alkylated alkynes, cis and trans dialkylated alkenes, trialkylated alkenes, 1,1 dialkylated alkenes, n-octane and the Isopar E used in this study. All of the spectra were obtained with 4 cm^{-1} resolution and with a 5 mm long pathlength at room temperature and pressure.

LIST OF SPECTRA

Figure A-30: FT-NIR Spectrum (4,000 - 12,000 cm⁻¹) of Ethylene in Isopar E Solution

Figure A-31: FT-NIR Spectrum (4,000 - 12,000 cm⁻¹) of Propylene in Isopar E Solution

Figure A-32: FT-NIR Spectrum (4,000 - 12,000 cm⁻¹) of 1-Butene in Isopar E Solution

Figure A-33: FT-NIR Spectrum (4,000 - 12,000 cm⁻¹) of 1-Pentene 99.9 % pure

Figure A-34: FT-NIR Spectrum (2,500 - 12,000 cm⁻¹) of 1-Hexene 99.9 % pure

Figure A-35: FT-NIR Spectrum (2,500 - 12,000 cm⁻¹) of 1-Octene 99.9 % pure

Figure A-36: FT-NIR Spectrum (2,500 - 12,000 cm⁻¹) of 1-Decene 99.5 % pure

Figure A-37: FT-NIR Spectrum (2,500 - 12,000 cm⁻¹) of Trans-2-Octene 98 % pure

Figure A-38: FT-NIR Spectrum (2,500 - 12,000 cm⁻¹) of Trans-3-Octene 99 % pure

Figure A-39: FT-NIR Spectrum (4,000 - 12,000 cm⁻¹) of Trans-4-Octene 99 % pure

Figure A-40: FT-NIR Spectrum (2,500 - 12,000 cm⁻¹) of Cis-2-Octene 96 % pure

Figure A-41: FT-NIR Spectrum (2,500 - 12,000 cm⁻¹) of Cis-3-Octene 96 % pure

Figure A-42: FT-NIR Spectrum (2,500 - 12,000 cm⁻¹) of Ciss-4-Octene 98 % pure

Figure A-43: FT-NIR Spectrum (2,500 - 12,000 cm⁻¹) of Cis-3-Methyl 3-Heptene 98 %

pure

Figure A-44: FT-NIR Spectrum (2,500 - 12,000 cm⁻¹) of Trans-3-Methyl 3-Heptene 98

% pure

Figure A-45: FT-NIR Spectrum (2,500 - 12,000 cm⁻¹) of Isopar E

Figure A-46: FT-NIR Spectrum (2,500 - 12,000 cm⁻¹) of n-Octane 99 % pure

Figure A-47: FT-NIR Spectrum (2,500 - 12,000 cm⁻¹) of 2-Ethyl-1-Hexene 99 % pure

Figure A-30: FT-NIR Spectrum ($4,000$ $12,000 \text{ cm}^{-1}$) of Ethylene in Isopar E Solution

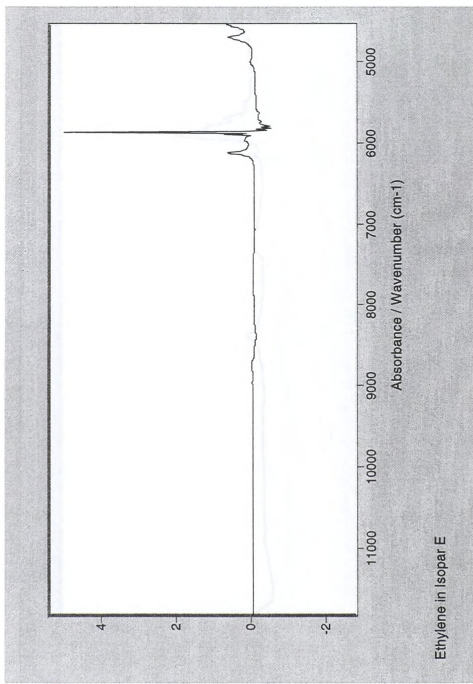


Figure A-31: FT-NIR Spectrum (4,000 - 12,000 cm^{-1}) of Propylene in Isopar E Solution

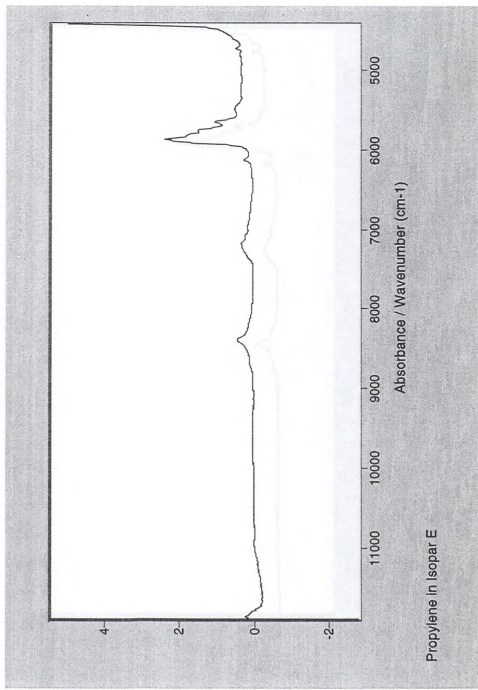


Figure A-32: FT-NIR Spectrum (4,000 - 12,000 cm^{-1}) of 1-Butene in Isopar E Solution

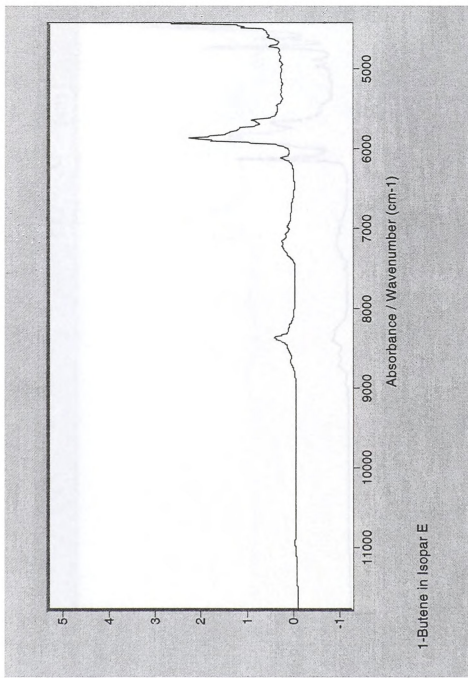


Figure A-33: FT-NIR Spectrum (4,000 - 12,000 cm^{-1}) of 1-Pentene 99.9 % pure

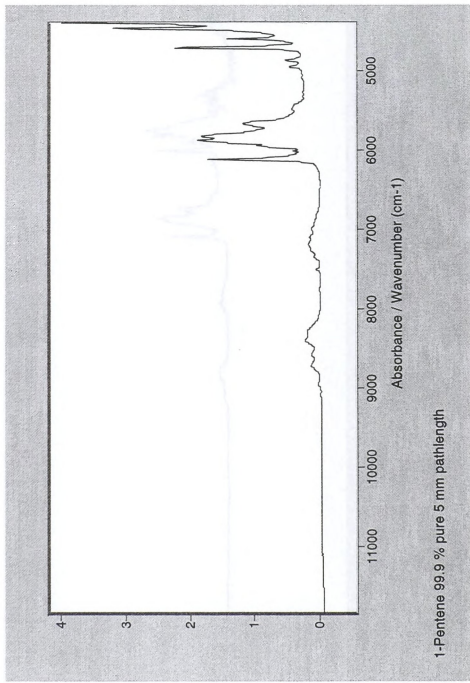


Figure A-34: FT-NIR Spectrum (2,500- 12,000 cm⁻¹) of 1-Hexene 99.9 % pure

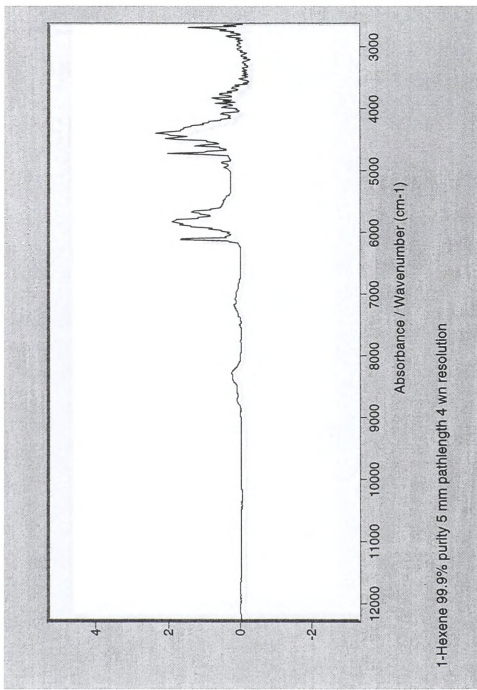




Figure A-35: FT-NIR Spectrum (2,500- 12,000 cm^{-1}) of 1-Octene 99.9 % pure

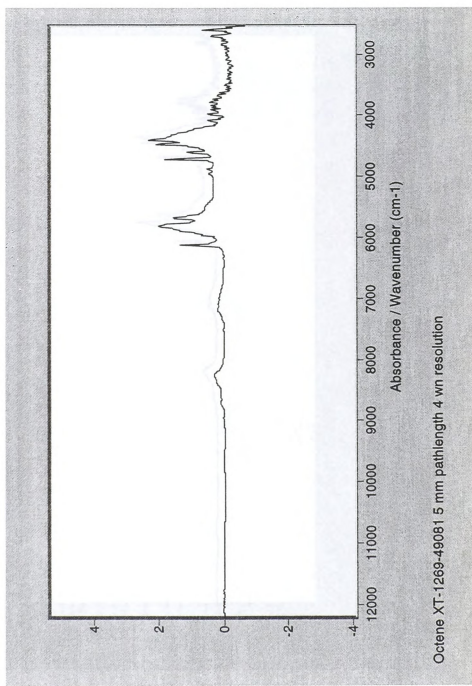


Figure A-36: FT-NIR Spectrum (2,500- 12,000 cm^{-1}) of 1-Decene 99.5 % pure

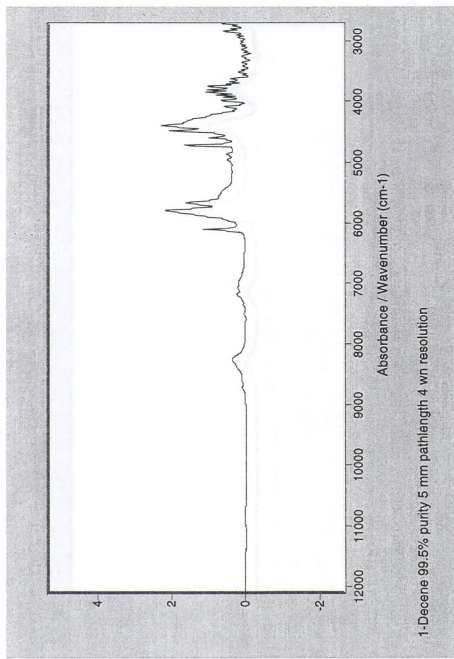




Figure A-37: FT-NIR Spectrum ($2,500\text{-}12,000\text{ cm}^{-1}$) of Trans-2-Octene 98 % pure

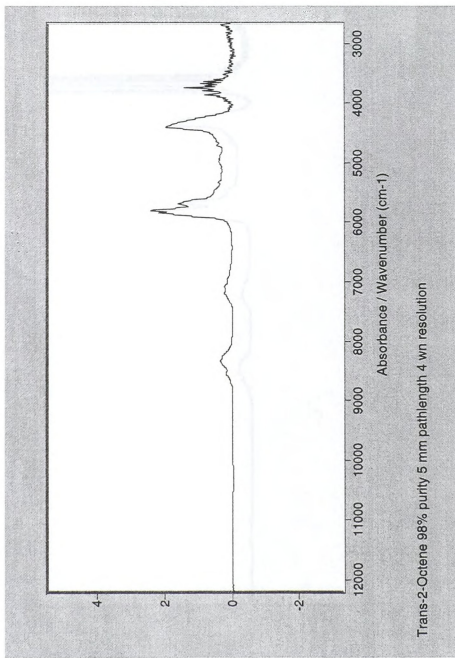




Figure A-38: FT-NIR Spectrum (2,500–12,000 cm⁻¹) of Trans-3-Octene 99 % pure

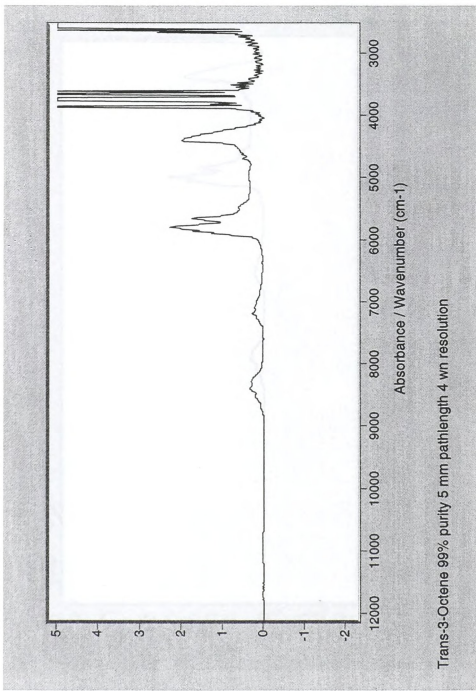




Figure A-39: FT-NIR Spectrum (4,000 - 12,000 cm^{-1}) of Trans-4-Octene 99 % pure

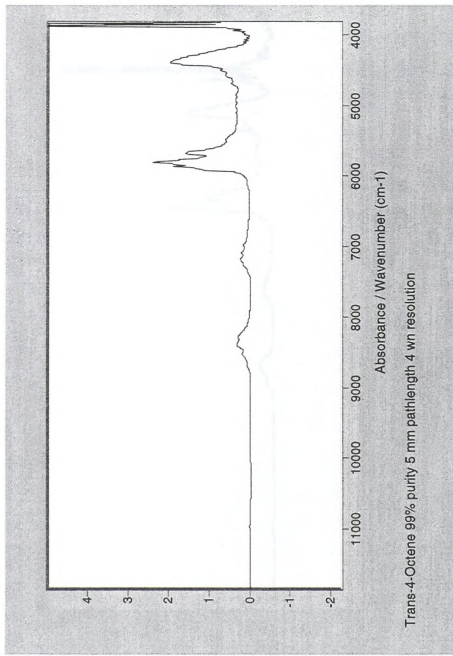




Figure A-40: FT-NIR Spectrum (2,500 - 12,000 cm^{-1}) of Cis-2-Octene 96 % pure

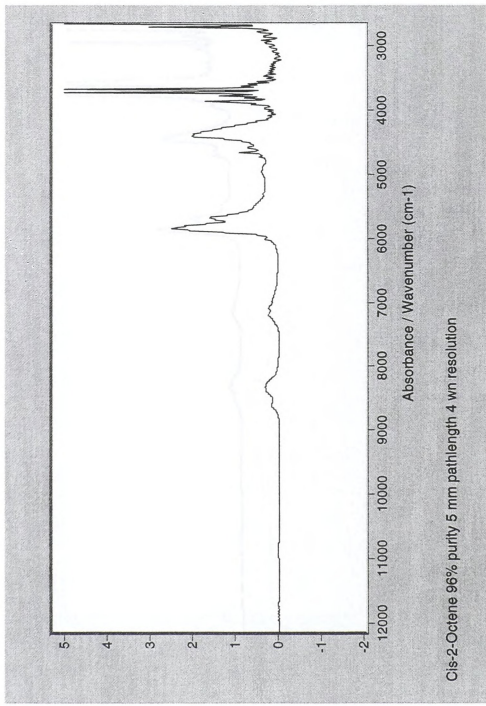


Figure A-41: FT-NIR Spectrum ($2,500$ - $12,000\text{ cm}^{-1}$) of Cis-3-Octene 96 % pure

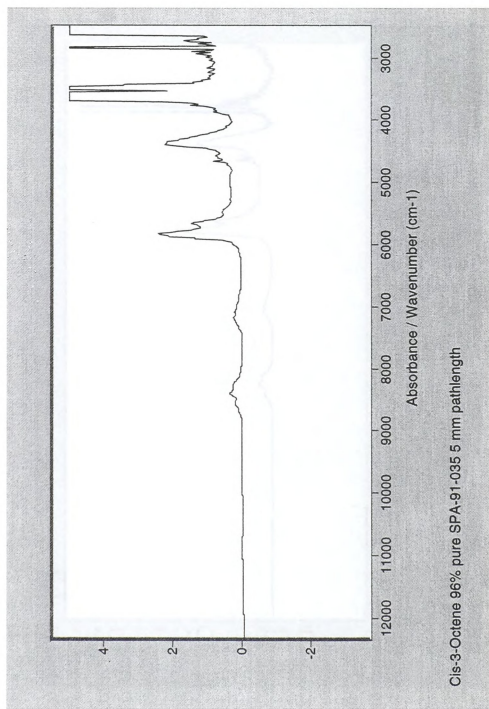


Figure A-42: FT-NIR Spectrum ($2,500 - 12,000 \text{ cm}^{-1}$) of Cis-4-Octene 98 % pure

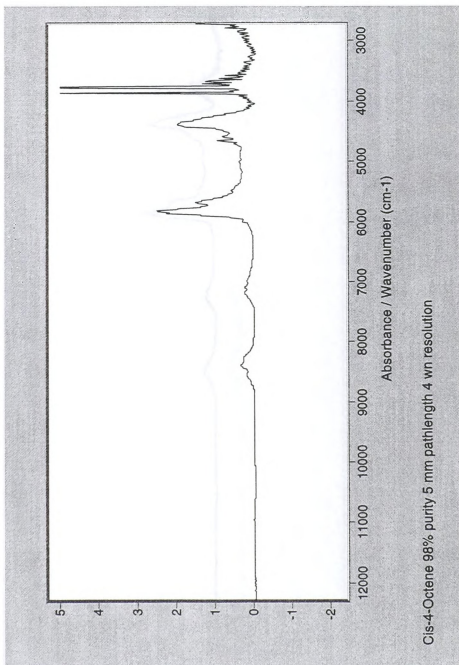


Figure A-43: FT-NIR Spectrum (2,500 - 12,000 cm^{-1}) of Cis-3-Methyl 3-Heptene 98 % pure

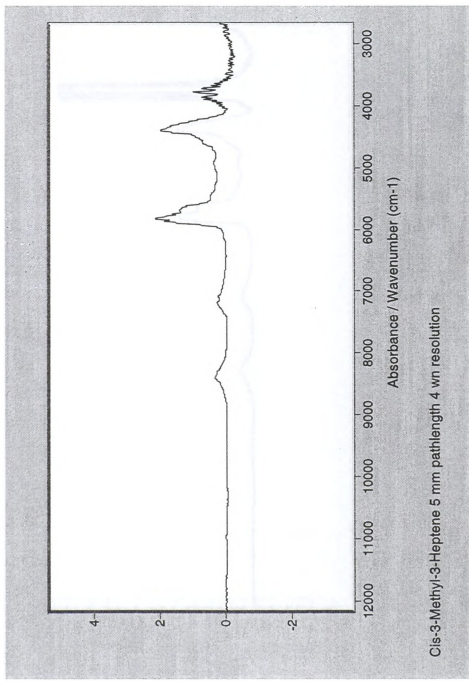


Figure A-44: FT-NIR Spectrum ($2,500 - 12,000 \text{ cm}^{-1}$) of Trans-3-Methyl-3-Heptene 98 % pure

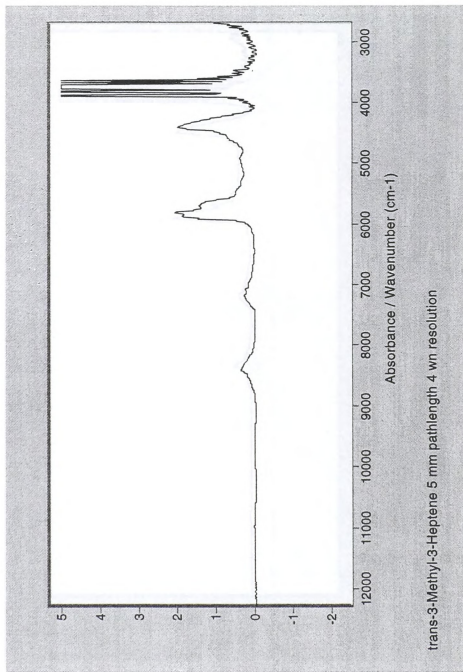


Figure A-45: FT-NIR Spectrum (2,500 - 12,000 cm^{-1}) of Isopar E

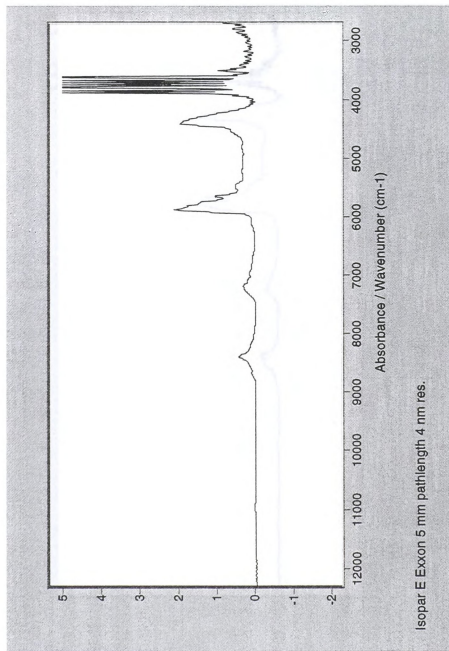




Figure A-46: FT-NIR Spectrum (2,500 - 12,000 cm^{-1}) of n-Octane 99 % pure

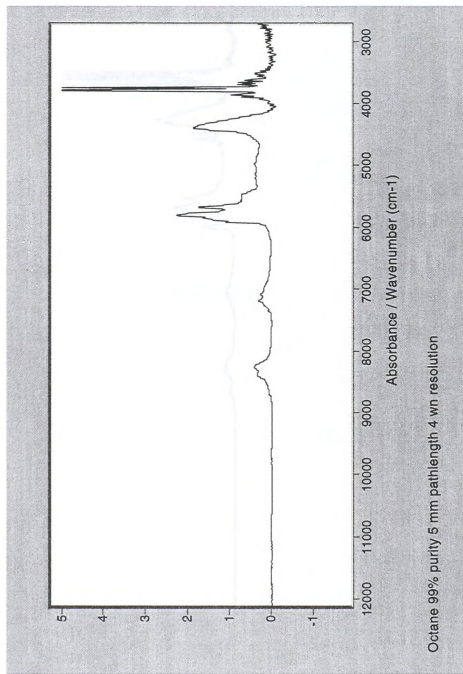
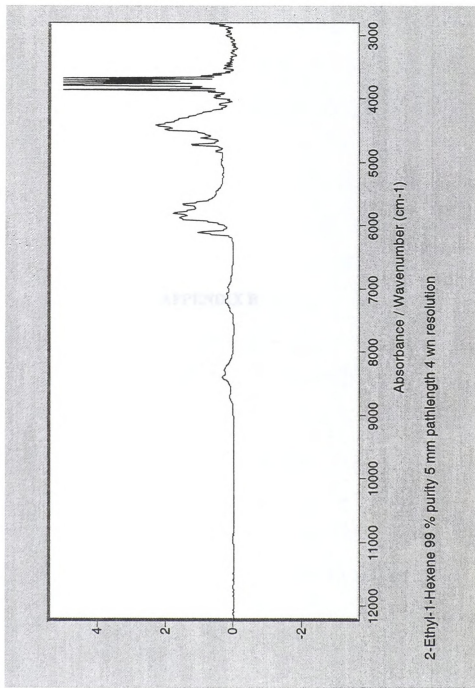




Figure A-47: FT-NIR Spectrum (2,500 - 12,000 cm^{-1}) of 2-Ethyl-1-Hexene 99 % pure



APPENDIX B

APPENDIX B

This section contains the excel spread sheets showing the calculations of the liquid phase concentration for each run.

LIST OF TABLES

Table B-1: Excel Spread Sheet Showing the Liquid Phase Concentration Calculations for Run # 07

Table B-2: Excel Spread Sheet Showing the Liquid Phase Concentration Calculations for Run # 08A

Table B-3: Excel Spread Sheet Showing the Liquid Phase Concentration Calculations for Run # 08B

Table B-4: Excel Spread Sheet Showing the Liquid Phase Concentration Calculations for Run # 09

Table B-5: Excel Spread Sheet Showing the Liquid Phase Concentration Calculations for Run # 10

Table B-6: Excel Spread Sheet Showing the Liquid Phase Concentration Calculations for Run # 11

Table B-7: Excel Spread Sheet Showing the Liquid Phase Concentration Calculations for Run # 12

Table B-8: Excel Spread Sheet Showing the Liquid Phase Concentration Calculations for Run # 13

Table B-9: Excel Spread Sheet Showing the Liquid Phase Concentration Calculations for Run # 14

Table B-10: Excel Spread Sheet Showing the Liquid Phase Concentration Calculations for Run # 15

Table B-11: Excel Spread Sheet Showing the Liquid Phase Concentration Calculations for Run # 17

Table B-12: Excel Spread Sheet Showing the Liquid Phase Concentration Calculations for Run # 18

Table B-13: Excel Spread Sheet Showing the Liquid Phase Concentration Calculations for Run # 21

Table B-14: Excel Spread Sheet Showing the Liquid Phase Concentration Calculations for Run # 22

Table B-15: Excel Spread Sheet Showing the Liquid Phase Concentration Calculations for Run # 23

Table B-16: Excel Spread Sheet Showing the Liquid Phase Concentration Calculations for Run # 24

Table B-17: Excel Spread Sheet Showing the Liquid Phase Concentration Calculations for Run # 25

Table B-18: Excel Spread Sheet Showing the Liquid Phase Concentration Calculations for Run # 27

Table B-19: Excel Spread Sheet Showing the Liquid Phase Concentration Calculations for Run # 28

Table B-1: Excel Spread Sheet Showing the Liquid Phase Concentration Calculations for Run # 07

Table B-1 (Cont.): Excel Spread Sheet Showing the Liquid Phase Concentration Calculations for Run # 07

Table B-2: Excel Spread Sheet Showing the Liquid Phase Concentration Calculations for Run # 08A



Table B-2 (Cont.): Excel Spread Sheet Showing the Liquid Phase Concentration Calculations for Run # 08A

Table B-3: Excel Spread Sheet Showing the Liquid Phase Concentration Calculations for Run # 08B

Table B-3 (Cont.): Excel Spread Sheet Showing the Liquid Phase Concentration Calculations for Run # 08B

RUN#00B											
Liquid C8	Liquid ISOPAR	Liquid C2	Liquid C8	Liquid ISOPAR	Liquid C2	Liquid C8	Liquid ISOPAR	Liquid C2	Liquid C8	Liquid ISOPAR	C2
1MOL	1MOL	1MOL	1g	Lg	Lg	WT%	WT%	MOL F	MOL F	Po, ATM	Po, ATM
0.6189	0.3041	0.3041	76.12	8.53	8.53	89.92%	10.08%	0.6705	0.3295	16.72	8.25
0.6189	0.3041	0.3041	76.12	8.53	8.53	89.92%	10.08%	0.6705	0.3295	16.72	8.25
0.6189	0.3041	0.3041	76.12	8.53	8.53	89.92%	10.08%	0.6706	0.3294	16.64	8.29
0.6207	0.3107	0.3107	76.35	8.72	8.72	89.75%	10.25%	0.6664	0.3336	24.15	4.34
0.6207	0.3107	0.3107	76.35	8.72	8.72	89.75%	10.25%	0.6665	0.3335	24.15	4.34
0.6207	0.3106	0.3106	76.35	8.71	8.71	89.76%	10.24%	0.6665	0.3335	24.09	4.37
0.6342	0.3141	0.3141	78.01	8.81	8.81	89.85%	10.15%	0.6688	0.3312	36.49	-3.37
0.6343	0.3141	0.3141	78.01	8.81	8.81	89.85%	10.15%	0.6688	0.3312	36.53	-3.40
0.6343	0.3141	0.3141	78.01	8.81	8.81	89.85%	10.15%	0.6688	0.3312	36.53	-3.40

Table B-4: Excel Spread Sheet Showing the Liquid Phase Concentration Calculations for Run # 09



Table B-4 (Cont.): Excel Spread Sheet Showing the Liquid Phase Concentration Calculations for Run #09

Table B-5: Excel Spread Sheet Showing the Liquid Phase Concentration Calculations for Run # 10

Table B-5 (Cont.): Excel Spread Sheet Showing the Liquid Phase Concentration Calculations for Run # 10

Table B-6: Excel Spread Sheet Showing the Liquid Phase Concentration Calculations for Run # 11



Table B-6 (Cont.): Excel Spread Sheet Showing the Liquid Phase Concentration Calculations for Run # 11

Liquid C8 /MOL	Liquid ISOPAR C8 /g	Liquid C8 /ISOPAR	Liquid C8 /WT%	Liquid W7% /MOL F	Liquid ISOPAR /MOL F	Liquid C8 /MEAS	Liquid C8 /CALC	Vapor C8 /ATM	Vapor Po,ATM /vMOL	Vapor C8 /ISOPAR	Vapor ISOPAR /vMOL	Liquid C8 /ISOPAR	Liquid C8 /ISOPAR g
0.1029	0.5314	11.54	65.37	15.01%	84.99%	0.1622	0.15	0.14	0.02	0.13	0.0001	0.1029	0.5314
0.1029	0.5314	11.54	65.37	15.01%	84.99%	0.1622	0.15	0.14	0.02	0.13	0.0001	0.1029	0.5314
0.1029	0.5314	11.54	65.37	15.01%	84.99%	0.1622	0.15	0.14	0.02	0.13	0.0001	0.1029	0.5314
0.1026	0.5306	11.51	65.26	14.99%	85.01%	0.1620	0.34	0.36	0.05	0.29	0.0004	0.1026	0.5306
0.1026	0.5306	11.51	65.26	14.99%	85.01%	0.1620	0.34	0.36	0.05	0.29	0.0003	0.1026	0.5306
0.1025	0.5305	11.51	65.26	14.99%	85.01%	0.1620	0.34	0.36	0.05	0.29	0.0004	0.1025	0.5305
0.1020	0.5292	11.45	65.09	14.96%	85.04%	0.1616	0.68	0.77	0.11	0.66	0.0009	0.1020	0.5292
0.1020	0.5291	11.44	65.08	14.95%	85.05%	0.1616	0.68	0.77	0.11	0.66	0.0009	0.1020	0.5291
0.1019	0.5291	11.44	65.08	14.95%	85.05%	0.1615	0.68	0.78	0.11	0.66	0.0010	0.1019	0.5291
0.1010	0.5268	11.34	64.80	14.89%	85.11%	0.1609	0.8391	1.34	1.55	0.25	0.0019	0.1010	0.5268
0.1010	0.5268	11.34	64.80	14.89%	85.11%	0.1609	0.8391	1.34	1.55	0.25	0.0019	0.1010	0.5268
0.1010	0.5268	11.33	64.79	14.89%	85.11%	0.1609	0.8391	1.34	1.56	0.25	0.0019	0.1010	0.5268
<i>A+B7)</i>													
<i>T(K)</i>													

Liquid C8 MOL is the number of moles of 1-octene in liquid phase obtained by subtracting the number of moles of 1-octene in the vapor phase from the total number of liquid isopar MOL is the # of moles of isoparE in liquid phase obtained by subtracting the # of moles of isoparE in the vapor phase from the total # of moles of isopar

Liquid C8 g is the weight of 1-octene in liquid phase obtained by multiplying the number of moles of 1-octene in the liquid phase with the molecular weight of octene
Liquid ISOPAR g is the weight of isoparE in liquid phase obtained by multiplying the number of moles of isoparE in the liquid phase with the molecular weight of isopar

Liquid C8 wt% is the weight percent of 1-octene in liquid

Liquid C8 MOL F is the mol fraction of 1-octene in liquid

Liquid ISOPAR MOL F is the mol fraction of isoparE in liquid

A+B7)

C8 Po,ATM is the partial pressure of C8/mol fraction of C8

ISOPAR Po,ATM is the partial pressure of isoparE=(P of isoparE)*mol fraction of isoparE

CALC P,ATM is the sum of the partial pressures of the C8 and isoparE which converges to the measured pressure.

Table B-7: Excel Spread Sheet Showing the Liquid Phase Concentration Calculations for Run # 12

Table B-7 (Cont.): Excel Spread Sheet Showing the Liquid Phase Concentration Calculations for Run # 12

Liquid C8	Liquid ISOPAR	Vapor C8	Vapor ISOPAR	Liquid C8	Liquid ISOPAR												
/MOL	/MOL	/g	/g	/MOL	/WT%	/MOL	/ATM	/MOL	/ATM	/MOL	/MOL	/MOL	/MOL	/MOL	/MOL	/MOL	/MOL
0.2055	0.4381	23.06	53.89	29.97%	70.03%	0.3193	0.6807	0.15	0.27	0.04	0.11	0.0009	0.0012	0.2055	0.4381	23.06	53.88
0.2055	0.4381	23.06	53.88	29.97%	70.03%	0.3193	0.6807	0.15	0.28	0.04	0.11	0.0009	0.0013	0.2055	0.4381	23.06	53.88
0.2055	0.4381	23.06	53.88	29.97%	70.03%	0.3193	0.6807	0.15	0.28	0.04	0.11	0.0009	0.0013	0.2055	0.4381	23.06	53.88
0.2058	0.4381	23.09	53.89	30.00%	70.00%	0.3196	0.6804	0.34	0.36	0.10	0.24	0.0006	0.0013	0.2058	0.4381	23.09	53.89
0.2058	0.4381	23.10	53.89	30.00%	70.00%	0.3196	0.6804	0.34	0.36	0.10	0.24	0.0006	0.0013	0.2058	0.4381	23.10	53.89
0.2058	0.4381	23.09	53.89	30.00%	70.00%	0.3196	0.6804	0.34	0.36	0.10	0.24	0.0006	0.0013	0.2058	0.4381	23.09	53.89
0.2054	0.4373	23.04	53.78	29.99%	70.01%	0.3196	0.6804	0.68	0.68	0.22	0.45	0.0010	0.0021	0.2054	0.4373	23.04	53.78
0.2054	0.4373	23.04	53.78	29.99%	70.01%	0.3196	0.6804	0.68	0.68	0.22	0.46	0.0010	0.0021	0.2054	0.4373	23.04	53.78
0.2054	0.4373	23.04	53.78	29.99%	70.01%	0.3196	0.6804	0.68	0.68	0.22	0.46	0.0010	0.0021	0.2054	0.4373	23.04	53.78
0.2037	0.4351	22.86	53.51	29.93%	70.07%	0.3189	0.6811	1.38	1.55	0.49	0.89	0.0027	0.0043	0.2037	0.4351	22.86	53.51
0.2037	0.4351	22.86	53.51	29.93%	70.07%	0.3189	0.6811	1.38	1.55	0.49	0.89	0.0027	0.0043	0.2037	0.4351	22.86	53.51
0.2037	0.4350	22.85	53.51	29.93%	70.07%	0.3189	0.6811	1.38	1.56	0.49	0.89	0.0027	0.0043	0.2037	0.4350	22.85	53.51

Table B-8 (Cont.): Excel Spread Sheet Showing the Liquid Phase Concentration Calculations for Run # 13

RUN#13	PT1MKS	PT4GP	TYES1	P_ATM	CORR	C8	ISOPAR	C2	SUM	DENSITY	VOLUME	VOLUME	VAPOR	VAPOR	VAPOR
				P_ISPA	P_ATM	VP_ATM	Po_ATM	Po_ATM	V	g/mL	VL	VL	ISOPAR	C8	C2
48.61	41.47	59.65	37.1	2.52	0.1224	0.1591	0.0025	0.1476	2.37	173.0	0.6815	0.1197	0.1416	0.0001	0.00076
48.73	41.47	59.68	37.4	2.55	0.1224	0.1603	0.0025	0.1487	2.39	173.0	0.6813	0.1198	0.1415	0.0001	0.00076
48.73	41.47	59.94	37.1	2.52	0.1227	0.1606	0.0025	0.1490	2.37	173.0	0.6812	0.1198	0.1415	0.0001	0.00077
59.73	59.10	84.37	53.7	3.66	0.3139	0.3475	0.0065	0.3224	3.33	178.2	0.6615	0.1234	0.1379	0.0003	0.00152
59.73	59.10	84.59	53.7	3.65	0.3162	0.3497	0.0066	0.3244	3.32	178.3	0.6613	0.1234	0.1379	0.0003	0.00152
59.73	59.10	84.65	53.7	3.65	0.3170	0.3504	0.0066	0.3251	3.32	178.3	0.6613	0.1234	0.1379	0.0003	0.00153
0.12	78.70	108.77	71.7	4.88	0.6959	0.6706	0.0144	0.6221	4.24	183.7	0.6418	0.1272	0.1341	0.0006	0.00267
-0.48	78.70	108.87	71.7	4.88	0.6978	0.6721	0.0145	0.6235	4.24	183.7	0.6417	0.1272	0.1341	0.0006	0.00267
-0.48	79.02	108.86	72.0	4.90	0.6975	0.6718	0.0145	0.6233	4.26	183.7	0.6417	0.1272	0.1341	0.0006	0.00267
-0.48	106.78	137.50	96.8	6.59	1.2961	1.2961	0.0320	1.2024	5.36	190.6	0.6185	0.1319	0.1294	0.00012	0.00462
-0.36	107.11	137.58	97.1	6.61	1.5478	1.3009	0.0321	1.2053	5.35	190.6	0.6184	0.1320	0.1293	0.00012	0.00463
-0.36	107.11	137.58	97.1	6.61	1.5478	1.3009	0.0321	1.2069	5.37	190.6	0.6184	0.1320	0.1293	0.00012	0.00463
<i>PTSET1 is the readout of the first pressure transducer PT4GP is the readout of the second pressure transducer</i>															
<i>TYES1 is the oven set point temperature</i>															
<i>CORR P_ISPA is corrected pressure according to the calibration of the pressure transducer ($y=mx+n$) xreadout of MRSPT1</i>															
<i>P_ATM is corrected pressure In units of atm.</i>															
<i>C8 VP_ATM is the vapor pressure of C8 at the set point temperature calculated by using Antoine Constants according to $\log(P)=A-B/(T+C)$</i>															
<i>ANTOINE CONSTANTS ATM, C, for IsoparE and 1-Octene are:</i>															
<i>C8 ISOPARE VP_ATM is the vapor pressure of IsoparE calculated similar to C8</i>															
<i>C8 Po_ATM is the partial pressure of IsoparE = $(Vp \text{ of IsoparE})/\text{molar fraction of C8}$</i>															
<i>ISOPARE Po_ATM is the partial pressure of IsoparE = $(Vp \text{ of IsoparE})/\text{molar fraction of IsoparE}$</i>															
<i>C2 Po_ATM is the partial pressure of C2.</i>															
<i>SUM of the molar volume of the components (C2,C8,IsoparE) obtained from sum of the each component molar mass divided by its density</i>															
<i>DENSITY of the mixture obtained by the molar mass divided by the total molar volume</i>															
<i>VOLUME of the liquid phase (Liter) = total mass of the original liquid divided by density</i>															
<i>VAPOR C8 MOL is the # of moles of 1-octene in vap. phase obtained by using state of the gas equation (par. pres. of the C8 vap. phase volume)/0.82067TK</i>															
<i>VAPOR ISOPAR MOL is the # of moles of IsoparE in vap. Phase obtained by using state of the gas equation (par. pres. of the IsoparE vap. phase volume)/0.82067TK</i>															
<i>VAPOR C2 MOL is the # of moles of C2 in vap. phase obtained by using state of the gas equation (partial pressure of the C2 vap. phase volume)/0.82067TK</i>															
<i>For the density equation D=A+Bt</i>															
MASS, g	WT%														
C8/ISOPAR	80.6	2.00			C2	1.23%	1.00	0.0356	0.03515	1.4447					
C2	1.00	0.00			C8	1.98%	1.61	0.0144	0.0208	2.3288					
					ISOPAR E	96.80%	78.99	0.6422	0.9277	114.1132	ISOPAR E	0.73468	-8.25E-04		
VESSEL VOLUME					TOTAL	100.00%	81.60	0.6922	1.0000	117.8867	C8	0.73502	-9.17E-04		
											C2	0.46757			



Table B-8 (Cont.): Excel Spread Sheet Showing the Liquid Phase Concentration Calculations for Run # 13



Table B-9: Excel Spread Sheet Showing the Liquid Phase Concentration Calculations for Run # 14

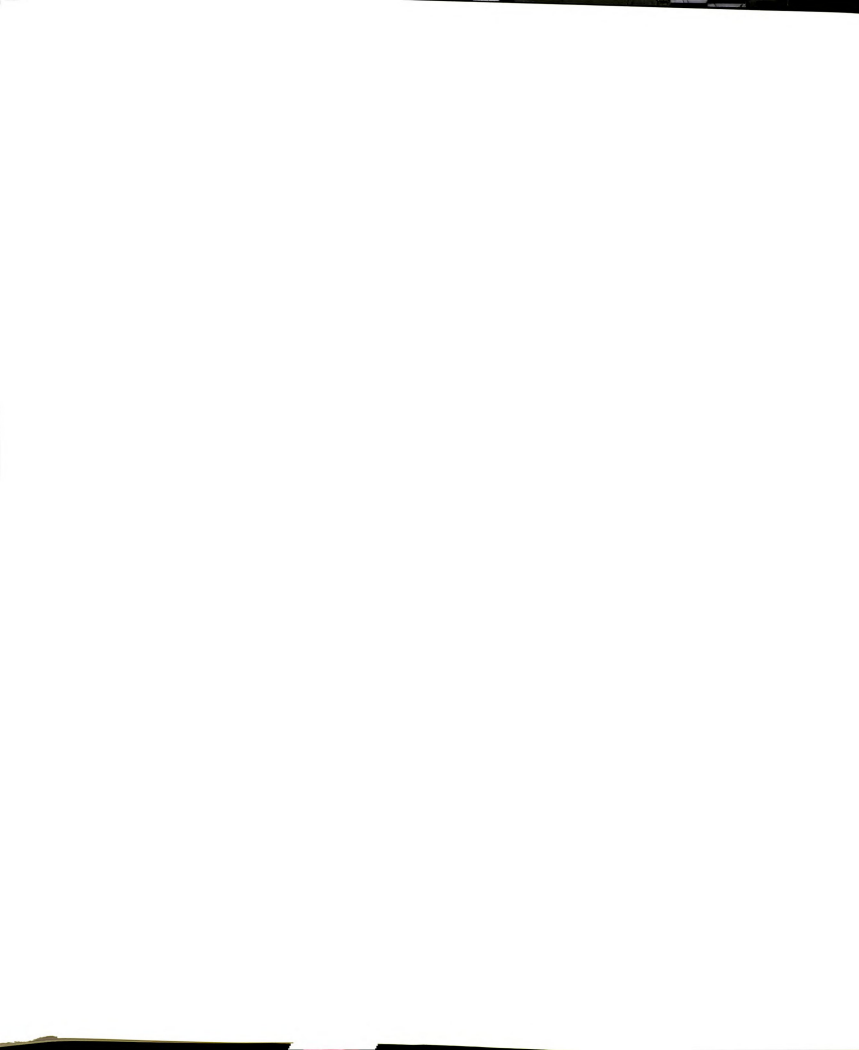


Table B-9 (Cont.): Excel Spread Sheet Showing the Liquid Phase Concentration Calculations for Run # 14

LIQUID C8 MOL is the number of moles of 1-octene in liquid phase obtained by subtracting the number of moles of 1-octene in the vapor phase from the total number of moles of octene									
LIQUID ISOPAR MOL is the # of moles of IsoparE in liquid phase obtained by subtracting the # of moles of IsoparE in the vapor phase from the total # of moles of IsoparE									
LIQUID C2 MOL is the # of moles of ethylene in liquid phase obtained by subtracting the # of moles of ethylene in the vapor phase from the total # of moles of C2.									
LIQUID C8 g is the weight of 1-octene in liquid phase obtained by multiplying the number of moles of 1-octene in the liquid phase with the molecular weight of octene									
LIQUID ISOPAR g is the weight of IsoparE in liquid phase with the molecular weight of IsoparE									
LIQUID C2 g is the weight of ethylene in liquid phase obtained by multiplying the number of moles of ethylene in the liquid phase with the molecular weight of ethylene									
LIQUID C8 wt% is the weight percent of 1-octene in liquid									
LIQUID C2 wt% is the weight percent of ethylene in liquid									
LIQUID C8 MOL F is the mol fraction of 1-octene in liquid									
LIQUID C2 MOL F is the mol fraction of ethylene in liquid									
LIQUID C8 wt% is the partial pressure of C8 = $(V_p \text{ of C8}) / \text{mol fraction of C8}$									
LIQUID C2 wt% is the partial pressure of IsoparE = $(V_p \text{ of IsoparE}) / \text{mol fraction of IsoparE}$									
CALC P_ATM is the sum of the partial pressures of the C2, C8 and IsoparE which converges to the measured pressure.									
C8	LIQUID ISOPAR	LIQUID C2	LIQUID C8	LIQUID C2	LIQUID C8	LIQUID ISOPAR	LIQUID C2	LIQUID C8	LIQUID ISOPAR
1 MOLE	1 MOLE	1 MOLE	1 MOLE	1 MOLE	1 MOLE	1 MOLE	1 MOLE	1 MOLE	1 MOLE
0.0136	0.6080	0.0877	1.53	74.79	2.46	1.94%	94.94%	3.12%	0.0192
0.0136	0.6080	0.0876	1.53	74.79	2.46	1.94%	94.94%	3.12%	0.0192
0.0136	0.6073	0.0836	1.52	74.70	2.35	1.94%	95.07%	2.98%	0.0193
0.0136	0.6073	0.0835	1.52	74.70	2.34	1.94%	95.08%	2.98%	0.0193
0.0136	0.6073	0.0837	1.52	74.70	2.35	1.94%	95.07%	2.99%	0.0193
0.0136	0.6063	0.0806	1.52	74.58	2.26	1.94%	95.17%	2.88%	0.0194
0.0136	0.6063	0.0805	1.52	74.58	2.26	1.94%	95.18%	2.88%	0.0194
0.0136	0.6063	0.0805	1.52	74.57	2.26	1.94%	95.18%	2.88%	0.0194
0.0135	0.6045	0.0777	1.52	74.36	2.18	1.94%	95.27%	2.79%	0.0194
0.0135	0.6045	0.0776	1.52	74.36	2.18	1.94%	95.27%	2.79%	0.0194

Table B-10: Excel Spread Sheet Showing the Liquid Phase Concentration Calculations for Run # 15

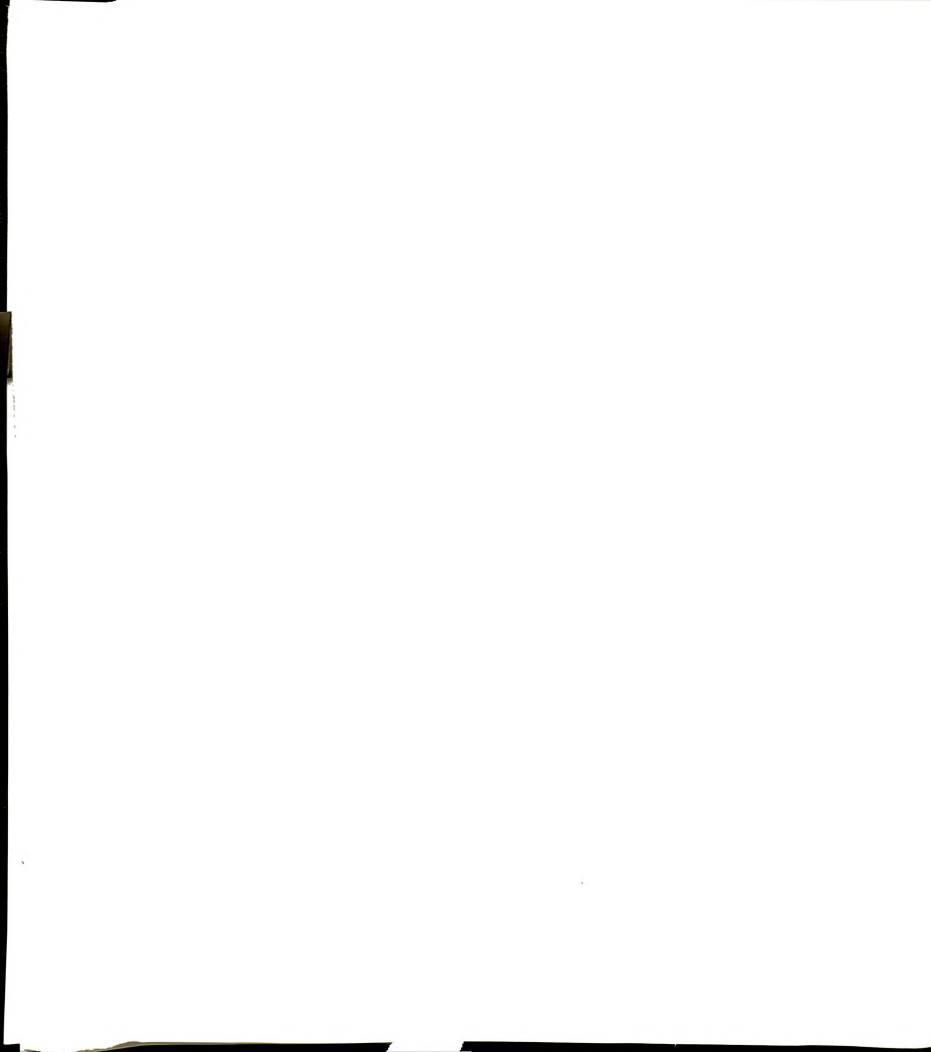


Table B-10 (Cont.): Excel Spread Sheet Showing the Liquid Phase Concentration Calculations for Run # 15

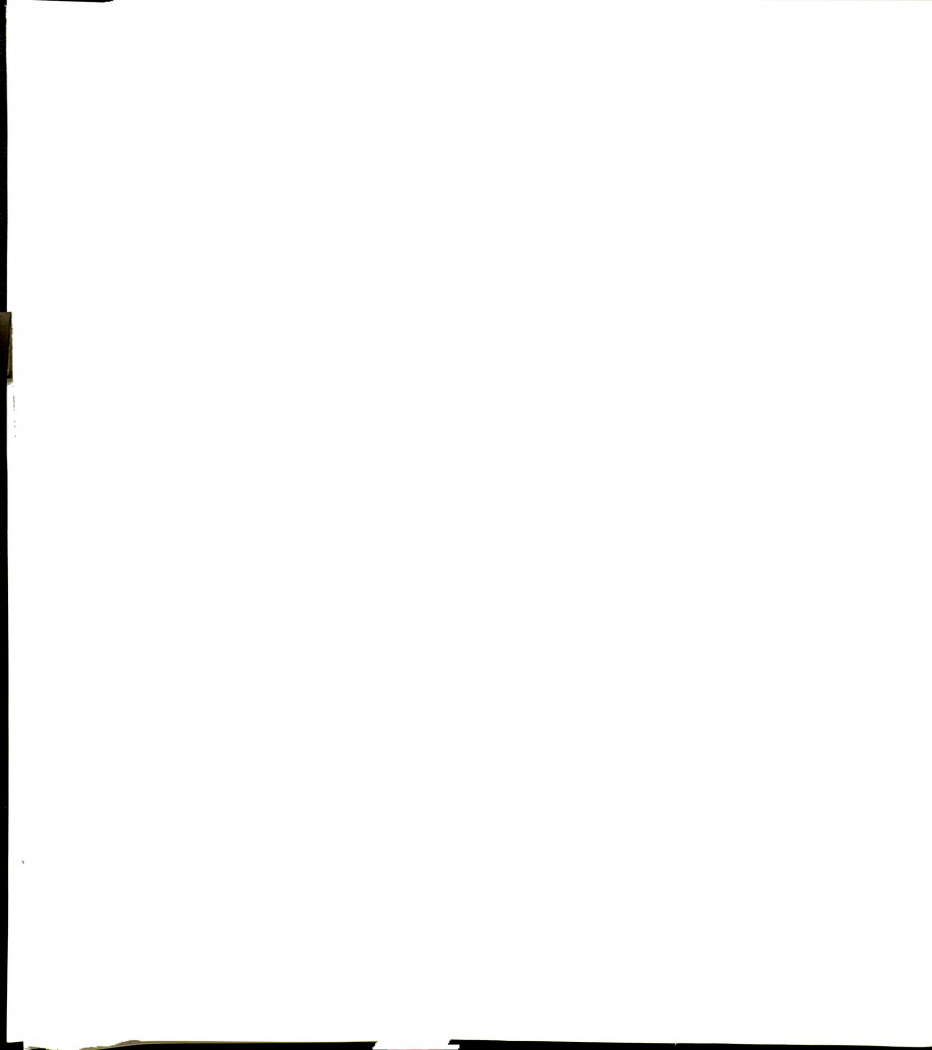


Table B-11: Excel Spread Sheet Showing the Liquid Phase Concentration Calculations for Run # 16

RUN#16		CORR	C8	ISOPAR	C2	SUM	DENSITY	VOLUME	VOLUME	VAPOR	VAPOR	C2
PT5SET	PT4GP	TYES1	P _{ATM}	VP _{ATM}	P _{0_ATM}	P _{0_ATM}	V	g/ml	V _L	V _L	ISOPAR	C2
74.13	72.08	25.75	85.4	0.0239	0.0423	0.0015	5.78	150.0	0.7183	0.1112	0.1378	0.00019
77.54	76.09	29.12	88.6	6.03	0.0286	0.0018	0.0383	5.99	150.0	0.7183	0.1112	0.1378
79.87	79.02	31.76	90.8	6.18	0.0329	0.0021	0.0429	6.13	150.0	0.7183	0.1112	0.1378
109.49	113.31	59.88	118.4	8.06	0.1224	0.1603	0.0079	0.1253	7.92	150.0	0.7183	0.1112
109.49	112.98	59.95	118.4	8.06	0.1228	0.1607	0.0079	0.1256	7.92	150.0	0.7183	0.1112
109.49	113.31	59.99	118.4	8.06	0.1229	0.1609	0.0079	0.1258	7.92	150.0	0.7183	0.1112
137.12	145.31	84.77	144.2	9.81	0.3183	0.3516	0.0205	0.2748	9.51	150.0	0.7183	0.1112
137.45	144.99	84.83	144.5	9.83	0.3190	0.3522	0.0206	0.2753	9.54	150.0	0.7183	0.1112
137.45	144.99	84.87	144.5	9.83	0.3194	0.3526	0.0206	0.2756	9.53	150.0	0.7183	0.1112
166.07	177.97	109.05	171.1	11.64	0.7015	0.6750	0.0452	0.5277	11.07	150.0	0.7183	0.1112
166.40	178.29	109.16	171.4	11.66	0.7038	0.6768	0.0454	0.5291	11.09	150.0	0.7183	0.1112
166.40	178.29	109.20	171.4	11.66	0.7048	0.6776	0.0455	0.5297	11.09	150.0	0.7183	0.1112
215.99	222.05	137.62	204.4	13.91	1.5454	1.2992	0.0997	1.0157	12.79	150.0	0.7183	0.1112
216.32	222.38	137.92	205.0	13.95	1.5573	1.3076	0.1004	1.0222	12.83	150.0	0.7183	0.1112
PT5SET is the readout of the first pressure transducer												
PT4GP is the readout of the second pressure transducer												
TYES1 is the oven set point temperature												
COPR P_{PSIA} is corrected pressure according to the calibration of the pressure transducer (v=m*x+n) x= readout of MKSPT1												
P_{ATM} is corrected pressure in units of atm.												
C8 VP_{ATM} is the vapor pressure of C8 at the set point temperature calculated by using Antoine Constants according to Log(p)=A-B/(T+C)												
ANTOINE CONSTANTS ATM, C_i for IsoparE and 1-Octene are:												
ISOPARE VP_{ATM} is the vapor pressure of IsoparE = (P₀ of C8) * molar fraction of IsoparE												
C8 Po_{ATM} is the partial pressure of C8 = (P₀ of C8) * molar fraction of C8												
ISOPAR Po_{ATM} is the partial pressure of IsoparE = (P₀ of IsoparE) * molar fraction of IsoparE												
C2 Po_{ATM} is the partial pressure of C2 = equal to Ptotal - (partial pressure of C8) - (partial pressure of IsoparE)												
SUM of the molar volume of the components ((C2, C8, IsoparE) obtained from sum of the each components molar masses devided by its density												
DENSITY of the mixture obtained by the molar mass devided by the total molar volume												
VOLUME of the Liquid phase (Liter) = total mass of the original liquid divided by density												
VOLUME of the vapor phase (Liter) = total volume of the vessel - volume of the liquid phase												
VAPOR C8 MOL is the # of moles of C8 in vap. phase obtained by using state of the gas equation (par. pres. of the C8 vap. phase Vol) / 0.8206°TK												
VAPOR ISOPAR MOL is the # of moles of IsoparE in vap. phase obtained by using state of the gas equation (partial pressure of IsoparE) / 0.8206°TK												
VAPOR C2 MOL is the # of moles of C2 in vap. phase obtained by using state of the gas equation (partial pressure of C2) / 0.8206°TK												
MASS, g												
WT%												
C2												
C8												
ISOPAR E												
TOTAL												
VESSEL VOLUME												
MASS, g												
WT%												
C2												
C8												
ISOPAR E												
TOTAL												
MASS, g												
WT%												
C2												
C8												
ISOPAR E												
TOTAL												
MASS, g												
WT%												
C2												
C8												
ISOPAR E												
TOTAL												
MASS, g												
WT%												
C2												
C8												
ISOPAR E												
TOTAL												
MASS, g												
WT%												
C2												
C8												
ISOPAR E												
TOTAL												
MASS, g												
WT%												
C2												
C8												
ISOPAR E												
TOTAL												
MASS, g												
WT%												
C2												
C8												
ISOPAR E												
TOTAL												
MASS, g												
WT%												
C2												



Table B-11 (Cont.): Excel Spread Sheet Showing the Liquid Phase Concentration Calculations for Run # 16

Liquid	Liquid	Liquid	Liquid	C8	ISOPAR	C2	Liquid	Liquid	C8	ISOPAR	C2	Liquid	Liquid	C8	ISOPAR	C2	Liquid	CALC	MEAS
C8 / MOL	ISOPAR / MOL	C2 / MOL	Ig / MOL	Lg	WT%	WT%	MOL F	MOL F	Po, ATM	P, ATM	P, ATM								
0.0478	0.5797	0.0816	5.37	71.31	2.29	6.80%	90.30%	2.90%	0.0675	0.8175	0.1151	0.00	0.03	5.78	5.81				
0.0478	0.5797	0.0808	5.37	71.30	2.27	6.80%	90.33%	2.87%	0.0675	0.8184	0.1141	0.00	0.04	5.99	6.03				
0.0478	0.5797	0.0803	5.37	71.30	2.25	6.80%	90.34%	2.85%	0.0676	0.8190	0.1135	0.00	0.04	6.13	6.18				
0.0478	0.5793	0.0741	5.36	71.25	2.08	6.82%	90.54%	2.64%	0.0682	0.8261	0.1057	0.01	0.13	7.92	8.06				
0.0478	0.5793	0.0741	5.36	71.25	2.08	6.82%	90.54%	2.64%	0.0682	0.8261	0.1057	0.01	0.13	7.92	8.06				
0.0478	0.5793	0.0741	5.36	71.25	2.08	6.82%	90.54%	2.64%	0.0682	0.8261	0.1057	0.01	0.13	7.92	8.06				
0.0477	0.5786	0.0694	5.36	71.17	1.95	6.83%	90.69%	2.48%	0.0686	0.8316	0.0998	0.02	0.29	9.50	9.81				
0.0477	0.5786	0.0694	5.36	71.17	1.95	6.83%	90.69%	2.48%	0.0686	0.8317	0.0997	0.02	0.29	9.52	9.83				
0.0477	0.5786	0.0694	5.36	71.17	1.95	6.83%	90.69%	2.48%	0.0686	0.8317	0.0997	0.02	0.29	9.52	9.83				
0.0476	0.5776	0.0654	5.35	71.05	1.84	6.83%	90.82%	2.35%	0.0690	0.8363	0.0947	0.05	0.56	11.03	11.64				
0.0476	0.5776	0.0654	5.35	71.05	1.83	6.83%	90.82%	2.34%	0.0690	0.8364	0.0947	0.05	0.57	11.05	11.66				
0.0476	0.5776	0.0654	5.35	71.04	1.83	6.83%	90.82%	2.34%	0.0690	0.8363	0.0947	0.05	0.57	11.05	11.66				
0.0474	0.5758	0.0618	5.32	70.82	1.73	6.84%	90.94%	2.23%	0.0693	0.8406	0.0902	0.11	1.09	12.71	13.91				
0.0474	0.5758	0.0617	5.32	70.82	1.73	6.84%	90.94%	2.22%	0.0693	0.8407	0.0901	0.11	1.10	12.74	13.95				

Liquid C8 MOL is the number of moles of 1-octene in liquid phase obtained by subtracting the number of moles of 1-octene in the vapor phase from the total number of moles of octene

Liquid ISOPAR MOL is the # of moles of IsoparE in liquid phase obtained by subtracting the # of moles of IsoparE in the vapor phase from the total # of moles of IsoparE

Liquid C2 MOL is the # of moles of ethylene in liquid phase obtained by subtracting the # of moles of ethylene in the vapor phase from the total # of moles of C2.

Liquid C8 g is the weight of 1-octene in liquid phase obtained by multiplying the number of moles of 1-octene in the liquid phase with the molecular weight of octene

Liquid ISOPAR g is the weight of IsoparE in liquid phase obtained by multiplying the number of moles of IsoparE in the liquid phase with the molecular weight of IsoparE

Liquid C2 g is the weight of ethylene in liquid phase obtained by multiplying the number of moles of ethylene in the liquid phase with the molecular weight of ethylene

Liquid C8 wt% is the weight percent of 1-octene in liquid

Liquid ISOPAR wt% is the weight percent of IsoparE in liquid

Liquid C2 wt% is the weight percent of ethylene in liquid

Liquid C8 MOL F is the mol fraction of 1-octene in liquid

Liquid ISOPAR MOL F is the mol fraction of IsoparE in liquid

Liquid C2 MOL F is the mol fraction of ethylene in liquid

C8 Po, ATM is the partial pressure of C8 = (Vp of C8) * mol fraction of C8

ISOPAR Po, ATM is the partial pressure of IsoparE = (Vp of IsoparE) * mol fraction of IsoparE

C2 Po, ATM is the partial pressure of C2 = (Vp of C2) * mol fraction of C2

CALC P, ATM is the sum of the partial pressures of the C2, C8 and IsoparE which converges to the measured pressure.

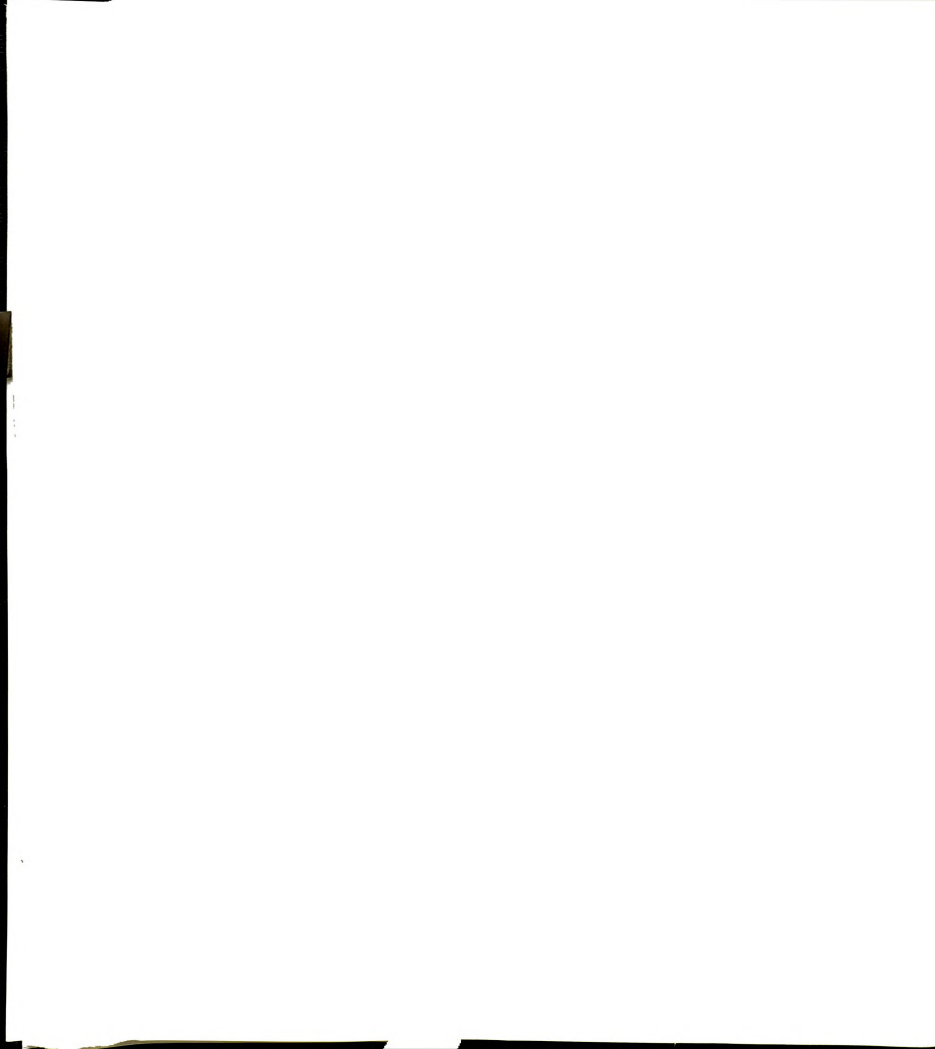


Table B-12: Excel Spread Sheet Showing the Liquid Phase Concentration Calculations for Run # 17



Table B-12 (Cont.): Excel Spread Sheet Showing the Liquid Phase Concentration Calculations for Run # 17

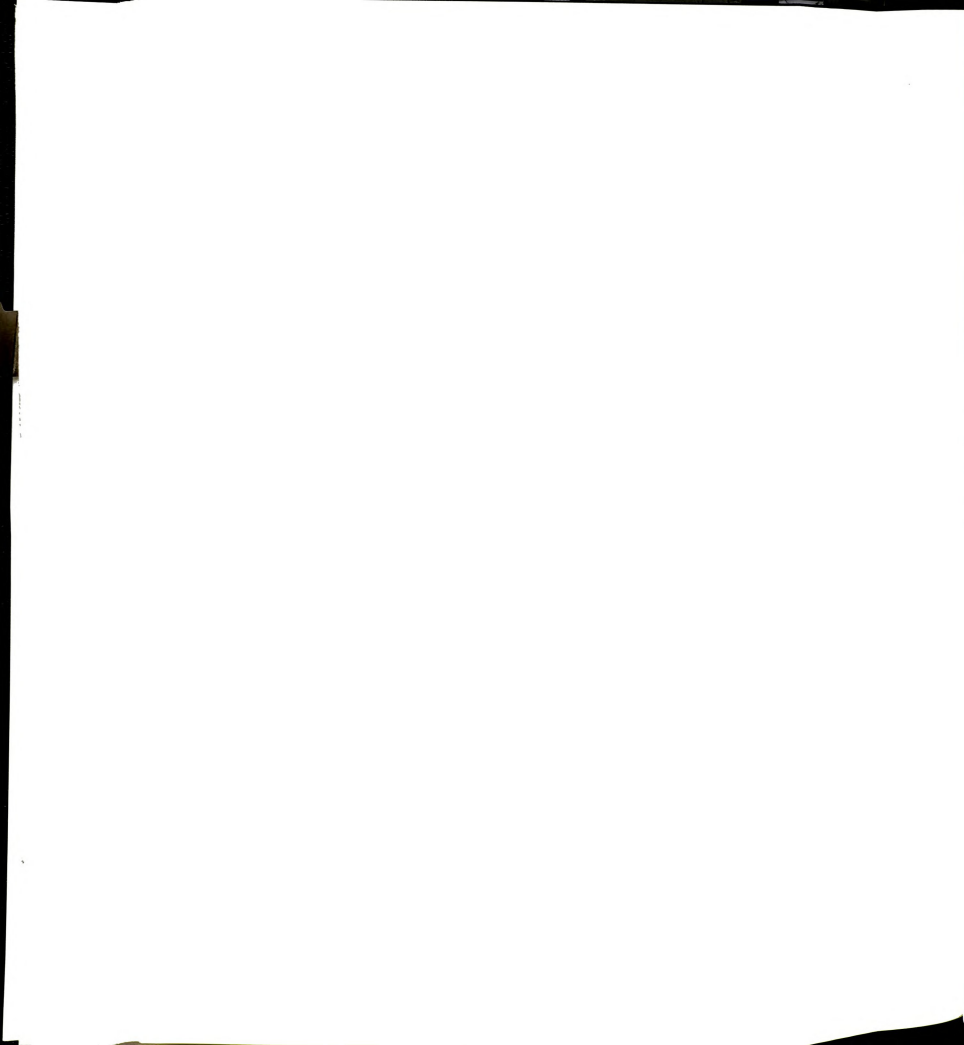


Table B-13: Excel Spread Sheet Showing the Liquid Phase Concentration Calculations for Run # 18



Table B-13 (Cont.): Excel Spread Sheet Showing the Liquid Phase Concentration Calculations for Run # 18



Table B-14: Excel Spread Sheet Showing the Liquid Phase Concentration Calculations for Run # 21



Table B-14 (Cont.): Excel Spread Sheet Showing the Liquid Phase Concentration Calculations for Run # 21



Table B-15: Excel Spread Sheet Showing the Liquid Phase Concentration Calculations for Run # 22



Table B-15 (Cont.); Excel Spread Sheet Showing the Liquid Phase Concentration Calculations for Run # 22



Table B-16: Excel Spread Sheet Showing the Liquid Phase Concentration Calculations for Run # 23



Table B-16 (Cont.): Excel Spread Sheet Showing the Liquid Phase Concentration Calculations for Run # 23

Liquid C8 is the number of moles of 1-octene in liquid phase obtained by subtracting the number of moles of 1-octene in the vapor phase from its total number of moles of octene.

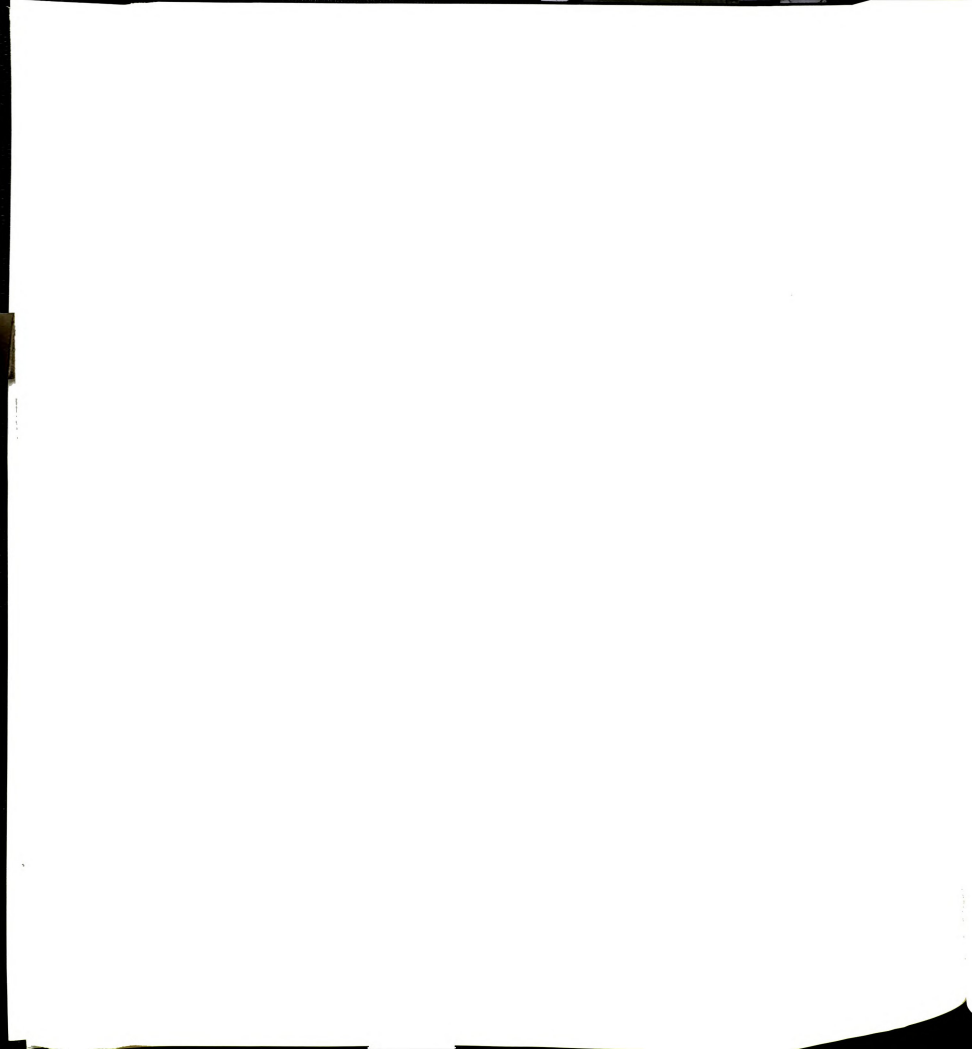


Table B-17: Excel Spread Sheet Showing the Liquid Phase Concentration Calculations for Run # 24



Table B-17 (Cont.): Excel Spread Sheet Showing the Liquid Phase Concentration Calculations for Run # 24



Table B-18: Excel Spread Sheet Showing the Liquid Phase Concentration Calculations for Run # 25



Table B-18 (Cont.): Excel Spread Sheet Showing the Liquid Phase Concentration Calculations for Run # 25



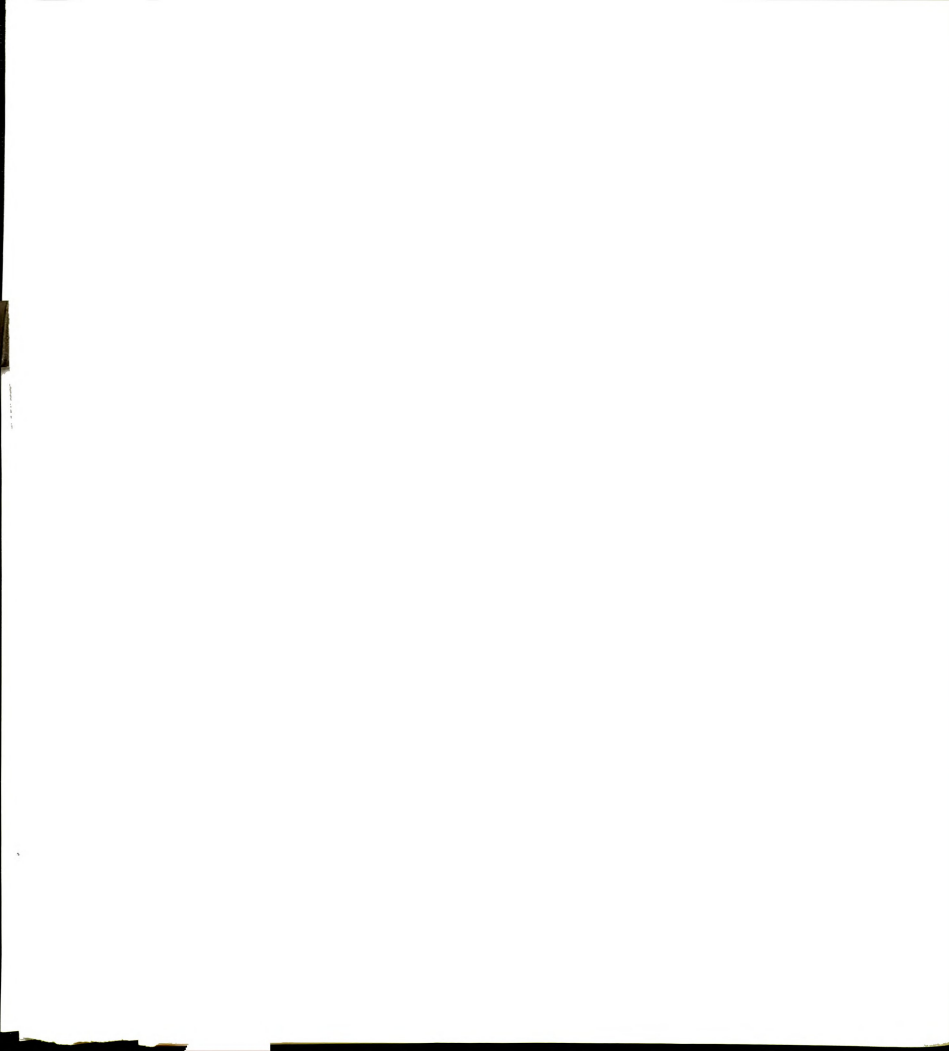
Table B-19: Excel Spread Sheet Showing the Liquid Phase Concentration Calculations for Run # 28



Table B-19 (Cont.): Excel Spread Sheet Showing the Liquid Phase Concentration Calculations for Run # 28



APPENDIX C



APPENDIX C

This section contains the data used in PLS modeling concentration for each file number correlating to each run

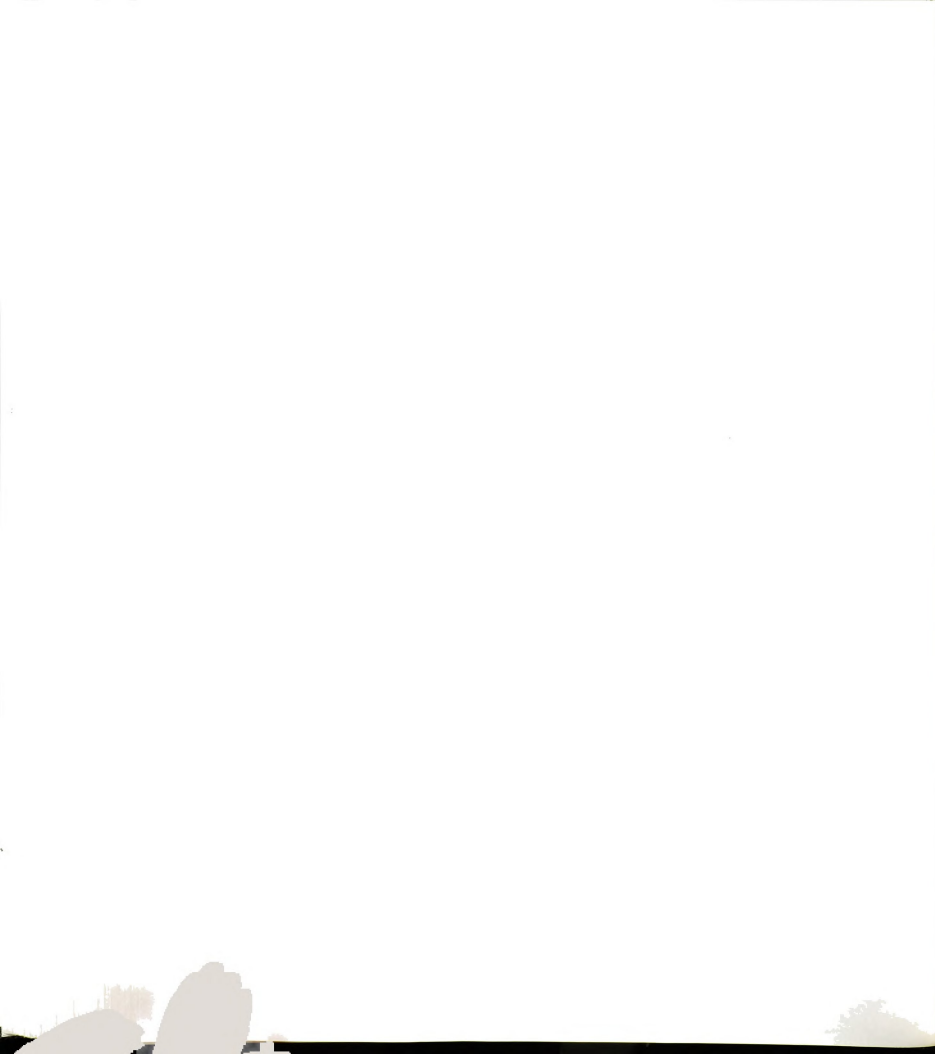


Table C-1: Data Files and the Correlating Concentrations Used in PLS Model

Data File Number	C2 wt Fraction	C8 wt Fraction	Isopar wt Fraction
DT0A790	0.00455	0	0.99545
DT0A800	0.00356	0	0.99644
DT0A810	0.00338	0	0.99662
DT0A845	0.06961	0	0.93039
DT0A860	0.0687	0	0.9313
DT0A870	0.06784	0	0.93216
DT0A880	0	0.01991	0.98009
DT0A895	0	0.01954	0.98046
DT0A910	0	0.01836	0.98164
DT0A940	0	0.06992	0.93008
DT0A950	0	0.06951	0.93049
DT0A960	0	0.06871	0.93129
DT0A985	0	0.15009	0.84991
DT0A999	0	0.14993	0.85007
DT0A1010	0	0.1495	0.8505
DT0A1020	0	0.14889	0.85111
DT0A1040	0	0.29969	0.70031
DT0A1050	0	0.30001	0.69999
DT0A1060	0	0.29995	0.70005
DT0A1080	0	0.29928	0.70072
DT0A1110	0.00784	0.01985	0.97231
DT0A1120	0.00649	0.01987	0.97363
DT0A1130	0.00533	0.01989	0.97478
DT0A1150	0.00414	0.01989	0.97598
DT0A1180	0.03119	0.01938	0.94943
DT0A1190	0.02987	0.01941	0.95073
DT0A1200	0.02883	0.01942	0.95175
DT0A1210	0.0279	0.01942	0.95268
DT0A1270	0.05536	0.0189	0.92575
DT0A1290	0.05256	0.01895	0.92849
DT0A1300	0.05027	0.01899	0.93074
DT0A1310	0.04831	0.01901	0.93268
DT0A1320	0.02903	0.06798	0.90299
DT0A1340	0.0272	0.06811	0.90469
DT0A1350	0.02606	0.06819	0.90575
DT0A1360	0.02531	0.06822	0.90647



Table C-1 (Cont.): Data Files and the Correlating Concentrations Used in PLS Model

DT0A1370	0.02487	0.06818	0.90694
DT0A1390	0.01218	0.06916	0.91867
DT0A1400	0.01113	0.06924	0.91963
DT0A1410	0.01047	0.06928	0.92024
DT0A1420	0.00985	0.0693	0.92085
DT0A1430	0.00945	0.06925	0.9213
DT0A1450	0.05639	0.06606	0.87755
DT0A1460	0.05251	0.06633	0.88115
DT0A1470	0.05023	0.06649	0.88327
DT0A1480	0.04827	0.06661	0.88512
DT0A1490	0.04631	0.0667	0.88699
DT0A1570	0.0392	0.17296	0.78784
DT0A1580	0.03596	0.17356	0.79049
DT0A1590	0.03414	0.17388	0.79198
DT0A1600	0.03259	0.17412	0.79329
DT0A1610	0.0313	0.17421	0.79449
DT0A1630	0.00807	0.17858	0.81336
DT0A1640	0.00744	0.1787	0.81386
DT0A1650	0.00689	0.17879	0.81432
DT0A1660	0.00631	0.17884	0.81484
DT0A1670	0.00595	0.17874	0.81532
DT0A1680	0.03768	0.17323	0.78908
DT0A1690	0.03676	0.17342	0.78982
DT0A1700	0.03618	0.17351	0.7903
DT0A1720	0.03565	0.17356	0.79078
DT0A1730	0.03504	0.17353	0.79144
DT0A1740	0.10604	0.2682	0.62575
DT0A1760	0.09901	0.27033	0.63066
DT0A1770	0.09462	0.27164	0.63374
DT0A1780	0.09126	0.27261	0.63614
DT0A1800	0.08862	0.27326	0.63812
DT0A1805	0.009	0.29734	0.69366
DT0A1820	0.00767	0.29777	0.69456
DT0A1830	0.00684	0.29801	0.69516
DT0A1840	0.00608	0.29814	0.69578
DT0A1860	0.00522	0.29807	0.69671
DT0A1870	0.04198	0.28743	0.67058
DT0A1880	0.03832	0.28856	0.67312
DT0A1890	0.03614	0.2892	0.67466
DT0A1900	0.0343	0.28968	0.67602
DT0A1920	0.03284	0.28987	0.67728
DT0A1930	0.06347	0	0.93653
DT0A1945	0.05921	0	0.94079
DT0A1955	0.057	0	0.943
DT0A1970	0.05567	0	0.94433
DT0A1985	0.05502	0	0.94498

LIST OF REFERENCES

LIST OF REFERENCES

1. Beebe, K.R., Blaser, W.W., Bredeweg, R.A., Chauvel, J.P., Harner, R.S., LaPack, M., Leugers, A., Martin, D.P. Wright, L.G. Yalvac, E.D. *Anal.Chem.*, **1993**, 65, 199R-216R.
2. Yalvac, E.D. Paper No. 536, 16th Annual Meeting of the Federation of Analytical Chemistry and Spectroscopy Societies, **1989**, Chicago, Illinois.
3. Yalvac, E.D., Paper No. 209, 17th Annual Meeting of the Federation of Analytical chemistry and Spectroscopy Societies, **1990**, Cleveland, Ohio.
4. Yalvac, E.D., Bredeweg, R.A., Albers, D.R. Paper No. 66, 18th Annual Meeting of the Federation of Analytical Chemistry and Spectroscopy Societies, **1991**, Anaheim, California, 1991.
5. Yalvac, E.D., Bredeweg, R.A. *Process Quality and Control*, **1992**, 6(2-3), 91-6.
6. DesJardin, M.A., Doherty, S.J., Gilbert, J.R. LaPack, Shao, J., *Process Control and Quality*, **1995**, 6(4), 219-29.
7. Aaljoki, K., Hukkanen, H., Jokinen, P., *Process Control and Quality*, **1994**, 6(2-3), 125-33.
8. Mayes, D.M., Koza, D.S., Cavinato, A.G., *Process Control and Quality*, **1993**, 5(1), 1-9.
9. Babji, B.S., Saraf, S.N., *Process Quality and Control*, **1993**, 4(3), 181-197.
10. Heesch, W.A., Greminger, D.C., Yalvac, E.D., *Process Control and Quality*, **1992**, 2(3), 215-25.
11. Cardis, T.M., *Process Control and Quality*, **1994**, 6(2-3), 109-15.
12. Nielsen, J., *Process Control and Quality*, **1992**, 2(4), 371-85.
13. Morabito, P.L., Melcher, R.G., *Process Control and Quality*, **1992**, 3(1-4), 35-43.
14. Garrison, A.A., Moore, C.F., Roberts, M.J., Hall, P.D., *Process Control and Quality* **1992**, 3(1-4), 57-65.



15. Moessner, R.C., Process Control and Quality, **1992**, 2(3), 237-49.
16. O'Rourke, P.E., JNMM, **1989**, 18(1), 85.
17. Harner, R.S., Proc. SPIE-Int Soc. Opt. Eng., **1992**, 1681 (Opt. Based Meth. Process Analysis), 256.
18. Burgess, L.W., Afrumowitz, M.A., Proc. SPIE-Int. Soc. Opt. Eng. **1992**, 1637 (Environ. Process. Monit. Technol.), 118.
19. Doyle, W.M., Proc. Control Qual., **1992**, 2, 11.
20. LaPack, M.A., Tou, J.C., Enke, C.G., Anal. Chem., **1991**, 63(15), 1631.
21. Srinivas, G., Chuang, S.C., J. Phys. Chem., **1994**, 98(11), 3024-31.
22. Callis, J.B., Illman, D.L., Kowalski, B.R., Anal. Chem., **1987**, 59(9), 624A.
23. Blaser, W.W., Ruhl, H.D., Bredeweg, R.A., Am. Lab., **1989**, 21(1), 69.
24. Clevett, K.J., Bioprocess Technol., **1990**, 47.
25. Guillemin, C.L., J. Chromatogr. **1988**, 441(1), 1.
26. Farquharson, S., Chauvel, J.P., J. proc. SPIE-Int. Soc. Opt. Eng., **1988**, 918, 80.
27. McPeters, H., Anal Chim. Acta., **1990**, 238, 83.
28. Doyle, W.M., Jennings, N., Spectroscopy, **1990**, 5, 34.
29. Saltzman, R.S., Mathews, M., Dell, C.D., ISA Calgary 89 Symp., **1989**, 217.
30. Herzberg, G., Infrared and Raman Spectra, D. Van Norstrand Co.: New York, **1945**.
31. Gordy, W., Martin, P. C., J. Chem. Phys. **1939**, 7, 99-102.
32. Gordy, W., Phys. Rev. **1946**, 69, 604-607.
33. Plyler, E. K., Benedict, W. S., Ibid, **1952**, 49, 1-6.
34. Rank, D. H., Rix, H. D., Wiggins, T. A., J. Opt. Soc. Am. **1953**, 43, 157-162.
35. Wiggins, T. A., Shull, E. R., Rank, D. H., Ibid, **1953**, 21, 1368-1373.



- 36 Goddu, F. R., Delker, D. A., Anal Chem.**1960**, 32, 1, 140-141.
- 37 Huges, R. H., Martin, R. J., Coggeshall, N. D., J. Chem. Phys., **1956**, 24, 489.
- 38 Coggeshall, N. D., Anal. Chem., **1950**, 22, 30, 381-395.
- 39 Griffiths, P. R., deHaseth, J. A., Fourier Transform Infrared Spectrometry, John Wiley & Sons:New York **1986**.
- 40 Esposito. L. D., Koenig, J. L., Fourier Transform Infrared Spectroscopy, Academic Press:New York, **1978**.
- 41 Spiro, I. J. Schlessinger, M., Infrared Technology Fundamentals, Marcel Dekker: New York, **1989**
- 42 Karge, H.G., Boldingh, E., Catal. Today, **1988**, 3(5), 379-386.
- 43 Yin, Y., Te, M., Jiao, F., Su, G., Proc. Int. Conf. Pet. Refin. Petrochem. Process., **1991**, 2, 614-20.
- 44 Chuand, S.C., Pien, S.I., J. Mol. Catal., **1989**, 55(1-3), 12-22.
- 45 Xia, C., Sun, Y., Li, D., Fenzi Cuihua, **1989**, 3(1), 62-71.
- 46 Garland, M., Bor, G., Inorg. Chem., **1989**, 28(3), 410-413.
- 47 Pan, W., Liu, J.; Li, S.; Xia, Y.; Liu, D., (Dep. Chem. Chem. Eng., Qinghua Univ., Beijing, Peop. Rep. China). Gaodeng Xuexiao Huaxue Xuebao (Zhuankan), **1982**, 107-13.
- 48 Mirbach, M.J., Mirbach, M.F., Saus, A., Topalsavoglou, N., Tuyet, N.P., J. Am. Chem. Soc., **1981**, 103(25) 7590-4
- 49 Moser, W.R.; Papile, C.J.; Brannon, D.A.; Duwell, R.A.; Weininger, S.J., J. Mol. Catal., **1987**, 41(3), 271-92.
- 50 Sheridan, R., Rein, A., Research and Development, 1991, 33(10).
- 51 Landau, R.N., Rein, A.J., Research and Development, 1993, 35(13), 39-40.
- 52 Giusto, R.A., Sevnt RC User forum USA, Proceedings, Mettler-Toleddo, Inc, Hightstown, NJ, **1993**.



53. Moser, W.R., Berard, J.R., Peter, J.M., Burger, R.J., Applied Spec., **1992**, 46(7), 1105-12.
54. Altman, L.J., Jalkian, R., US Patent, **1993**, Patent No., 5,407,830.
55. Rekoske, J.E. Barreau, M.A., Ind. Eng. Chem. Res., **1995**, 34(9), 2931-9.
56. Atkinson, R., Tuazon, E.C., Aschmann, S.M., Environ. Sci. Technol., **1995**, 29(9), 1860-6.
57. Atkinson, R., Tuazon, E.C., Aschmann, S.M., Environ. Sci. Technol., **1995**, 29(6), 1674-80.
58. Espeel, P.H., De Peuter, G., Tielen, M.C., Jacops, P.A., J. Phys. Chem., **1994**, 98(44), 11588-96.
59. Jiang, S., Li, C., Xin, Q., Cuihua Xuebao, **1993**, 14(3), 229-33.
60. Cariati, F., Rindone, B., Phys.=CHem. Behav. Atmos. Polut., 1990, 400-7.
61. Martens, A., Crouzet, P., Eur. Pat. Appl., **1989**, EP-345182.
62. Wenig, T.W., Ames Lab Report, IS-T-1313; **1989**, Order No. DE870109337, 220pp.
63. Moser, T.P. Ames Lab. Report, IS-T-1307, **1987**, Order No. DE87010935, 143pp.
64. Wenig, T.W. Schrader, G.L., J. Phys. Chem., **1987**, 91(22), 5674-80.
65. Wenig, T.W. Schrader, G.L., J. Phys. Chem., **1987**, 91(7), 1911-18.
66. Wenig, T.W. Schrader, G.L., J. Phys. Chem., **1986**, 90(24), 6480-8.
67. Koizumi, H. Suzuki, Y., Bunseki Kagaku, **1983**, 32(8), 489-93.
68. Dobrov, V.S., Klimentko, P.L., Sopkina, A.K., Gordash, Y.T., Malova, L.G., Neftepererab. Neftekhim, **1980**, 19, 41-5
69. Sojak, L., Ostrovsky, I., Kubinec, R., Kraus, A., J. Chromatogr., **1992**, 609(1-2), 283-8.
70. Listemann, M.L., Waller, F.J., Herman, F.L., Spectroscopy, 1993, 8(5), 40-5.
71. Gurka, D.F., Titus, R., Anal Chem., **1986**, 58(11), 2189-94.

72. Morin, P. Caude, M., Rosset, R., J. Chromatogr., 1987, 407, 87-108.
73. Takeuchi, K., Hanaoka, T., Matsuzaki, T., Sugi, Y., Ogasawara, S., Abe, Y., Misono, T., Stud. Surf. Sci. Catal., **1995**, 92, 269-74.
74. Johnson, S.A., Rinkus, R.M., Diebold, T.C., Maroni, V.A., Appl. Spectrosc., **1988**, 42(8), 1369-75.
75. Lachenal, G., Vibrational Spectroscopy, **1995**, 9, 93-100.
76. Khettry, A., Hansen, M. G., Antec, **1995**, 2824-2831.
77. DeThomas, F. A., Hall, J. W., Monfre, S. L., Talanta, **1994**, 41, 3, 425-431.
78. Mijovic, J., Andjelic, S., Kenny, J., Polymers for Advanced Technologies, **1995**
79. Osborn, B. G., Fearn, T., Near Infrared Spectroscopy in food Analysis, Wiley, New York, **1980**.
80. Watson, C. A., Anal. Chem., **1977**, 49, 9, 835A-840A.
81. Archibald, D., Miller, C. E., Lin, L. T., Honigs, D.E., Apl. Spectrosc., **1988**, 42, 1549.
82. Maggard, S.M., US Patent, **1990**, Pat. No., 0,506,391.
83. Parisi, A.F., Nogueiras, L., Prieto, H., Anal. Chim. Acta., 1990, 238(1), 95-100.
84. Brackemann, H., Buback, M., Voegele, H.P., Makromol. Chem., **1986**, 187(8), 1977-92.
85. Buback, M., Tups, H., Physica B+C, **1986**, 139-140(1-3), 626-8.
86. Lysaght, M.J., Air Force Inst. of Tech., Report No., AIFT/CI/CIA-91-013D, **1991**, 258 pp.
87. United States Patent, **1992**, Pat. Num. 5,151,474.
88. United States Patent, **1992**, Pat. Num. 5,155,184.
89. United States Patent, **1984**, Pat. Num. 4,469,853.
90. Sharaf, M.A., Illman, D.L., Kowalski, B.R., Chemometrics, **1986**, John Wiley & Sons, New York.

91. Haaland, D.M., Thomas, E.V., *Anal. Chem.* **1988**, 60, 1193.
92. Haaland, D.M., Thomas, E.V., *Anal. Chem.* **1988**, 60, 1202.
93. Haaland, D.M., *Anal. Chem.* **1988**, 60, 1208.
94. Brown, C.W., *Spectroscopy*, **1986**, 1(4), 32.
95. Jackson, J.E., *A User Guide to Principle Components*, **1991**, John Wiley, New York.
96. Massart, D.L., Brereton, R.G., Dessy, R.E., Hopke, P.K., Spiegelman, C.H., Wegscheider, W., Eds. *Chemometrics Tutorials*, **1990**, Elsevier, Amsterdam.
97. Kowalski, B.R., *Chemometrics, Mathematics and Statistics in Chemistry.*, **1983**, D. Reidel Publishing Co., Dordrecht, Holland.
98. Thomas, E.V., Haaland, D.M., *Anal. Chem.*, **1990**, 62, 1091-99.
99. Marjoriemi, M., Mantysalo, E., *J. Am Leather Chem. Assoc.*, **1992**, 87, 249-58.
100. Lin, J., Brown, C.W., *Appl. Spectrosc.* **1993**, 47, 239.
101. Wei, W., Mo, Z., Yao, S., *Anal. Chim. Acta*, **1991**, 25, 143-8.
102. Blanco, M., Coello, J., Iturriaga, H., Maspoch, S., de la Pezuela, C., *Talanta*, **1993**, 40, 1671-6
103. Varadi, M., Hruschka, W., Norris, K.H., *Acta. Aliment.* **1992**, 21, 95-106.
104. Arakaki, L.S.L., Burns, D.H., *Appl. Spectrosc.*, **1992**, 46(12), 1919-28
105. Bellon, V., *Sens. Actuators, B* **1993**, 12, 57-64.
106. Kettaneh-Wold, N., *Chemom. Intell. Lab. Syst.*, **1992**, 14, 57-69.
107. Gauglitz, G., Kraus, G., *GIT Fachz. Lab.* 1992, 36, 232-5, *Chem. Abstr.* 1992, 268, 115-22.
108. Ni, Y., *Anal. Chim. Acta.*, **1993**, 284(1), 199-205.
109. Van de Voort, F., Sedman, J., Emo, G., Ismail, A.A., *J. AOAC Int.*, **1992**, 75(5), 780-5.



110. Miller, C.E., *Appl. Spectrosc.*, **1989**, 43(8), 1435-43.
111. Ketterer, M.E., Biddle, D.A., *Anal. Chem.*, **1992**, 64, 1819-23.
112. Lysaght, M.J., Kelly, J.J., Callis, J.B., *Fuel*, **1993**, 72, 623-31.
113. Lee, M.H., Cavinato, A.G., Mayes, D.M., Rasco, B.A., *J. Agric. Food Chem.*, **1992**, 40, 2176-81.
114. F. Seitz, *Modern Theory of Solids*, **1940** Mc Graw-Hill, New York.
115. Bridgman, P.W., *Physics of High Pressure*, **1949**, G. Bell and Sons, Ltd., London.
116. Frank, C.W., *Electronic Transition and the High Pressure Chemistry and Physics of Solids*, **1973**, Chapman and Hall, London.
117. Ferraro, J.R., *Vibrational Spectroscopy at High External Pressures*, **1984**, Academic Press, Inc., New York.
118. Griffith, J.S., *The Theory of Transition Metal Ions*, **1964**, Cambridge University Press, London.
119. Fisher, D.C., Drickamer, H.G., *J. Chem Phys.*, **1971**, 54, 4825.
120. Bargeron, C.B., Drickamer, H.G., *J. Chem Phys.*, **1971**, 55, 3471.
121. Drier, T., Schiff, G., *J. Chem. Phys.*, 1994, 100(9), 6275-89.
122. Uliivi, L., Lu, Z., Tabisz, G.C., *Phys. Rev., A: Gen. Phys.*, 1989, 40(2), 642-51.
123. Morin, P.H., Beccard, B., Caude, M., Rosset, R., *J. of High Res. Chromatog. & Choromatog. Communications*, 1988, 11, 697-705.
124. Taha, S., Tosson, M., *Thermochim. Acta*, **1994**, 236 (1-2), 217-226.
- 125 Lin, S.B., Koenig, J.L., *J. Polym. Sci., Polym. Phys. Ed.*, **1983**, 21(10), 2067-83.
126. Fernandez Bertran, J., La Serna, B., *J. Mol. Struct.*, **1979**, 56(2)283-8.
127. Fukushima, K., Kawai, T., *J. Mol. Struct.*, **1984**, 112 (1-2), 51-7.
128. Campbell, J.H., Fisher, J.F., Jonas, J., *J. Chem Phs.*, **1974**, 61(1),346-60.



129. Karlsson, A., Klaeboe, P., Nielsen, C.J., J. Raman Spectrosc., **1992**, 23(3), 167-80.
130. Tanabe, K., Hiraishi, J., Tamura, T., J. Mol. Struct., **1976**, 33(1), 19-37.
131. Van der Veken, B.J., Coppens, P., Sanders, R.S., Daeyaert, F.F., Durig, J.R., J. Mol. Struct. **1992**, 272, 305-46.
132. Fernandez-Ballester, G., Castresana, J., Arrondo, J.L.R., Ferragut, J.A., Gonzalez-Ros, J.M., Biochem. J., **1992**, 288(2), 421-6.
133. Kato, M., Taniguchi, Y., J. Phys. Chem., **1994**, 98 (10), 2688-93.
134. Carles, M., Eloy, D., Pujol, L., Bodot, H., J. Mol. Struct., 1987, 156(1-2), 43-58.
135. Hoshino, N., Inabe, T., Mitani, T., Maruyama, Y., Bull. Chem. Soc. Jpn., **1988**, 61(12), 4207-14.
136. Minomura, S., Drickamer, H.G., J. Chem Phys., **1961**, 35 903.
137. Perez-Albuerne, E.A., Drickamer, H.G., J. Chem Phys., **1965**, 43, 1381.
138. Sherman, W.F., Wilkinson, G.R., Advances in Infrared and Raman Spectroscopy, **1980**, Heydon, London.
139. Snyder, R.W., Sheen, C.W., Painter, P.C., Applied Spectroscopy, **1988**, 42(3), 503-8
140. Efimov, Y.Y., Naberukhin, Y.I., Opt. Spektrosk. **1982**, 52(6), 999-1003.
141. Gordon, I.G., Adv. Magnetic Resonance, **1968** 3, 1.
142. Gordon, R.G., J. Chem. Phys. **1963**, 39, 2788.
143. Arroume, M., Idrissi, A., Turrell, G., J. Molecular Struct., **1992**, 266, 153-158.
144. Sugitani, A., Ikawa, S., Konaka, S., Chem. Phys., **1990**, 142, 423-30.
- ^{145.} Gordon, I.G., Adv. Magnetic Resonance, **1968** 3, 1.
- ^{146.} Gordon, R.G., J. Chem. Phys. **1963**, 39, 2788.
147. Ingle, J.D., Crouch, S.R., Spectrochemical Analysis, **1988**, Prentice Hall, New Jersey.
148. McOmber, J.I., Shriver, D.F., Ratner, M.A., Ferraro, J.R., J. Phys. Chem. Solids, **1982**, 43, 903.



149. Adams, D.M., Tan, T.K., J. Phys. Chem. Solids, **1981**, 42, 559.
150. Wu, C.K., J. Polymer Science, **1974**, 12, 2493-506.
151. Adams, D.M., Ekejiuba, I.O.C., J. Chem. Soc. Faraday Trans., **1981**, 77, 851.
152. Ferraro, J.R., Coord. Chem. Rev., **1979**, 29, 1.
153. Adams, D.M., Sharma, S.K., J. Chem. Soc. Faraday Trans., **1978**, 2 (74), 1355.
154. Adams, D.M., Appleby, R., Inorg. Chim. Acta., **1978**, 26, 643.
155. Adams, D.M., Sharma, S.K., J. Mol. Struct., **1981**, 71, 121.
156. Breitinger, D., Kirsten, U., J. Solid State Chem., **1977**, 22, 233.
157. Dultz, W., Krause, H., Winchester, L.W., J. Chem. Phys., **1977**, 67, 2560.
158. Greig, D., Shriver, D.F., Ferraro, J.R., J. Chem. Phys., **1977**, 66, 5248.
159. Gardiner, D.J., Walker, N.A., Dare-Edwards, M.P., Spectrochimica Acta., 1987, 43A(1), 21-34.
160. Gardiner, D.J., Walker, N.A., Dare-Edwards, M.P., Spectrochimica Acta., 1987, 43A(10), 1241-47.
161. Haaland, D. M., Easterling, R. G., Appl. Spec., **1980**, 34, 539.
162. Haaland, D. M., Easterling, R. G., Appl. Spec., **1982**, 36, 665.
163. Haaland, D. M., Easterling, R. G., Vopicka, D. A., Appl. Spec., **1985**, 39, 73.
164. Brown, C. W., Lynch, P. F., Obremski, R. F., Lavery, D. S., Anal. Chem., **1982**, 54, 1472.
165. Haaland, D. M., Practical Fourier Transform Infrared Spectroscopy, Academic Press, Inc.: New York, **1990**.
166. Martens, H., Naes, T., Multivariate Calibration, Wiley, New York, **1989**.
167. Thomas, E. V., Anal Chem., **1994**, 66, 795A

168. Brown, S.D., Blank, T.B., Sum, S.T., Weyer, L.G., Anal. Chem., **1994**, 66 (12), 315R.
169. User Guide, PLSplus/IQ, Galactic Industries Co. **1996**, Salem, NH.
170. Bellamy, L. J.; The Infrared Spectra of Complex Molecules, John Wiley & Sons, New York, **1975**.
171. Dollish, F. R., Fateley, W. G., Bentley, F. F. Characteristic Frequencies of Organic Compounds, John Wiley & Sons:New York, **1974**.
172. Nyquist, R. A. The Interpretation of Vapor-Phase Spectra, Group Frequency Data, Sadtler Research Laboratories, **1984**.
173. Pouchert, C. J., The Aldrich Library of FT-IR spectra, Aldrich Chemical Company, Inc., 1985.
174. Rea, D. G., Anal. Chem. **1960**, 32, 1638.
175. Crawford, Jr., B. L., Lancaster, J. E., Inskeep, R. G., J. Chem. Phys. **1953**, 21, 678.
176. Lin-Vien, D., Colthup, N. B., Fataley, W. G., Grasselli, J. G., The handbook of Infrared and Raman Characteristic Frequencies of Organic Molecules, Academic Press, Inc., San Diego, CA, **1991**.
177. Thompson, H. W., Torkington, P., Trans. Faraday Soc. **1945**, 41, 246.
178. Rasmussen, R. S., Brattain, R. R., J. Chem. Phys. **1947**, 15, 120.
179. Rasmussen, R. S., Brattain, R. R., J. Chem. Phys. **1947**, 15, 131.
180. Rasmussen, R. S., Brattain, R. R., J. Chem. Phys. **1947**, 15, 135.
181. McMurray, H. L., Thornton, V., Anal. Chem., **1952**, 24, 318.
182. Colthup, N. B., Daly, L. H., Wiberley, S. E.; Introduction to Infrared and Raman Spectroscopy; Academic Press:San Diego, **1990**.
183. Struve, W. S.; Fundamentals of Molecular Spectroscopy, John Wiley & Sons: New York, **1989**.
184. Barrow, G. M.; Introduction to Molecular Spectroscopy, McGraw-Hill: York, **1962**.
185. Kaye, W.; Spectrochemica Acta, **1954**, 6, 257-287.



186. Gaytguer, G.; J.Phys. Radium, **1953**, 14, 19-24.
187. Mecke, R., Discuss. Faraday Soc., **1950**, 9, 161-171.
188. Vaan Ness, H.C., Abbott, M.M., Classical Thermodynamics of Nonelectrolyte Solutions, **1982**, McGraw-Hill, New York.
189. Reid, R.C., Prausnitz, J.M., Poling, B.E., The Properties of Gases and Liquids, **1987**, 4th Edition, McGraw-Hill, New York.
190. Navarro-Viloslada, F., Perez-Arribas, L.V., Leon-Gonzalez, M.E., Polo-Diez, L.M., Anal. Chim. Acta., 313, **1995**, 93-101.
191. Rohrback, B.G., Trends in Anal. Chem. **1991**, 10(9), 269-261.
192. Kelly, J.J., Barlow, C.H., Jinguiji, T.M., Callis, J.B., Anal. Chem. **1989**, 61(4), 313-320.
193. Malinowski, E.R., Factor Analysis in Chemistry, **1991**, 2nd edition, Wiley, New York.
194. Geladi, P., Anal. Chim. Acta., **1986**, 185, 1-17.
195. Haaland, D.M., Computer-Enhanced Analytical Spectroscopy, **1992**, V3, 1-30, Plenum Press, New York.
196. Harris, J.M., Frans, S.D., Poston, P.E., Wong, A.L., IN Computer-Enhanced Analytical Spectroscopy; Meuzelaar, H.L.C. Ed., Plenun Press, New York, **1990**, 2,3-36.
197. Miller, J.N., Analyst, **1991**, 116,3-14.
198. Brown, P.J., Anal. Proc., **1990**, 27,303-6.
199. Mark, H., Anal. Chim. Acta, **1989**, 223, 75-93.
- 200 Adams, J.M., Chemometrics in Analytical Spectroscopy, The Royal Society of Chemistry, **1995**, Cambridge, England.
201. Meloun, M., Miliitky, J., Forina, M., Chemometrics for Analytical Chemistry, **1992**, Ellis Horwood, LTD., West Sussex, England.



202. Brereton, R.G., Chemometrics Application of Mathematics and Statistics to Laboratory Systems, **1990**, Ellis Horwood LTD., West Sussex, England.

MICHIGAN STATE UNIV. LIBRARIES



31293015635745